NOVEMBER
1977

laser technology

MICROWAVES

In this issue:

- Lower crosspole levels for frequency reuse
- FORTRAN program convolves two signals
- A novel third-harmonic oscillator for ECM systems

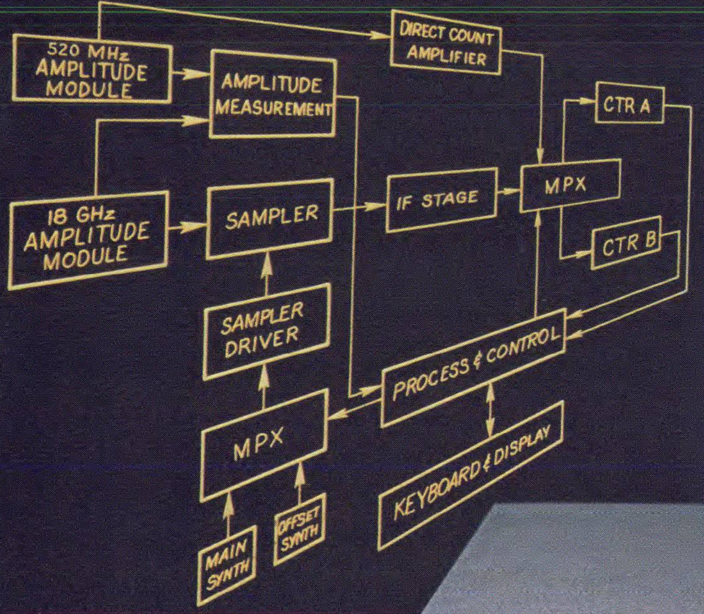

MICRO-PROCESSOR CONTROLLED COUNTER DISPLAYS FREQUENCY AND VOLTAGE TOGETHER

MICROWAVES

November 1977
Vol. 16, No. 11

news

9 With outputs of milliwatts to megawatts, millimeter-wave radar is coming on strong
12 US, European firms race for new EW markets, as Japanese manufacturers sprint to catch up
14 Lockheed wins Air Force approval to build Precision Location/Strike System
18 Industry
23 Washington
28 International
34 Meetings
37 R & D
40 For Your Personal Interest. . .

editorial

44 Where do you stand?

technical

48 **Lower Crosspole Levels For Safe Frequency Reuse.** Marc Spellman of Harris ESD analyzes three transmission phenomena that reduce the availability of communications links with frequency reuse.
62 **Oscipliers: K-Band VCOs You Build With Bipolars.** R.G. Winch of Teledyne Microwave introduces the bipolar replacement for Gunn-based VCO's. This novel circuit is faster than conventional YIG-tuned oscillators and in addition, dipenses with post-VCO multipliers and doubler stages.
68 **Convolution Program Tests Two Interfering Signals.** Fred E. LaPlante of RCA Alaska Communications, Inc., shows how to avoid the stumbling block of convolution with this comprehensive FORTRAN routine.

departments

74 **Cover Feature:** Microprocessor-controlled frequency counter thinks fast, acts smart and costs less
75 New Products
85 New Literature
87 Advertisers' Index
88 Product Index

About the cover: The brains behind HP's new 5342A automatic frequency counter is a microprocessor. It allows the instrument to do things other counters can't even think about. See story on p. 74.

coming next month: Passive Components

- **Filters.** An investigation of filters stabilized by MIC dielectric resonators shows high Q values and little variation with temperature.
- **Mixers.** Sources of third-order intermodulation distortion are traced and analyzed, and several methods of suppression are evaluated.
- **Transmission lines.** A complete library of subroutines, written in FORTRAN, handle all common problems with lossless or lossy lines.

Publisher
Howard Bierman

Editor
Stacy V. Bearse

Associate Editor
Robert Wollins

Washington Editor
Paul Harris
Snyder Associates
1050 Potomac St. NW
Washington, DC 20007
(202) 965-3700

Editorial Assistant
Gail Murphy

Production Editor
Sherry Lynne Karpen

Art Director
Robert Meehan

Art Illustrator
Janice Tapp

Production
Dollie S. Viebig, Mgr.
Anne Molfetas

Circulation
Barbara Freundlich, Dir.
Sherry Karpen,
Reader Service

Directory Coordinator
Janice Tapp

Editorial Office
50 Essex St.,
Rochelle Park, NJ 07662
Phone (201) 843-0550
TWX 710-9910-5071

A Hayden Publication
James S. Mulholland, Jr., President

MICROWAVES is sent free to individuals actively engaged in microwave work. Prices for non-qualified subscribers:

	1 Yr.	2 Yr.	3 Yr.	Single Copy
U.S.	$25	$40	$ 60	$3.00
Foreign	$40	$70	$100	$4.00

Additional Product Data Directory reference issue, $15.00 each (U.S), $27.00, (Foreign), POSTMASTER, please send Form 3579 to Fulfillment Manager, MicroWaves, P.O. Box 13801, Philadelphia, PA. 19101.

Back Issues of MicroWaves are available on microfilm, microfiche, 16mm or 35mm roll film. They can be ordered from Xerox University Microfilms, 300 North Zeeb Road, Ann Arbor, MI 48106. For immediate information, call (313) 761-4700.

Hayden Publishing Co., Inc., James S. Mulholland, President, printed at Brown Printing Co., Inc., Waseca, MN.

Lower Crosspole Levels For Safe Frequency Reuse

Three transmission phenomena combine to reduce the availability of communications links with frequency reuse. An understanding of their effects is the first step toward improving performance.

Here's a list of six statements pertaining to frequency reuse communications systems. Which are true and which are false?

- Rain drops affect polarization coupling because of their shape.
- Multipath gives rise to coupling between orthogonally polarized signals.
- Faraday rotation has no effect on terrestrial links.
- Faraday rotation affects only linearly polarized waves.
- There are ways to predict the availability of a system employing frequency reuse.
- There are ways to improve the availability of any frequency reuse system.

If you took more than a few seconds to evaluate each of the above statements, don't feel bad. Questions like these are at the heart of transmission media problems associated with frequency reuse systems employing orthogonal polarization. To get a better grasp of the facts about signal depolarization, first review the basics. (Just for the record, all six statements are true).

Frequency reuse is a response to spectrum conservation demands, and is accomplished by applying one signal channel to one polarization and a second channel to an orthogonal polarization. Hence, the term "frequency reuse."

Frequency reuse with orthogonally polarized channels doubles the bandwidth efficiency of a system. For ideal antennas with ideal transmission media, the 3-dB increase in bits/Hz of spectrum is accomplished with a corresponding 3-dB increase in transmitted power. However, since neither antennas nor transmission media are ideal, other steps are required to maintain the quality of communications achieved in the nonfrequency-reuse system. The nonideal antennas and transmission media are manifested by a finite signal-to-interference ratio (or crosspole isolation), S/I. S is the power in the receiver channel associated with the transmission of the like polarization, and I is the power in the same receiver channel associated with the transmission of orthogonal polarization.

The degradation in an antenna's S/I ratio results from the finite limit of polarization isolation for antenna feeds and therefore is due to increasing I. The degradation in S/I attributable to the transmission media may be a two-fold effect. First, there is a coupling of power from one polarization to the other, which like the antenna effect, primarily increases I and thus reduces S/I. Second, there are circumstances that may result in selective fading of S and not I, thus degrading S/I due to a decrease in S as opposed to an increase in I.

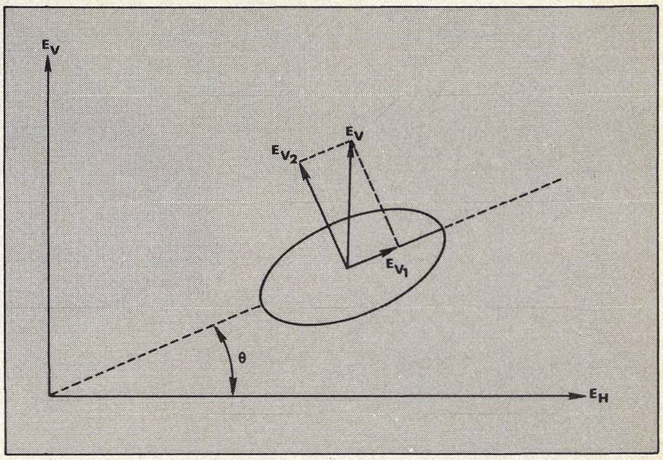

1. Rain drop misalignment with horizontal and vertical axes. *The vertical electric field isn't parallel with the drop's major axis while the horizontal electric field is not aligned with the rain drop's minor axis.*

The three most devastating transmission media phenomena that impact polarization isolation are rain, multipath propagation and the Faraday effect. In addition, antennas are a significant contributor to crosspole coupling. Of the three media effects, rain has received the most attention from path planners. Rain both absorbs and scatters microwave energy. Multipath propagation resulting from refraction, diffraction or reflection also degrades crosspolarization isolation.

Unlike the effects of rain, multipath-induced crosspole is probably limited to terrestrial links and does not impact satellite links. Only recently have quantitative data and theoretical postulations on multipath-induced crosspole found their way into the literature[1,2]. The Faraday effect impacts satellite links only. Furthermore, since it is not a deorthogonalizing effect, but merely results in a polarization rotation, it may be compensated for rather easily and is therefore not as significant as either rain or multipath.

If only rain fell straight . . .

If rain drops were perfectly spherical and fell in a straight line, they would not contribute to cross polarization coupling. This is because crosspole coupling—the reciprocal of crosspole isolation—results from a misalignment of the major and minor axis of a rain drop and the electrical field

Marc Spellman, Associate Principal Engineer, Harris ESD, P. O. Box 37, Melbourne, FL 32901.

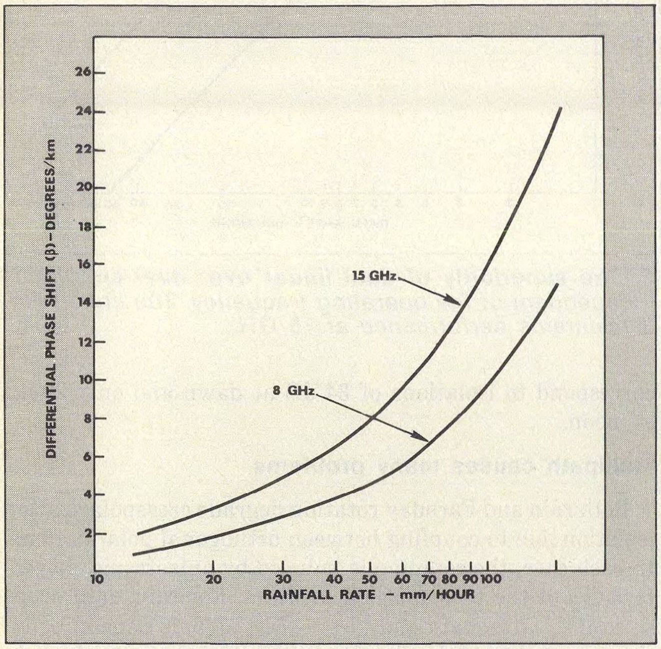

***2. A greater differential phase shift** occurs at high signal frequencies and at a more intense rainfall.*

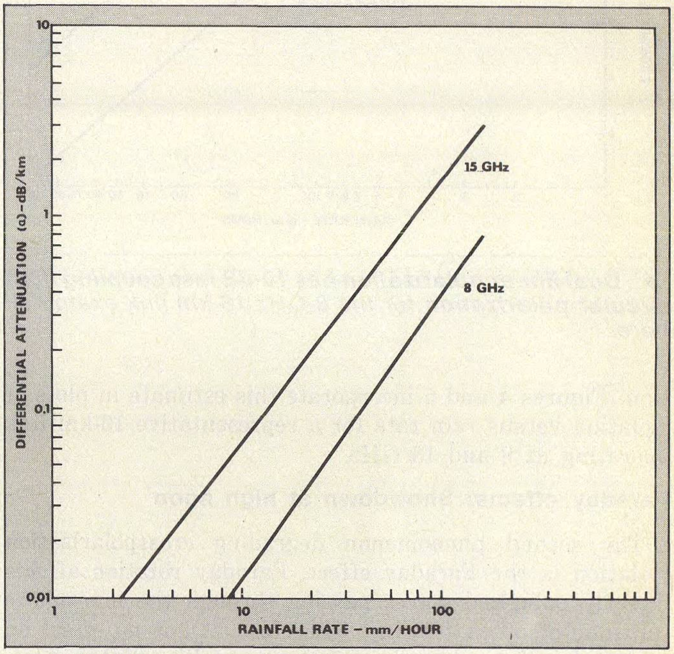

3. Microwave energy absorption increases at higher frequencies, resulting in a larger differential attenuation.

impinging on it.

The misalignment causes a differential phase shift , β, and a differential attenuation, α, between the electric field components, both parallel and perpendicular to the rain drops' axes of symmetry (Fig. 1). Signal frequency, rain rate and the type of polarization pair all affect the magnitude of the polarization decoupling.

Figure 2 illustrates how two of these variables—rain rate and frequency—affect the differential phase shift, β. Note the increase in phase shift at the higher frequency. The same frequency relationship holds when differential attenuation, α, is plotted as a function of rain rate (Fig. 3). This data, derived from calculations,[3] also points out that a greater rain rate increases both differential phase shift and differential attenuation.

The polarization pair being used must be considered to relate α and β to crosspolarization coupling levels. Links with dual linear polarizations (horizontal and vertical) experience different crosspolarization coupling than do the same links using dual circular polarization (left-handed and right-handed). The coupling level for a dual circularly polarized system can be approximated[4] by:

$$C_c = 20 \log \left| \frac{1 - e^{-\ell(\alpha + j\beta)}}{1 + e^{-\ell(\alpha + j\beta)}} \right| \qquad (1)$$

Here, β and α are differential phase shift and differential attenuation per unit length (taken from Figs. 2 and 3), and ℓ is the path length. A key assumption implicit in this expression is that the rain rate is constant over the path length.

If a system employs dual linear polarization, an additional parameter, the raindrop canting angle, impacts crosspolarization coupling. The canting angle is the angle between the major axis of the image of an oblate spheroidal rain drop projected on the plane normal to the direction of propagation and the horizontal in that same place. The functional dependence of linear crosspole coupling on the canting angle is:[5]

$$C_L = 20 \log \left| \frac{(1 - e^{-\ell(\alpha + j\beta)}) \tan \theta}{1 + e^{-\ell(\alpha + j\beta)} \tan^2 \theta} \right| \qquad (2)$$

where θ is the canting angle and ℓ, α and β are the same as in Eq. 1.

Equations 1 and 2 demonstrate that the isolation between orthogonal circular polarized waves will always be poorer than between orthogonal linear polarized waves. The only exception is for a 45-degree canting angle for which the two expressions are identical. In reality, there is not one canting angle for any particular rain, but rather, there is a canting angle distribution. This distribution determines the degree to which linear polarization isolation is superior to circular polarization isolation when rain is the sole cause of coupling. Although not enough[5] raindrop canting angle distribution measurements are available to make precise predictions of the advantages of linear polarization, estimates[6], supported by experimentation, suggest a 10-dB improvement in isola-

(continued on p. 50)

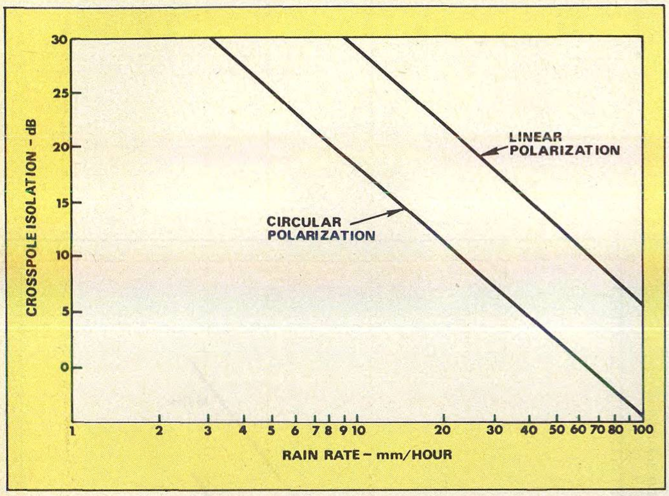

4. Dual linear polarization has 10-dB less coupling than circular polarization *for the 8-GHz 16-km link examined here.*

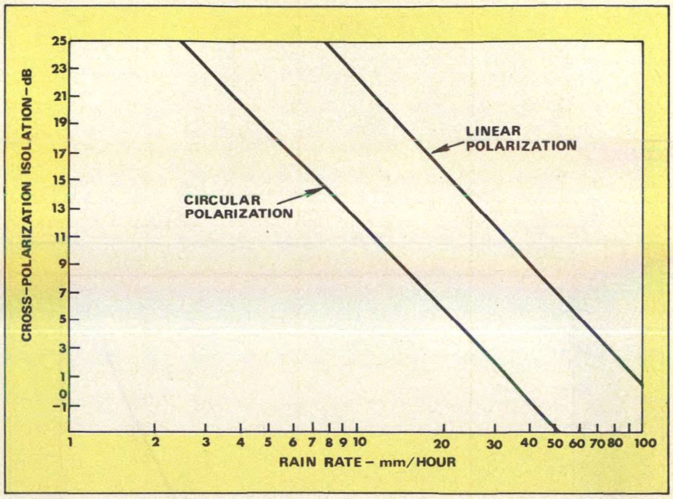

5. The superiority of dual linear over dual circular *is independent of the operating frequency. The link in Fig. 3 maintains performance at 15 GHz.*

tion. Figures 4 and 5 incorporate this estimate in plots of isolation versus rain rate for a representative 16-km link operating at 8 and 15 GHz.

Faraday effects: Showdown at high noon

The second phenomenon degrading crosspolarization isolation is the Faraday effect. Faraday rotation affects linearly polarized waves passing through the ionosphere (altitude of 50 to 400 km). Therefore, it has no effect on terrestrial links but does impact satellite links. Also, circularly polarized waves are not affected by Faraday rotation, since the further rotation of circularly polarized electric fields does not result in any cross coupling. Additionally, the rotation experienced by linearly polarized waves is the same for any electric field orientation, and therefore, the orthogonality of dual linearly polarized channels is not impacted by Faraday rotation. Since orthogonality is maintained, cross-channel coupling can be removed by rotation of the receiving antenna feed.

The magnitude of the Faraday rotation depends on frequency, as well as the sun's position relative to the antenna. The peak rotation at noon can be approximated by:

$$R = \frac{90°}{F^2}$$

where F is the signal frequency in GHz. The minimum rotation at dawn is approximately:

$$R = \frac{18°}{F^2}$$

where F is again in GHz. An additional but as yet unquantified factor which impacts the magnitude of Faraday rotation is solar flares. Coupling levels due to Faraday rotation are equal to 20 log sin ø, where ø is the rotation angle. Therefore, at 11 GHz, the rotation varies from 0.15 degrees at dawn to 0.74 degrees at noon. For perfectly aligned antennas, this results in a range of polarization isolations of 52 dB at dawn to 38 dB at noon time. At 4 GHz, the rotation is much more severe, varying from 1.1 degrees at dawn to 5.6 degrees at noon. These rotations correspond to isolations of 34 dB at dawn and only 20 dB at noon.

Multipath causes many problems

Both rain and Faraday rotation degrade crosspolarization isolation due to coupling between orthogonal polarizations. In each case, the coupling is induced by anisotropic characteristics of the transmission medium. For rain, rain drops selectively attenuate and phase-shift signals depending on the orientation of the electric field with respect to the rain drop. For Faraday rotation, the earth's static magnetic field causes the ionosphere to be anisotropic, resulting in phase shift and attenuation variations of circularly polarized waves depending on their sense of rotation.

The crosspole degradation due to multipath, however, principally results from a selective fading of the desired sig-vis-a-vis the undesired or interfering signal. The coupling of signal power between orthogonal polarizations, necessary for crosspole degradation, may or may not be associated with the multipath mechanism. It has been speculated[2] that coupling may result from depolarization caused by foreground scattering, off-axis receiving antenna characteristics, or higher-order waveguide modes.

(continued on p. 52)

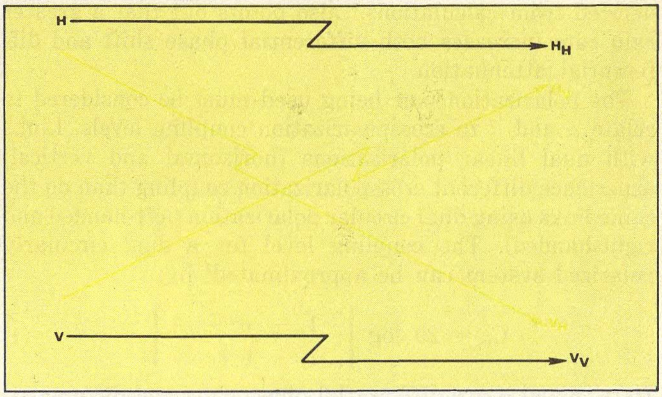

6. Horizontal and vertical signals fade together, *but their cross-coupled components do not. This phenomena creates multipath interference.*

Whatever the source of coupling, it is well below the expected and measured coupling due to on-axis antenna imperfections and misalignments. However, the former coupling, unlike the latter coupling, does not fade together with the in-line signal[1,2]. And, this creates the degradation in crosspole isolation. Figure 6 illustrates in-line and cross-coupled signals for a linearly polarized frequency re-use link. Both H_H and V_H as well as V_V and H_V do not fade together.[7,8] But, H_H and V_V do fade simultaneously.[7,9] These results imply that cross pole interference $\left(\frac{V_H}{V_V} \text{ and } \frac{H_V}{H_H}\right)$ is impacted by multipath.

Predicting link availability

The combination of reduced crosspole isolation and antenna effects have their greatest effect on the link availability of a frequency reuse system. A reuse link contends with interfering signals not present in a basic link (the coupled crosspole signal), and as a result, a reuse system has a lower link availability than a basic system.

Availability is a measurement of the time a fixed level of performance is provided by an antenna system. The easiest way to detail an availability comparison between the two types of antenna systems is with an example. Assume a 16-km terrestrial link. This, of course, eliminates an effect from Faraday rotation. For purposes of examination, multipath contributions will also be neglected.

In order to develop an availability prediction (the probability of acceptable link performance for a specified link

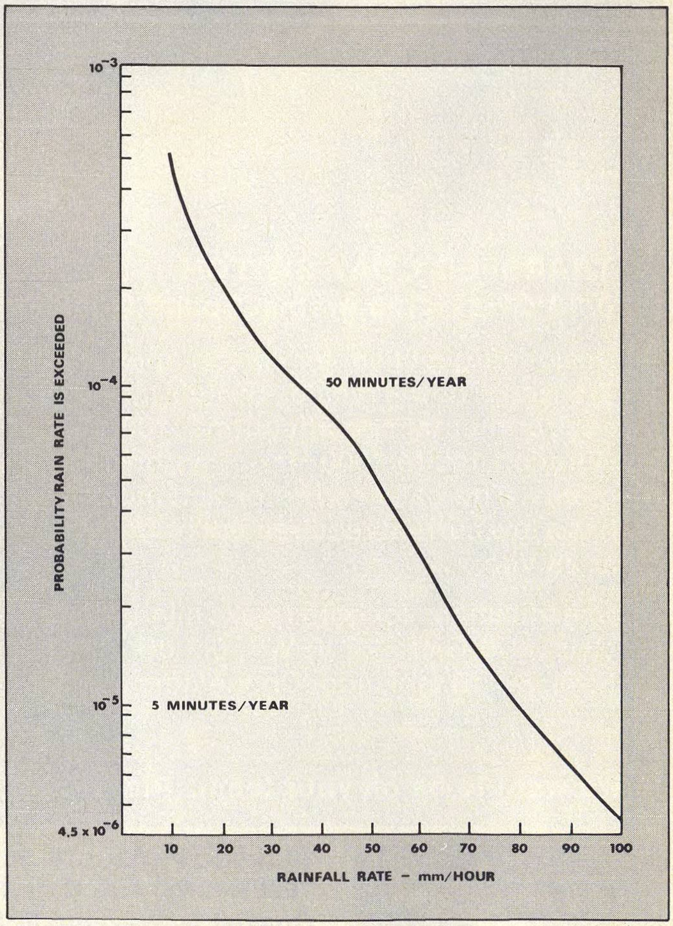

***7. A point rain model** is the first step in a link prediction analysis.*

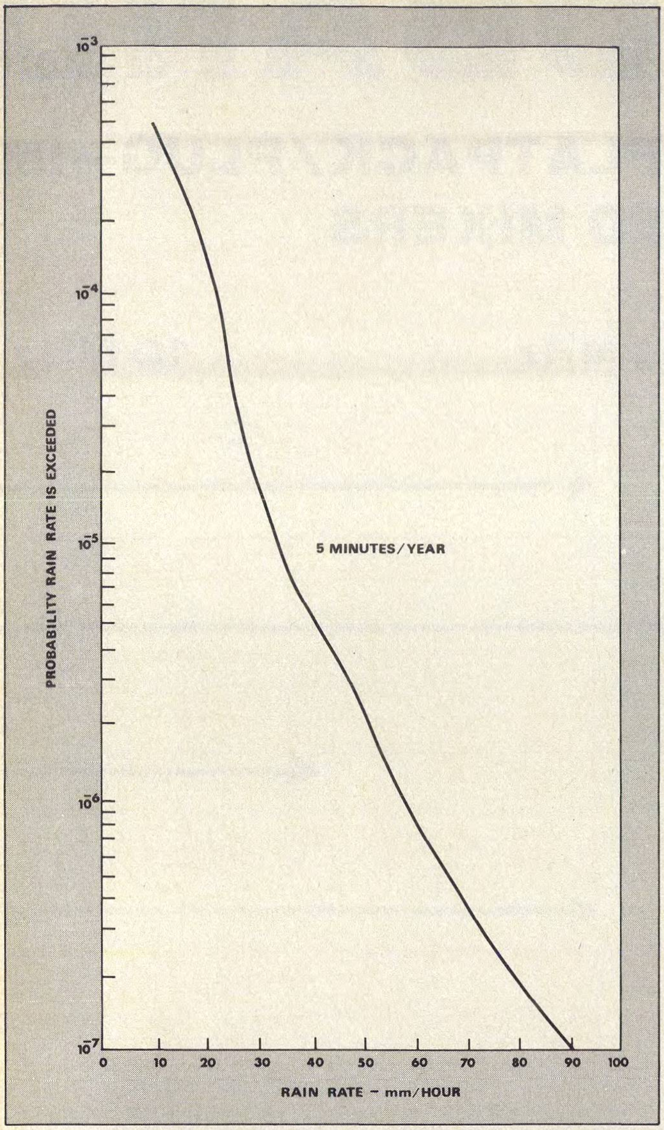

*8. **A path rain rate** can be extrapolated from a point rain model. Here a path rain rate is plotted for a 16-km path.*

margin), a rain model must be postulated. Figure 7 is a rain model[10] representative of a temperate climate. For example, it illustrates that a point rainfall rate of 80 mm/hr or greater occurs with a probability of 1 in 10^5, or approximately 5 minutes a year.

Probabilities of point rainfall rates are, however, insufficient for determining a desired availability prediction. What is needed is the probability of path rainfall rates, where a path rainfall rate is defined as the space average of the point rates along a path. Path rates as such are extremely difficult to observe or measure. They must be inferred from point data, and it is not obvious how rainfall statistics for a long path are related to those from a point. Obviously, point rates will not extend uniformly over a large area.

Generally, point rates are related to path rates through such characteristics as storm size, shape, persistence and velocity of translation. In turn, these characteristics are intimately related to rain rate. Predictions[11], based on the relationship between path rainfall rates and point rainfall rates, state that an annual distribution of 1-hr point rates approximates an annual distribution of instantaneous 50-km path rates. This ergodic relationship between point and

(continued on p. 57)

space averaged rain rates can be extended to include additional time-path length pairs. Extrapolating these results leads to the representative plot shown in Fig. 8 which shows path rain rate probabilities for a 16-km path.

Having established a rain probability model, the effect of rain on both attenuation and cross coupling can now be determined. Attenuation is addressed initially. Attenuation of microwaves by rain has been considered[12, 13] since 1945.

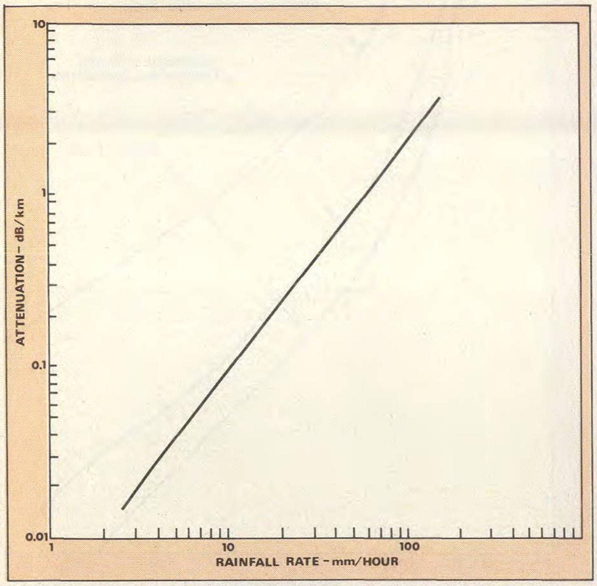

***Both scattering and absorption** create this attenuation curve at 8 GHz.*

Figure 9 shows graphs of path attenuation in dB-per-kilometer versus rainfall rate in millimeters-per-hour for an 8-GHz link. The determination of crosspole coupling versus rainfall rates has already been presented in Fig. 4.

The next step is to associate the crosspole, or interfering signal, with its resultant reduction in received signal-to-noise ratio. This will naturally depend on the modulation technique and its immunity to interfering signals. In this example, QPSK modulation is assumed. A worst-case situation where the in-line and cross-coupled (interfering) signals have coincident symbol timing and a carrier phase offset of 45 degrees is shown in Fig. 10. Here, a 10-dB crosspole coupling is seen to result in a 5-dB degradation in S/N. Figure 10 also illustrates S/N degradation when the phase of the interference is random.[14]

All the necessary information has now been presented to generate approximate availability curves for both basic and frequency reuse links. These are shown in Fig. 11 for the 8-GHz, 16-km link, operating in a temperate climate with QPSK modulation and assuming a random phase relationship. Three curves result. The first is for a basic link where frequency reuse is not employed and the system margin must compensate for only direct rain attenuation. The second is for a frequency reuse link employing dual linearly polarized waves. Here the system margin must compensate for both direct attenuation and the coupled crosspole interference. Interestingly, this curve falls to the right and above the first curve, indicating that for a given availability a greater system margin must exist or conversely for a specified system margin a reduced availability will

(continued on p. 58)

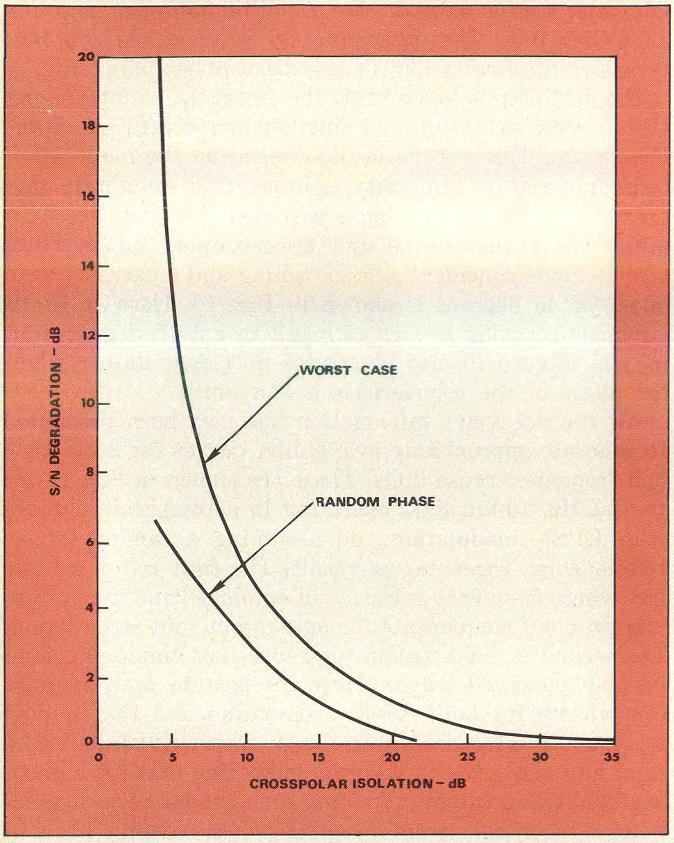

10. In-line and cross-coupled signals with coincident timing and a 45-degree phase offset creates a worst case signal-to-noise degradation.

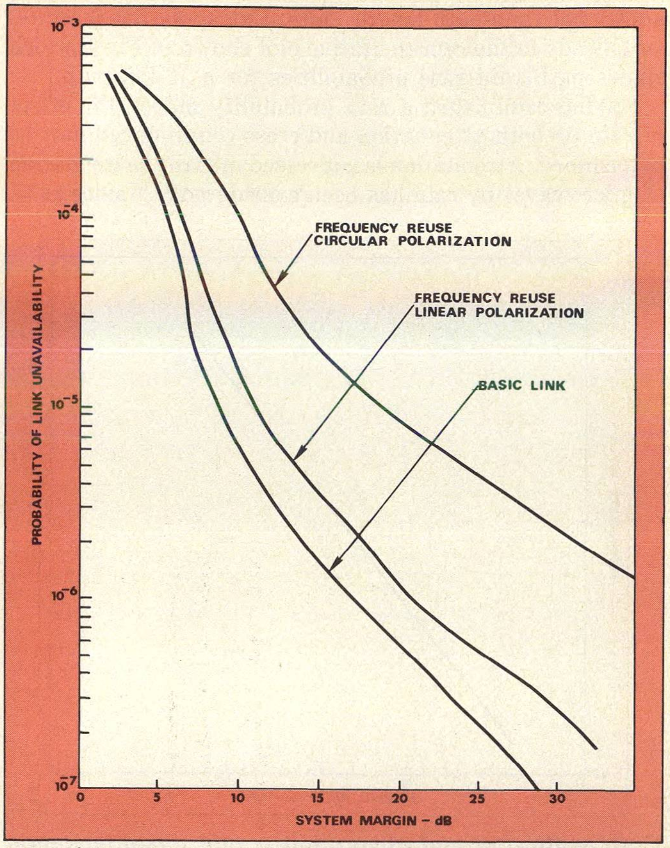

11. Availability curves prove that a linearly polarized reuse system is superior to a circularly polarized system. Neither presents as much availability as a basic link.

result. The third curve corresponds to a frequency reuse link employing dual circular polarization. Because of the greater coupling expected in a circularly polarized frequency reuse links, this curve falls further above and to the right.

Before considering some ways to increase the availability of frequency reuse links, the impact of the addition of the crosspole multipath effects to the above analysis is worth some discussion. First, the simultaneous occurrence of both strong rain induced, and multipath induced crosspole isolation degradation is extremely unlikely. The heavy rains that produce rain crosspole tend to break up the atmospheric stratification that is necessary for many of the multipath effects. Thus, peak crosspole couplings should not change. What does happen is that the likelihood that any particular margin will be exceeded increases. Thus, it would be expected that the curves should rise vertically, with the new curve shape depending upon the fade statistics of the link being scrutinized.

Increasing availability

The most apparent method to increase link availability but perhaps one that can be characterized as a "brute force" approach, is to merely provide more transmitted power. For a given availability, this corresponds to the horizontal displacement between the basic link curve (Fig. 11) and the appropriate crosspole curve (linear or circular). When comparing these power increments to the increments necessary to achieve bandwidth efficiently via more complex modulation schemes, they look rather attractive. However, there are situations, K-band links and satellite-to-ground links, for instance, where those increments are not attractive.

Another approach is to establish space diversity. Both rain and multipath tend to be very position/location sensitive. By establishing an alternate, physically separated transmission path, availability will be significantly enhanced. This, however, requires redundant equipment. Still another approach and perhaps the most elegant, is to include an adaptive polarization correction subsystem in the link equipment. Such subsystems have been built, demonstrated and implemented in both RF and IF ranges. They operate by nulling out the interfering signal in one link with a small sample of the in-line signal in the orthogonally polarized channel. These devices show the greatest potential for bringing the availability of the frequency reuse link up to the level of the basic link in a cost-effective manner.••

References

1. T. O. Mottl, "Dual Polarized Channel Outages During Multipath Fading," *BSTJ*, Vol. 56, No. 5 p. 675, May-June 1977.
2. S. H. Lin, "Impact of Microwave Depolarization During Multipath Fading on Digital Radio Performance," *BSTJ*, Vol. 56, No. 5, p. 645, May-June 1977.
3. J. A. Morrison, and T. S. Chu, "Perturbation Calculations of Rain-Induced Differential Attenuation and Phase Shift at Microwave Frequencies," *BSTJ*, Vol. 52, No. 10, pp. 1907-13, Dec. 1973.
4. R. R. Taur, "Rain Depolarization, Theory and Experiment," *Comsat Technical Review*, Vol. 4, No. 1, (Spring, 1974).
5. Watson and Arbabi, "Rainfall Crosspolarization of Linearly and Circularly Polarized Waves at Microwave Frequencies," *Electronic Letters*, Vol. 8, No. 11, (June, 1972).
6. Semplak, "Simultaneous Measurements of Depolarization of Rain Using Linear and Circular Polarizations at 18 GHz," *BSTJ*, (February, 1974).
7. Barnett, "Degradation of Cross-Polarization Discrimination During Rain and Multipath Fading at 4 GHz," IEEE, 1974, *ICC*, Conference Record, (June 17-19, 1974).
8. RADC Report data 02 (December, 1974).
9. Gill and Byrne, "2 GHz Digital Microwave Cross-Polarization Propagation Measurements," *Telecommunications*, pp. 45-48, (June, 1974).
10. Norbury and White, "Point Rainfall Rate Measurements at Slough, U.K.," Propagation of Radio Waves at Frequencies Above 10 GHz, *IEEE Conference Publication* No. 98.
11. H. E. Bussey, "Microwave Attenuation Statistics Estimated from Rainfall and Water Vapor Statistics," *Proceedings of the IRE*, (July, 1950).
12. Ryde and Ryde, "Attenuation of Centimeter Waves by Rain, Hail, Fog and Cloud," G. E. Co. Ltd., Wembly, England, (5-1945).
13. Medhurst, "Rainfall Attenuation of Centimeter Waves: Comparison of Theory and Measurement," *IEEE Transactions on Antennas and Propagation*, (July, 1965).
14. V. K. Prabhu, "Error Rate Considerations for Coherent Phase-Shift Keyed Systems with Cochannel Interference," *BSTJ*, 48, No. 3 pp. 743-767, (March, 1969).

Oscipliers: K-Band VCOs You Build With Bipolars

Meet the bipolar challenger for Gunn-based VCOs. Besides being faster than a conventional YIG-tuned oscillator, the novel circuit dispenses with post-VCO multipliers, too.

HEART of many electronic countermeasure (ECM) designs is the voltage-controlled oscillator (VCO). Today, the Ku-band VCO most often incorporates a Gunn or Impatt diode. Now the trend is toward ever-faster ECM systems. As a result of this quickening pace, the settling time requirement imposed on the VCO, now in the 20-ns region, excludes all YIG-tuned oscillators from future design considerations. So, perhaps the time is right for countermeasures equipment engineers to dust off their old, quick —but complex—bipolar VCO mockups.

Based on speed alone, the bipolar voltage-controlled oscillator is at least an order of magnitude faster than the YIG-tuned version. When configured in the doubling mode, a bipolar VCO can output 75 mW (preceding isolator/filter stages), tunable over a 30 per cent bandwidth at 9 GHz.

Sort out harmonics

Recent transistor oscillator designs indicate operation in the doubling mode up to X-band (Fig. 1). The doubler is followed by a separate X2 multiplier circuit to output the high Ku-band frequencies. But if you stop and think about it, this approach is wasteful in that it overlooks the fact that harmonics inherently generated in Ku-band due to the reactive nonlinearities within the transistors and varactors may themselves be used in a circuit configuration that bypasses the need for multipliers.

The bipolar transistor doubling circuit is by design a balanced circuit optimized for enhancement of even harmonics, such as the second, and for rejection of the fundamental. If the circuit is designed to optimize the fourth harmonic, for example, a X2 multiplier would not be required. And if the available harmonics are utilized to the fullest advantage, the designer will discover that not even a doubler is required.

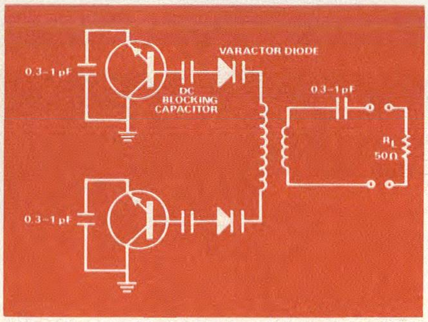

***1. Classic doubler-configured bipolar VCO,** to output frequencies at Ku-band, is followed by a multiplier (shown as 50-ohm load).*

By purposely unbalancing a transistor doubler, the fundamental can be mixed with the second harmonic to enhance the third. This describes an oscillating multiplier incorporating an idler circuit.

The result is a high-speed voltage-controlled oscillator that operates as a varactor-tuned third-harmonic multiplier. The novel VCO outputs 6 to 10 mW over the frequency range of 14 to 17 GHz. Since it incorporates elements of an oscillator and multiplier, the VCO has been nicknamed the "oscplier," and is briefly described.

A replacement for diode sources?

The oscplier is a more complex VCO, incorporating a modification to the basic bipolar doubler. Principally envisioned for use in ECM systems as the contender to the presently-used YIG-tuned Gunn or Impatt-based VCOs and in other high-frequency, high-speed medium power applications, the os-

(continued on p. 66)

Dr. R.G. Winch, Staff Scientist, Teledyne Microwave, 1290 Terra Bella Avenue, Mountain View, CA 94043.

Why is a varactor capable of frequency multiplication?

Both the non-linearities in bipolar transistors and varactors and the step-recovery nature of varactors, having graded junctions, produce the combined effect of generating harmonics with a high efficiency relative to the fundamental. Early theories assumed that the varactor diode was never driven into forward conduction and that the multiplication process was due entirely to the non-linearity reactance of the diodes in the reverse bias condition. The later step-recovery theory states that charge is stored in a diode during its first half cycle of input signal (0 to pi radians) during which time it is in a low-impedance, forward-conduction state. The stored charge is in the form of minority carriers that have been injected from one side of the pn junction to the other. If the minority carrier lifetime of material is designed to be greater than the period of the applied voltage (fundamental frequency) then recombination is inhibited and injected carriers are returned to the point of origin. Transistion time (δ) must be less than the period of the output harmonic $t_T \leq 1/f_H$. As the figure indicates, step recovery is very abrupt; the output signal is rich in harmonics which increase as δ decreases.••

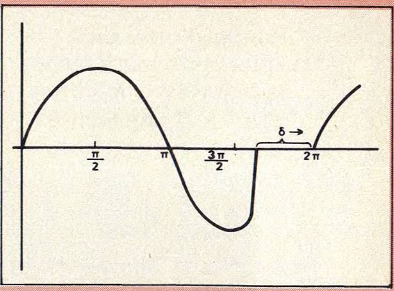

***Harmonic current generated** by step-recovery diode increases as δ decreases. Non-linearities of bipolars and graded-junction varactors generate harmonics.*

ciplier would be a better choice over the YIG-tuned VCO. The YIG device still remains attractive when tuning linearity over a wide bandwith is a prime design goal and speed is secondary.

Each transistor in the osciplier circuit (shown in Fig. 2) generates the fundamental and integral harmonic frequencies even when the resonant circuits are identical and contain lumped capacitors instead of varactors. The fundamental frequency plus harmonics are consequently presented to the varactors that follow. The output matching section improves the selectivity of the desired harmonic and conversely provides a degree of rejection to unwanted harmonics.

The circuit is optimized by a computer-aided nodal analysis. Taking the s-parameters of the transistors, the optimum feedback elements can maximize either their s_{11} or s_{22} values to provide a value greater than unity at the fundamental frequency.

Using the grounded-collector configuration, a tank circuit in series with the base terminal is satisfactory. The resonant circuits primarily consist of the transistor collector/base capacitance, varactor capacitance and bond-wire inductance. The resonant circuits of the two transistors differ since the resonant frequency of one is chosen to be at the fundamental frequency and the other at the doubled frequency.

The varactor diode resistance must be reduced to a minimum since resistive loading of the transistors reduces their s_{22} value and degradation of output power. Diodes exhibiting low punch-through with low breakdown voltage are recommended. This type of diode enables high oscillator mod-

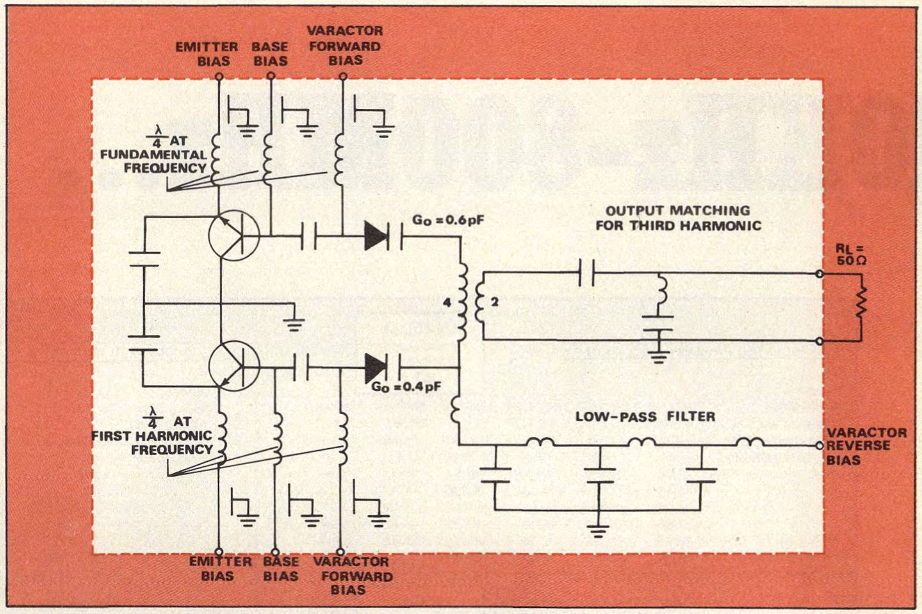

2. Simplified schematic of high-speed VCO, *the "osciplier." Unlike classic bipolar VCO (Fig. 1), osciplier output frequency is already at Ku-band.*

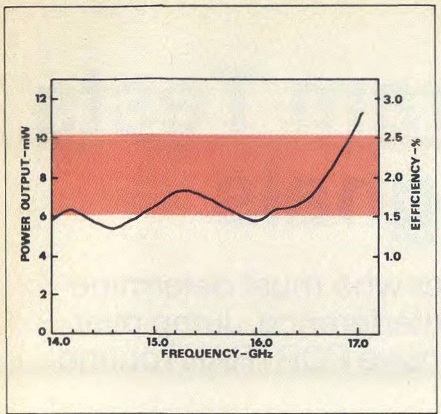

*3. **Osciplier performance curve** indicates a nominal efficiency that varies from 1.5 to 2.5 per cent equivalent output power ranges from 6 to 10 mW. Note that efficiency scale is adjusted to correspond with power output, while tuning voltage scale aligns with frequency.*

ulation sensitivity. Also, the high-Q diodes (> 4000 at 50 MHz) offer power output at higher efficiencies than do standard varactors.

Prototype performs well

The osciplier designed using this technique uses quarter-wave high-impedance bias lines tuned $\lambda/4$ at the fundamental on the top half of the circuit and $\lambda/4$ at the second harmonic on the bottom half. The varactors have capacitance values of 0.6 pF and 0.4 pF at zero volts. The tuning voltage is applied to the diodes through a low-pass filter to minimize the RC time constant that limits tuning speed. The output is matched to 50 ohms and then fed into an isolator followed by a bandpass filter to maintain a high immunity to frequency pulling and rejection of unwanted harmonics. As shown in Fig. 3, 10 V is applied to the varactors to tune the osciplier across the 14 to 17 GHz band. Frequency stability over an ambient of −54 to +75°C is maintained to within 10 MHz by a proportional-controlled heater.

This circuit was prototyped using packaged devices, but their physical size approaches an appreciable portion of a quarter wavelength; resulting parasitics can cause unwanted in-band resonances. Chip devices mounted on ceramic microstrip are the final approach used for production.

Nippon Electric Company, type NEC 219, stripline-packaged bipolar devices and Varian varactors were used in the prototype which employed an air-dielectric, stripline medium. After the prototype was built with packaged devices, the circuit was translated to ceramic microstrip. Output power and efficiency vs. frequency is depicted in Fig. 3. Osciplier bandwidth of 15 per cent was the design goal but wider bandwidth is possible using a wider tuning voltage range and broader-band bias input lines (e. g., low-pass filters). For example, if about 40 V is applied to the varactor for tuning, instead of the indicated 10 V, broader bandwidth can be implemented. However, this produces a frequency-voltage curve that is less linear; the oscillator has a slower "set-on" time.

The ultimate limit to third-harmonic osciplier bandwidth is 39 per cent, a limit imposed by the amplitude of the second harmonic being in band at 10 dB down from the third harmonic in this VCO design.

As indicated in Fig. 3, osciplier efficiency is from 1.5 to 2.5 per cent. However, the power output of the VCO includes a 2.5-dB loss due to the four-port isolator, output bandpass filter and operating temperature of +75°C. By comparison, the efficiency of a fundamental bipolar VCO operating in the same environment over a 20 per cent bandwidth is only about 5 per cent.••

Convolution Program Tests Two Interfering Signals

Convolution is a stumbling block to the engineer who must determine the noise power in an FDM-FM system due to interference. Jump over this mathematical obstacle with this comprehensive FORTRAN routine.

INTERFERENCE resulting from two FM radio signals can be shown to be a function of the convolution of the spectra of the two signals.[1] Presented here is a procedure, implemented in FORTRAN, that convolves two input spectra and presents data that can be used later in a standard interference program. While this is not intended to be a "cookbook" procedure, sufficient explanation is provided to allow a reader to modify the accompanying FORTRAN program to suit individual needs, or if preferred, to re-write the program in some other language such as BASIC or PL1.

This approach takes advantage of the fast Fourier transform (FFT). Methods of performing convolutions using the FFT algorithm were described as early as 1966.[2] More detailed descriptions of convolution using the discrete Fourier transform in general, and the FFT in particular, have appeared more recently.[3] However, most descriptions of FFT convolution gloss over the somewhat mechanical procedures of implementation which, while possibly out of place in theoretical papers, are vital to the individual who must solve a practical problem.

In preparing this program, an effort was made to keep the syntax as near to ANSI-standard FORTRAN as possible (see, "CONVOLVE: A FORTRAN program for the convolution of two microwave spectra"). Particular attention is directed to the call to FFT. No listing for this routine is given, as it is assumed that those interested in pursuing this subject will have some form of FFT already implemented in their computer. Although the version used here is derived from an IBM implementation, other sample routines are publically available[3] in both ALGOL and FORTRAN.

A look behind the program

Two significant factors must be considered when performing a convolution of input spectra. First, the input spectra must share a common sampling interval equal to, or less than, the smallest interval present in either input spectrum. Second, in order to satisfy the requirements of the FFT routine, samples must be equal to some power of two that is large enough to contain the spectrum with the largest bandwidth. While seemingly trite and obvious, these two points are essential if proper results are to be obtained. Also, these two criteria establish a limit on the amount of detail that can be processed and still remain within the memory limits to the computer used for the calculation.

A common sampling interval can best be obtained by re-sampling both input spectra at an interval, I, equal to the smallest interval present in either of the input spectra. The number of intervals, N, is then computed as:

N = smallest integer $\geq BW/I$

where I = sampling interval

BW = bandwidth of wider input spectra

Prior to re-sampling the spectra, the size of the array required for the FFT routine must be determined. Allowance must be made for both positive and negative frequency samples, and sufficient space must be reserved for the imaginary terms that will be produced by the FFT. The required array size, N_o, for each spectrum is:

$$N_o = 2^{(M+1)}$$

where M is the smallest integer $\geq \dfrac{\log 2N}{\log 2}$

Each input spectrum is them sampled at the new intervals using linear interpolation to find values not present in the original spectrum array. These new data points are stored in new arrays in a particular fashion. Data is stored in the normal fashion at one end of the array, and as a mirror image at the other end, in a form that indicates a complex number with a zero-value imaginary term. This is necessary since the FFT must see positive frequencies at the low end of the array and negative frequencies at the upper end.

A sample problem is shown in Fig. 1 to illustrate the method. While the example chosen is perhaps an extreme case, it illustrates interference between a single-channel FM radio and a 1,200-channel FDM multiplex system. This situation might be encountered with a single-carrier-per-channel (SCPC) earth station interfering with a common carrier microwave radio system.

The arrays are now transformed by the FFT routine and the results multiplied, term by term, as complex numbers.

If $A_i = \mathrm{Re}(A_i) + j\,\mathrm{Im}(A_i)$

and $B_i = \mathrm{Re}(B_i) + j\,\mathrm{Im}(B_i)$

then $C_i = A_i \cdot B_i = \{\mathrm{Re}(A_i) + j\mathrm{Im}(A_i)\} \cdot \{\mathrm{Re}(B_i) + j\mathrm{Im}(B_i)\} = \mathrm{Re}(C_i) + j\mathrm{Im}(C_i)$

where $\mathrm{Re}(C_i) = \mathrm{Re}(A_i) \cdot \mathrm{Re}(B_i) - \mathrm{Im}(A_i) \cdot \mathrm{Im}(B_i)$

$\mathrm{Im}(C_i) = \mathrm{Re}(A_i) \cdot \mathrm{Im}(B_i) + \mathrm{Re}(B_i) \cdot \mathrm{Im}(A_i)$

The inverse transform is then formed of this product array (C_i) yielding the convolution of the sidebands of the two input spectra. But keep in mind that this is not the total answer but only one component of it.[4] The convolution of two spectra that contain residual carriers consists of four components which must be summed to form the total convolution function $C(\beta)$.

$$C(\beta) = C_A(\beta) + C_B(\beta) + C_C(\beta) + C_D(\beta)$$

(continued on p. 70)

Fred E. LaPlante, Senior Engineer, RCA Alaska Communications, Inc., 629 E Street, Anchorage, AK 99501.

CONVOLVE: A FORTRAN program for the convolution of two microwave spectra

```
C - - - - - - - - - - - - - - - - - - - - - - - - - - - - - - - - - - - -
C
      SUBROUTINE INTCONV(F1,A1,N1,C1DB,F2,A2,N2,C2DB,FOUT,AOUT,N,WCC)
C
C - - - - - - - - - - - - - - - - - - - - - - - - - - - - - - - - - - - -
C
C     THIS PROGRAM WILL COMPUTE THE CONVOLUTION FUNCTION FOR TWO
C     MICROWAVE SPECTRA. THE MAXIMUM NUMBER OF POINTS WHICH CAN BE
C     HANDLED IS 512. THIS REPRESENTS, FOR EXAMPLE, A BANDWIDTH
C     OF 20mHz AND A MINIMUM FREQUENCY INCREMENT OF 40 kHz.
C
C     THIS PROGRAM USES CONVOLUTIONAL TECHNIQUES DESCRIBED IN FCC
C     REPORT FCC/OCE RS75-04 DATED APRIL 1975.
C
C            INPUT#1              INPUT#2              OUTPUT
C            =======              =======              ======
C          F1 - FREQUENCIES     F2 - FREQUENCIES     FOUT - FREQUENCIES
C          A1 - AMPLITUDES      A2 - AMPLITUDES      AOUT - AMPLITUDES
C          N1 - ARRAY SIZE      N2 - ARRAY SIZE      N - ARRAY SIZE
C          C1DB - CARRIER       C2DB - CARRIER       WCC - CARRIER SPIKE
C
C
C
      REAL F1(512),A1(512),F2(512),A2(512),F(2048),X(2048),H(2048),W(2048)
     &,WCSIG(2048),WCINT(2048),FOUT(512),AOUT(512),ARAY1(2048),ARAY2(2048)
     &,ARAY3(2048),ARAY4(2048),ARAY5(2048),ARAY6(2048)
C
      STRING TNAM,RNAM,INAM,DUMM
C
      EQUIVALENCE(ARAY1,WCSIG),(ARAY2,WCINT),(ARAY3,W),(ARAY4,FREQ),
     &(ARAY5,X),(ARAY6,H),(WTOT,W)
C
      COMMON /ARAYS/ARAY1,ARAY2,ARAY3,ARAY4,ARAY5,ARAY6
C
C******INITIALIZATION
C
      DATA ADJ/150./
      DO 1430 INIT=1,2048
      ARAY1(INIT)=0.
      ARAY2(INIT)=0.
      ARAY3(INIT)=0.
      ARAY4(INIT)=0.
      ARAY5(INIT)=0.
 1430 ARAY6(INIT)=0.
C
C*******GET INPUT SPECTRA FROM FILES AND SCALE TO MANAGEABLE LEVELS.
C
C   -  SIGNAL SPECTRUM
      C1PWR=10.0**((C1DB+ADJ)/10.0)
      DO 1500 J=1,N1
 1500 A1(J)=A1(J)+ADJ
C
C   -  INTERFERENCE SPECTRUM
      C2PWR=10.0**((C2DB+ADJ)/10.0)
      DO 1550 J=1,N2
 1550 A2(J)=A2(J)+ADJ
C
C******SELECT SMALLEST FREQ INCREMENT
C
      FINCR1=ABS(F1(2)-F1(1))
      FINCR2=ABS(F2(2)-F1(1))
      FINCR=FINCR1
      IF(FINCR2.LT.FINCR1)FINCR=FINCR2
C
C******SELECT LARGEST BANDWIDTH.
C
      BW1=(F1(N1)-F1(1))
      BW2=(F2(N2)-F2(1))
      BW=BW1
      IF(BW2.GT.BW1)BW=BW2
C
C******ESTABLISH COMMON SAMPLING POINTS AS "(LARGEST BW)/(SMALLEST INCR)".
C
      N=CEIL(BW/FINCR)
C
C   -  DETERMINE ARRAY SIZE FOR TRANSFORMATIONS
C      ARRAY SIZE IS DETERMINED AS BEING THE SMALLEST POWER OF TWO THAT
C      WILL PROVIDE ROOM FOR BOTH A POSITIVE AND NEGATIVE FREQUENCY
C      FUNCTION AS WELL AS ALLOWING SPACE FOR THE IMMAGINARY COMPONENT
C
      M=CEIL(ALOG10(2*N)/ALOG10(2.0))+1
      NO=2**M
      NH=NO/2
      NH1=NH-2
C
C   -  BUILD FREQUENCY ARRAY WITH PROPER SAMPLING INTERVAL.
      DO 1870 I=1,NH1,2
 1870 F(I)=FINCR*(I-1)/2
C
C******BUILD WORKING ARRAYS AT NEW SAMPLE POINTS.
C
      CALL SAMPLE(F1,A1,N1,F,X,NH1)
      CALL SAMPLE(F2,A2,N2,F,H,NH1)
C
C******COMPLETE SPECTRUM BY ADDING NEG FREQ VALUES AND SHIFTING.
C
C      ALSO CONVERT dB TO POWER RATIO.
      DO 2060 I=1,NH,2
C
C   -  DESIRED SIGNAL.
      X(I)=10.**(X(I)/10.)
      X(NO-I)=X(I)
C
C   -  INTERFERENCE SIGNAL.
      H(I)= 10.**(H(I)/10.)
      H(NO-I)=H(I)
 2060 CONTINUE
C
C******SAVE INPUT SPECTRUM ARRAYS FOR LATER PROCESSING
C
      DO 2120 IMOV=1,NO
      WCSIG(IMOV)=X(IMOV)
 2120 WCINT(IMOV)=H(IMOV)
C
C******CONVOLUTE INPUT SPECTRA.
C
C   -  TRANSFORM INPUT SPECTRA
C
      CALL FFT(X,M,1,ERR,$2670)
      CALL FFT(H,M,1,ERR,$2670)
C
C   -  FORM PRODUCT OF TRANSFORMED ARRAYS.
      DO 2240 I=1,NO,2
      W(I)=X(I)*H(I)-X(I+1)*H(I+1)
 2240 W(I+1)=X(I)*H(I+1)+H(I)*X(I+1)
C
C   -  GET INVERSE TRANSFORM OF PRODUCT ARRAY.
      CALL FFT(W,M,3,ERR,$2670)
C
C******DEVELOP CONVOLUTION FUNCTION FOR EACH CARRIER TO SPECTRUM CASE.
C
      DO 2380 I=1,NO,2
C
C   -  FOR INT CXR TO SIG SPECTRUM.
      WCSIG(I)=C2PWR*WCSIG(I)
C
C   -  FOR SIG CXR TO INT SPECTRUM.
      WCINT(I)=C1PWR*WCINT(I)
 2380 CONTINUE
C
C******DEVELOP TOTAL CONVOLUTION FUNCTION
C
      DO 2440 I=1,NO,2
      W(I)=2.*(W(I)+(C2PWR*WCSIG(I))+(C1PWR*WCINT(I)))
 2440 CONTINUE
C
C******COMPUTE SCALE CONVERSION FACTOR
C
      ADJPWR=10.0**(ADJ/10.)
      CORPWR=ADJPWR*ADJPWR
      CORDB=10.0*ALOG10(CORPWR)
C
C******PRODUCE FINAL UN-SCALED OUTPUT
C
C
      WCC=C1DB+C2DB
      DO 2600 I=1,NH1,2
      W(I)=10.*ALOG10(W(I))-CORDB
      IJ=IJ+1
      FOUT(IJ)=F(I)
 2600 AOUT(IJ)=W(I)
C
C******ROUTINE COMPLETE, QUIT
C
      RETURN
C
C
 2670 PRINT,"FFT ERROR",ERR
      STOP
      END
C
C - - - - - - - - - - - - - - - - - - - - - - - - - - - - - - - - - - - -
C
      SUBROUTINE SAMPLE(INX,INY,NIN,OUTX,OUTY,NOUT)
C
C - - - - - - - - - - - - - - - - - - - - - - - - - - - - - - - - - - - -
C
C******SAMPLE f(INX,INY) INTO g(OUTX,OUTY)
C
      REAL INX(NIN),INY(NIN),OUTX(NOUT),OUTY(NOUT)
C
      IA=1
      DO 2930 IB=1,NOUT,2
C
      IF(OUTX(IB).GT.INX(NIN)*1.01)GO TO 2910
      IF(OUTX(IB).LT.INX(1)*0.99)GO TO 2910
      IF(OUTX(IB).GT.INX(IA+1))IA=IA+1
C
      OUTY(IB)=RLINT(INY(IA),INY(IA+1),INX(IA),OUTX(IB),INX(IA+1))
      GO TO 2930
C
 2910 OUTY(IB)=0.0
C
 2930 CONTINUE
C
      RETURN
      END
C
C - - - - - - - - - - - - - - - - - - - - - - - - - - - - - - - - - - - -
C
      FUNCTION RLINT(X1,X3,Y1,Y2,Y3)
C
C - - - - - - - - - - - - - - - - - - - - - - - - - - - - - - - - - - - -
C
C******LINEAR INTERPOLATION BETWEEN X1 AND X3
C
      DIFFX=X3-X1
      DIFFY3=Y3-Y1
      DIFFY2=Y2-Y1
      IF(DIFFY3.EQ.0.)GO TO 3180
C
      RATIOY=DIFFY2/DIFFY3
C
      ADJX=DIFFX*RATIOY
C
      RLINT=X1+ADJX
C
      RETURN
 3180 RLINT=X1
      RETURN
      END
C
C - - - - - - - - - - - - - - - - - - - - - - - - - - - - - - - - - - - -
C
C     FUNCTION "CEIL(X)" RETURNS THAT INTEGER >= X
C
C
C     SUBROUTINE "FFT(ARRAY,SIZE,MODE,ERCODE,$ERADDRESS)"
C         ACCEPTS AS INPUTS :
C                  ARRAY - ARRAY CONTIAINING THE DATA TO BE TRANSFORMED
C                  SIZE  - DIMENSION OF THE ARRAY (MUST BE AN INTEGER
C                          POWER OF TWO)
C                  MODE  - FUNCTION TO BE PERFORMED:
C                                 0 - REAL ANALYSIS
C                                 1 - COMPLEX ANALYSIS
C                                 2 - REAL SYNTHESIS
C                                 3 - COMPLEX SYNTHESIS
C                  $ERADDRESS - ERROR RETURN
C        RETURNS AS OUTPUTS :
C                  ARRAY - THE TRANSFORMED RESULTS ARE HERE
C                  ERCODE - ERROR CODE FOR USE AT ERADDRESS
C
```

where $C_A(\beta)$ = convolution of the two residual carriers.
$C_B(\beta)$ = convolution of the desired signal residual carrier with the interfering sideband spectrum.
$C_C(\beta)$ = convolution of the interfering signal residual carrier with the desired sideband spectrum.
$C_D(\beta)$ = convolution of the two sideband spectra excluding the residual carriers.

The latter term, $C_D(\beta)$, is the one component produced thus far. $C_A(\beta)$ is simply the product of the two carrier amplitudes and is not included in the output function because the presence of $C_A(\beta)$ would distort later interference computations which involve interpolation of the magnitude of adjacent data points. Instead, the $C_A(\beta)$ term should be added into later computations when required, but after performing any interpolations in the vicinity of the carrier.

Terms $C_B(\beta)$ and $C_C(\beta)$ are products of a copy of each the original spectra multiplied by the other spectra's carrier amplitude.

One final matter must be considered, depending on the range of real number sizes that the user's computer will handle. As with most modern-day computers, the author's machine is limited to numbers between 10^{-38} and 10^{+38}. Thus, due to the small size of the power levels involved after conversion from decibels to watts, all inputs are scaled by adding a factor K (K = 150 dB). At the end of the routine, the answer is restored by subtracting a compensating factor of 2K. Each reader will have to select a value of K suit to individual situations.

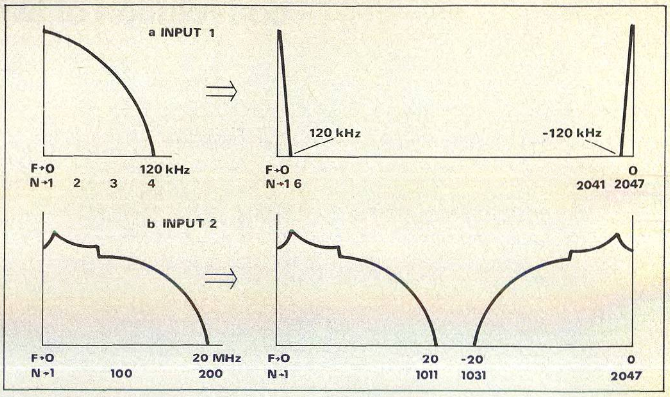

1. Data must be stored normally and as a mirror image. *This case illustrates interference between a single-channel FM radio (a) and a 1,200-channel FDM multiplex system (b).*

How well does this approach work? The FORTRAN program given here will provide answers that agree very closely with those obtained by a "graphical" technique[4] which, while intuitively satisfying, is much more expensive to run. ••

Acknowledgement

The considerable patience and assistance of George Sharp of the FCC is gratefully acknowledged.

References

1. Pontano, Fuenzalida and Chitre, "Interference Into Angle-Modulated Systems Carrying Multi-channel Telephony Signals," *IEEE Transactions on Communications*, p. 714, (June, 1973).
2. J. G. Stockham, "High Speed Convolution and Correlation," *Proceedings-Spring Joint Computer Conference*, p. 229, (1966).
3. Brigham, *The Fast Fourier Transform*, Prentice-Hall, New York, (1974).
4. Das and Sharp, "Convolution Method of Interference Calculation," *Federal Communications Commission Report FCC/OCE RS75-04*, (April, 1975).

DECEMBER
1977

MICROWAVES

laser technology

PASSIVE COMPONENTS

Dielectric Resonators Add Q To MICs
Understand Intermod In Mixer Diodes
Correct For Microstrip Line Thickness
Fortran Programs Do Smith-Chart Chores
Analyze Unusual Substrates By Calculator

Also:
New R & D Raises Impatt Efficiency • Balance Amplifier Power And Gain

MICROWAVES

December 1977
Vol. 16 No. 12

news

9 New impatt R&D drives up efficiency; processing key to improved specs
10 A more ideal GaAs mixer diode
14 Temperature-stable dielectric resonators replace expensive invar, boost Q in MICs
18 Glowing GaAs FET sheds light on new internal field structure
23 Industry
27 Washington
134 International
138 Meetings
142 R&D
144 For Your Personal Interest. . .

editorial

148 European customers: Eager, but somewhat disappointed

technical

Passive Components

150 **Dielectric Resonators Add Q To MIC Filters.** Michael Dydyk, of Motorola, Inc., discusses the need for small, high-Q resonators in filter designs—a need created by microwave integrated circuits. Dielectric disk resonators meet that need, he says, but traditional filter design must be modified.

162 **Consider A Single Diode To Study Mixer Intermod.** Daniel L. Cheadle, Watkins-Johnson Company, profiles the diode's conduction cycle as the key to analyzing third-order distortion. He offers a computer program that plows through sixth-order equations to find the best suppression method.

172 **Nine FORTRAN Subroutines Do Smith-Chart Chores.** Wilfred J. Remillard, a Professor at Northeastern University, supplies nine subroutines that analyze lossy or lossless transmission lines, transform coordinate systems, do Smith-chart rotations, and describe stub matching circuits.

178 **Easy-To-Plot Graphs Show Power-Gain Tradeoffs.** David Rosemarin and Moty Chorev describe a bilateral design method to take the confusion out of low power amplifier efficiency analysis.

184 **Take The Guesswork Out Of Thick Microstrip K.** Kurt P. Schwan, a staff member at the MIT Lincoln Laboratory, replaces guesswork involved when calculating the effective dielectric constant of thick microstrip with a simple graph.

186 **HP-65 Program Computes Microstrip Impedance.** Fred E. Gardiol, Professor, and J. F. Zürcher, Ecole Polytechnique Fédérale de Lausanne, tell how to use a calculator to describe, accurately, a microstrip line on any substrate. Their program displays effective dielectric constant, then computes impedance.

departments

188 Annual Index
190 Author's Guide
193 Application Notes
195 Product Feature
Ultra-fast RF power meter eases multi-detector power struggle
196 New Products
208 New Literature
211 Advertisers' Index
212 Product Index

About the cover: Improved dielectric resonators are casting a new light on filter and oscillator design. For more details on how to use these versatile ceramic disks, see stories on pages 14 and 150. Photo courtesy of Bell Laboratories, Murray Hill, NJ.

coming next month: Engineering career survey

We've asked readers to comment on their salary, education, career aims, job satisfaction, and general attitudes toward a career in microwave engineering. Next month, we'll compile their responses in a probing analysis of what it's like to be a microwave engineer in 1978. Find out where you stand among your colleagues . . . don't miss this special report.

Also included are articles on high-power amplifier design, a designer's guide to stripline circuits, news coverage of December's International Electron Devices Meeting, and a look at the revitalized concept of automobile radar.

Publisher
Howard Bierman

Editor
Stacy V. Bearse

Associate Editors
Robert Wollins
Robert E. Herbaugh

Washington Editor
Paul Harris
Snyder Associates
1050 Potomac St. N.W.
Washington, DC 20007
(202) 965-3700

Editorial Assistant
Gail Murphy

Production Editor
Jamie Matusow

Art Director
Robert Meehan

Art Illustrator
Janice Tapp

Production
Dollie S. Viebig, Mgr.
Anne Molfetas

Circulation
Barbara Freundlich, Dir.

Directory Coordinator
Janice Tapp

Editorial Office
50 Essex St.,
Rochelle Park, NJ 07662
Phone (201) 843-0550
TWX 710-990-5071

A Hayden Publication
James S. Mulholland, Jr., President

MICROWAVES is sent free to individuals actively engaged in microwave work. Prices for non-qualified subscribers:

	1 Yr.	2 Yr.	3 Yr.	Single Copy
U.S.	$25	$40	$ 60	$3.00
Foreign	$40	$70	$100	$4.00

Additional Product Data Directory reference issue, $15.00 each (U.S), $27.00, (Foreign). POSTMASTER, please send Form 3579 to Fulfillment Manager, MicroWaves, P.O. Box 13801, Philadelphia, PA. 19101.

Back Issues of MicroWaves are available on microfilm, microfiche, 16mm or 35mm roll film. They can be ordered from Xerox University Microfilms, 300 North Zeeb Road, Ann Arbor, MI 48106. For immediate information, call (313) 761-4700.

Hayden Publishing Co., Inc., James S. Mulholland, President, printed at Brown Printing Co., Inc., Waseca, MN.

Dielectric Resonators Add Q To MIC Filters

Microwave integrated circuits have created a need for small, high-Q resonators in filter designs. Dielectric disk resonators meet that need, but traditional filter design must be modified in several ways.

ALTHOUGH much is known about the behavior of dielectric resonators in free space, [1,2,3,4] and in conducting enclosures, [5,6] applying these studies to the design of dielectric resonators for microstrip is not a straightforward task. The close proximity of substrates and ground planes to the resonator significantly shifts the resonator's frequency and Q.

But, it is possible to design MIC filters using high-Q dielectric resonators by carefully examining all the resonator effects—frequency, unloaded Q, spurious response, etc., —and combining these results in a set of filter design equations.

An examination of the filter in Fig. 1 reveals a metal waveguide operating below cutoff for all modes in the frequency band of interest. The substrate at the bottom of the guide supports the resonators and the microstrip circuit, to which the end resonators are coupled. At resonance, the resonators excite the normal modes of a partially loaded waveguide, and coupling between resonators is achieved via the evanescent fields of these modes. Since the guide is at cutoff, the modes excited by the resonators vanish at some distance beyond the resonators, and the guide may be opened to permit connection to other microstrip components on the same substrate.

Although the resonators partly extend into the coupling region between the resonators, the coupling modes still appear like those of a uniform dielectric loaded waveguide as shown in Fig. 1. These modes are separated into orthogonal sets, termed LSE and LSM.[7]

For the filter examined here, only the LSE modes are excited by the resonator fields, and contribute to the coupling. The LSM modes will, however, be excited by the open-circuited microstrip transmission line used to couple to the resonators. It is essential that these modes are also evanescent; otherwise, resonance effects will occur in the filter box, causing unwanted spurious passbands.

Zero-in on resonant frequency

The design of a dielectric resonator, like the design of a metal cavity, depends on its natural resonant frequencies. Since exact solutions of dielectric resonators with shapes other than spheres or doughnuts cannot be rigorously computed, approximate techniques are necessary to solve the problem.

Both H and E resonant modes can be excited in a dielectric resonator. The H mode has a large normal magnetic field component at the boundary surfaces, while the E mode contains no predominant normal magnetic field component at the surfaces.

Dielectric resonator resonant frequencies are usually computed by assuming that the dielectric resonator is placed in unbounded space. In real conditions, however, dielectric resonators are placed in microwave structures, like waveguides, striplines, or microstrip transmission lines. Because these microwave structures are close to the resonators, they disturb the resonator's external fields, and alter their resonant frequency.

Consider cylindrical disk resonators, located as shown in Fig. 1. To determine the resonant frequency, assume that the resonator is housed in a contiguous magnetic-wall, cylindrical waveguide below cutoff. This waveguide is terminated by two conducting surfaces, representing the ground plane and the top cover of a microstrip transmission line, with a dielectric between the resonator and the ground plane. In the dielectric region, the guide is above cutoff, and a standing wave exists at resonance. In the air, and in the substrate region, the fields decay since this area appears as a waveguide below cutoff.

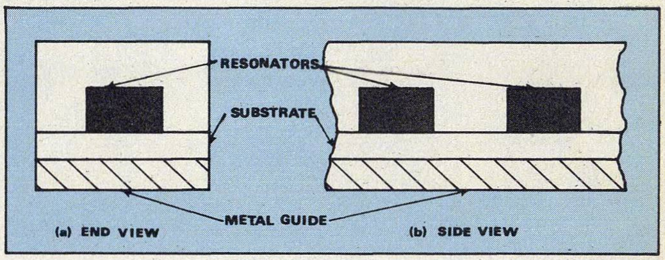

*1. **Basic filter geometry** includes dielectric resonators located on an MIC substrate. The waveguide circuit is below cutoff at the incident frequency.*

A complete solution for the resonant frequency of the dielectric resonator is obtained through the transverse resonance procedure. Carrying out the details of the boundary value problem, it becomes clear that the procedures even in the transverse direction are similar to those in any transmission line problem. The solutions[8] in the transverse directions consist of standing waves, with the transverse transmission line at resonance. Or, expressed mathematically:

$$Z_{1(x)} = \overrightarrow{Z} + \overleftarrow{Z} = 0 \qquad (1)$$

where the $\overrightarrow{Z}$ and $\overleftarrow{Z}$ are the impedances looking to the right and left of an arbitrary reference plane.

When this procedure is applied to the MIC dielectric resonator, with an equivalent circuit as shown in Fig. 2,

Michael Dydyk, Principal Staff Engineer, Motorola, Inc., Government Electronics Division, 8201 E. McDowell Road, P.O. Box 1417, Scottsdale, AZ 85252.

Table 1: MIC dielectric resonator specifications

Resonant frequency	10.0 GHz
Resonator material	Barium tetratitanate
Relative dielectric constant of resonator material	38.0
Substrate material	Teflon fiberglass
Relative dielectric constant of substrate material	2.54
Thickness of substrate	31 mils
Thickness of resonator (from Eq. 2)	70 mils
Thickness of air above resonator	100 mils
Radius of dielectric resonator	107.5 mils

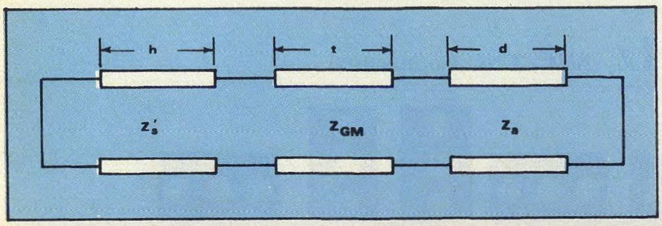

*2. **Resonant frequency calculations** are based on the waveguide filter equivalent circuit. The frequency is shifted by the presence of the dielectric resonators, distributed along the MIC substrate.*

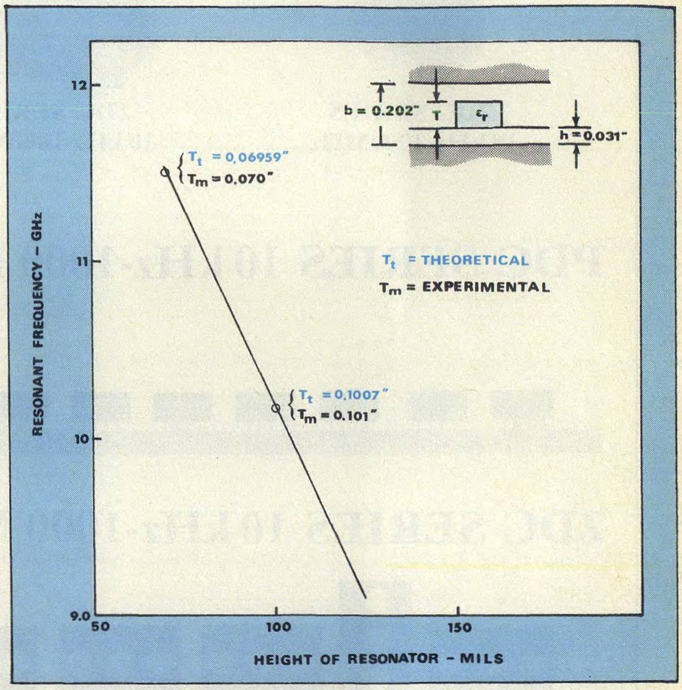

*3. **Adding the decaying field** in and around the cylindrical surface of the resonators to the resonant frequency calculation improves the agreement between experimental and theoretical results greatly.*

the following transcendental equation results:

$$\tan \gamma_i t = \frac{\gamma_i\,(\gamma_{oa} \tanh \gamma_{os} h + \gamma_{os} \tanh \gamma_{oa} d)}{\gamma_i^2(\tanh \gamma_{os} h)(\tanh \gamma_{oa} d) - \gamma_{os}\,\gamma_{oa}} \tag{2}$$

Equation 2 determines the resonant frequency when ϵ_s, ϵ_r, R, h, d and t are known, or the thickness of the resonator when the frequency is known. The radius, R, of the dielectric resonator must be selected a priori. The best way to do this is to find the radii which cause the following conditions when the resonator is no longer resonant:

$$\gamma_i = \gamma_{os} = 0 \tag{3}$$

$$R = 1.2025 \;\frac{c}{\omega}\left[\frac{1}{\sqrt{\epsilon_r}} + \frac{1}{\sqrt{\epsilon_s}}\right] \tag{4}$$

These theoretical results were verified by designing, fabricating, and evaluating an MIC dielectric resonator with specifications detailed in Table 1. The measured resonant frequency of this resonator is 11.5 GHz—15 per cent higher than the desired result. To improve this, it is necessary to include the decaying fields which exist around the cylindrical surface.

This analysis starts by assuming the existence of an external magnetic field, and then, using Maxwell's equations and boundary conditions arrives at the following result:

$$\beta_{ci}R \left[\frac{J_o(\beta ciR)}{J_1(\beta ciR)}\right] = -\alpha_{co}R \left[\frac{K_o(\alpha_{co}R)}{K_1(\alpha_{co}R)}\right] \tag{5}$$

The objective here is to find the effect of the decaying field on the roots of the Bessel Function, specifically $\beta_{ci}R$. For a given frequency and resonator radius, this is accomplished with Eq. 5 and the definitions of β_{ci} and α_{co}. The solution is completed when the ratio (2.405/R), appearing in all the definitions dealing with Eq. 2, is replaced with the newly found β_{ci}.

With this modification, the theoretical and experimental comparison is quite good, as shown in Fig. 3.

Solving for unloaded Q

The unloaded Q of any resonant structure is defined as 2π times the ratio of the maximum stored energy to the

(continued on p. 154)

energy lost in one cycle. For the filter examined here, energy storage takes place partly in the dielectric resonator, partially in the substrate, and partially in the air above the resonator. Similarly, the energy losses are due to the losses in the end walls, and the dielectric losses in the dielectric resonator and substrate. Unloaded Q is defined as:

$$Q_u = \frac{2\omega\,(W_r + W_s + W_a)}{P_{ac} + P_{sc} + P_r + P_s} \qquad (6)$$

The stored energy can be determined from:

$$W_i = \frac{\epsilon_o}{2} \iiint_v \epsilon(z)\,|E|^2\, dv \qquad (7)$$

The dielectric losses can be determined from:

$$P_i = \epsilon_o \omega \iiint \epsilon''(z)\,|E|^2 \quad dv \qquad (8)$$

Reducing the algebra:

$$\frac{W_i}{P_i} = \left[\frac{1}{2\omega \tan \delta(z)} \right] \qquad (9)$$

Equation 9 indicates that only W_i or P_i must be calculated. The energy lost in the conductors is determined from:

$$P_{ic} = R \iint |H_t|^2\, ds \qquad (10)$$

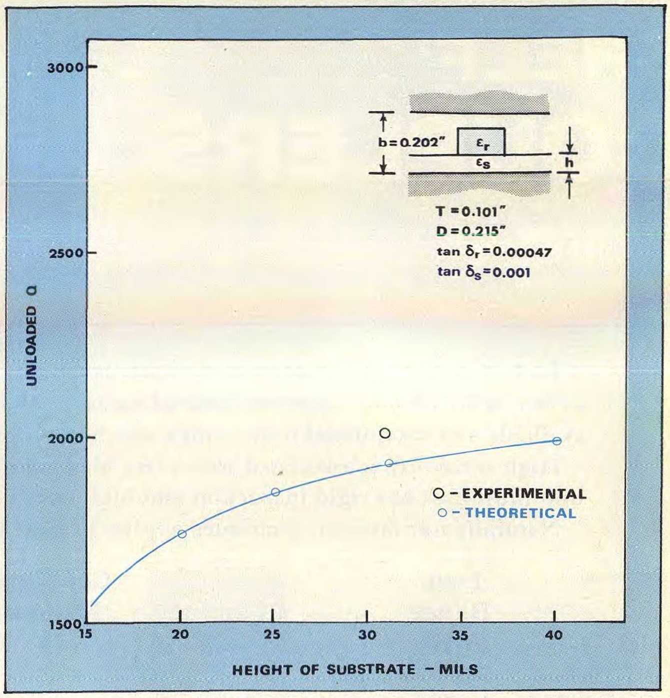

***4. Unloaded Q falls by one quarter** as substrate height falls by a factor of two. Notice that one experimental reading is in fair agreement with the theoretical result.*

List of symbols

ds	incremental surface area
dV	incremental volume
$E_{\theta r}$	electric field in the resonator
$E_{\theta s}$	electric field in the substrate
$E_{\theta a}$	electric field in the air above the resonator
A,B,C	arbitrary constants
ρ_{oi}	root of Bessel Function
r	the radial variable in cylindrical coordinates
$A\ell$	conducting loop areas
I_i	current in loop one
$\epsilon''(z)$	effective imaginary part of the permittivity representing dielectric loss, which takes the values ϵ_A'', ϵ_s''
tan $\delta(z)$	dielectric loss tangent, which takes the values $\tan\delta_r$, $\tan\delta_s$

L_m	mutual inductance between loops
H_2	field value at the location of conducting loop two
e_p	transverse components of electric field
e_{zp}	longitudinal components of electric field
a_p	amplitude factors of waves
α_{mn}	attenuation constant of waveguide
ψ_1	wave potential in the substrate
R	dielectric resonator radius
ω	frequency in radians
ϵs	relative dielectric constant of the substrate material
t	dielectric resonator thickness
h	substrate thickness
d	thickness of the air region above the dielectric resonator

C	speed of light
ϵ_r	relative dielectric constant of tl resonator material
P_{ac}	energy losses due to the finite co ductivity of the top cover
P_{sc}	energy losses due to the finite co ductivity of the ground plane
P_r	dielectric losses in the resonator
P_s	dielectric losses in the substrate
$\epsilon(z)$	dielectric constant, which takes tl values ϵ_r, ϵ_s and 1, corresponding the three different media
R	surface resistance of the grour plane and top cover
H_t	magnetic field tangential to the conductor surface
ψ_2	wave potential in the air region
ω	fractional bandwidth
μ_o	permeability of free space

To carry out the various integrations in Eqs. 7, 8, and 10, it is necessary to assume the existence of electric fields of the following forms, in the three different medias:

$$E_{\theta r} = A\, J_1\left(\frac{\rho_{01} r}{R}\right) \cos \gamma_1 Z \qquad (11)$$

$$E_{\theta s} = B\, J_1\left(\frac{\rho_{01} r}{R}\right) \sinh\left[\gamma_{os}\left(h + \frac{t}{2} + Z\right)\right] \qquad (12)$$

$$E_{\theta a} = C\, J_1\left(\frac{\rho_{01} r}{R}\right) \sinh\left[\gamma_{oa}\left(d + \frac{t}{2} - Z\right)\right] \qquad (13)$$

The constants A, B, and C are evaluated by matching boundary conditions and the magnetic fields required by Eq. 10 using Maxwell's equations.

The final result for the unloaded Q is:

$$Qu = \frac{\epsilon_r\left[t + \frac{\sin\gamma_1 t}{\gamma_1}\right] + \epsilon_s\left[\frac{\cos(\gamma_1 t/2)}{\sinh \gamma_{os} h}\right]^2\left[\frac{\sinh 2\gamma_{os} h - h}{2\gamma_{os}}\right] + \left[\frac{\cos(\gamma_1 t/2)}{\sinh\gamma_{oa} d}\right]^2\left[\frac{\sinh 2\gamma_{oa} d}{2\gamma_{oa}} - d\right]}{\epsilon_r \tan\delta_1\left[t + \frac{\sin\gamma_1 t}{\gamma_1}\right] + \epsilon_s \tan\delta_s\left[\frac{\cos(\gamma_1 t/2)}{\sinh\gamma_{os} d}\right]^2\left[\frac{\sinh 2\gamma_{os} h - h}{2\gamma_{os}}\right] + \frac{2R}{\omega\epsilon_o}\left[\frac{\cos(\gamma_1 t/2)}{\omega\mu_o}\right]^2\left[\left[\frac{\gamma_{os}}{\sinh\gamma_{os} h}\right]^2 + \left[\frac{\gamma_{oa}}{\sinh\gamma_{oa} d}\right]^2\right]} \qquad (14)$$

Equation 14 can be used to determine the unloaded Q of the MIC dielectric resonator, and to estimate the effect of the substrate height on the unloaded Q. Figure 4 indicates that the unloaded Q decreases by 25 percent for a substrate height reduction by a factor of two. Also shown in Figure 4 is the experimental measurement of unloaded Q.

Determine external Q by evaluating coupling

A dielectric resonator placed in the field of a propagating MIC transmission line will be magnetically coupled to the line. For most effective coupling, the magnetic-dipole axis of the resonator should be in the direction of the H field of the transmission line as shown in Fig. 5. The loaded, or external, Q of the resonator, therefore, must be known to insure the most efficient coupling takes place.

- $J_n(\beta_{ci}, R)$ Bessel Function of the first kind, order n
- $H_n(\alpha_{co}, R)$ Hankel Function of the first kind, order n
- $K_n(\alpha_{co}, R)$ Modified Bessel Function of the first kind, order n
- α_{co} $\bullet\gamma_{co}$
- W_r stored energy in the resonator
- W_s stored energy in the substrate
- W_a stored energy in the air above the resonator
- S center to center spacing between resonators
- a,b waveguide cross-sectional dimensions
- ℓ_c waveguide cavity length
- n,P denote the number of variations of the fields in the x and z direction respectively

- $\beta_{ci} = \sqrt{\left(\frac{\omega}{c}\right)^2 \epsilon_r - \beta^2}$ propagation constant in the transverse direction inside the resonator
- $\alpha_{co} = \sqrt{\beta^2 - \left(\frac{\omega}{c}\right)^2}$ propagation constant in the transverse direction outside the resonator
- $K_{y1} = \sqrt{\left(\frac{\omega}{c}\right)^2 \epsilon_s - KZ^2 - \left(\frac{\eta\pi}{a}\right)^2}$ propagation constant in the x direction in the substrate
- $K_{y2} = \sqrt{\left(\frac{\omega}{c}\right)^2 - KZ^2 - \left(\frac{\eta\pi}{a}\right)^2}$ propagation constant in the x direction in the air region
- $g_{J(J'=0,1,2\ldots)}$ low pass prototype elements
- $\gamma_1 = \sqrt{\left(\frac{\omega}{c}\right)^2 \epsilon_r - \left(\frac{2.405}{R}\right)^2}$ phase constant in the Z direction
- $\gamma_{oa} = \sqrt{\left(\frac{2.405}{R}\right)^2 - \left(\frac{\omega}{c}\right)^2}$ decay rate in air
- $\gamma_{os} = \sqrt{\left(\frac{2.405}{R}\right)^2 - \left(\frac{\omega}{c}\right)^2 \epsilon s}$ decay rate in the substrate

A useful formula may be derived for Q_{EXT} through the use of certain simplifying assumptions.[9] The principal assumption is that the dielectric resonator may be replaced by one inductive loop tuned to resonance by a series capacitor (Fig. 6). The stored energy and the magnetic dipole moment are then the same for the two situations. These quantities are:

$$M = A\ I_1 \quad (15)$$

and

$$W_m = \frac{L\ I_1^2}{2} \quad (16)$$

The loop couples an impedance, Z, in series with the line. Applying elementary circuit theory to Fig. 6 yields:

$$X = \frac{Z}{j} = \frac{-(\omega_o Lm)^2}{2\omega_o L\left(\frac{f-f_o}{f_o}\right)} \quad (17)$$

From which:

$$Q_{EXT} = \frac{2\ \omega_o L\ Z_o}{(\omega_o Lm)^2} \quad (18)$$

Next, use the following relations for the voltage induced in the loop by the current I:

$$\frac{dB}{dt} = j\ \omega\ \mu_o H \quad (19)$$

$$V_1 = j\omega_o L_m I = j\omega\mu_o \iint_A H \bullet dA \quad (20)$$

Combining Eqs. 15 through 20:

$$Q_{EXT} = \frac{2W_m\lambda_o Z_o}{\mu_o M_1{}^2\pi n}\left[\frac{IA}{\iint_A H \bullet dA}\right]^2 \quad (21)$$

Interestingly, the factor

$$F = \frac{\mu_o M_1{}^2}{2W_m} \quad (22)$$

had occurred in previous analysis, and is a function of the dimensional and electrical parameters of a dielectric resonator, substrate dielectric constant, and height and closeness of the top cover.

When applying MIC dielectric resonators to bandpass filters, the resonators should be located near a maximum current point. This is achieved by terminating the inner conductor of the microstrip transmission line in a short circuit near the resonator, or in an open circuit a quarter wavelength beyond the resonator. The latter approach is more suitable for microstrip applications because the total stored energy will be the sum of the energy stored in the dielectric resonator and the microstrip transmission line resonator. As a first-order approximation, neglect the energy stored in the microstrip transmission resonator. Then the external Q for the bandpass filter is:

$$Q_{EXT}\Big|_{BPF} = \frac{1}{2} Q_{EXT}\Big|_{BSF} \quad (23)$$

To apply Eq. 21 to microstrip transmission line, it is necessary to evaluate the squared term, which is not a simple matter. A solution of this ratio was obtained through an electrostatic boundary value problem. However, the end result did not have the correct slope of external Q versus distance from the inner conductor. Until a suitable formula

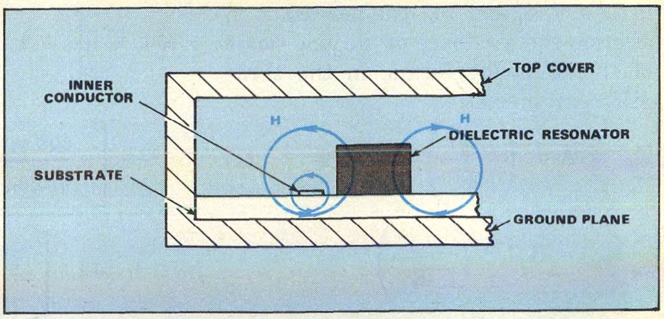

5. Coupling between a dielectric resonator and an MIC line *is affected by fields around the inner conductor and the substrate. The largest coupling occurs with the resonator's axis parallel to the H fields.*

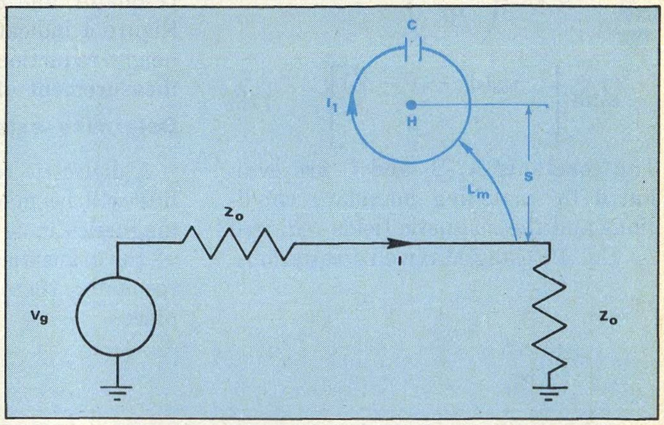

6. Circuit equivalent *used in the coupling equations contains mutual inductance between the resonator and the transmission line.*

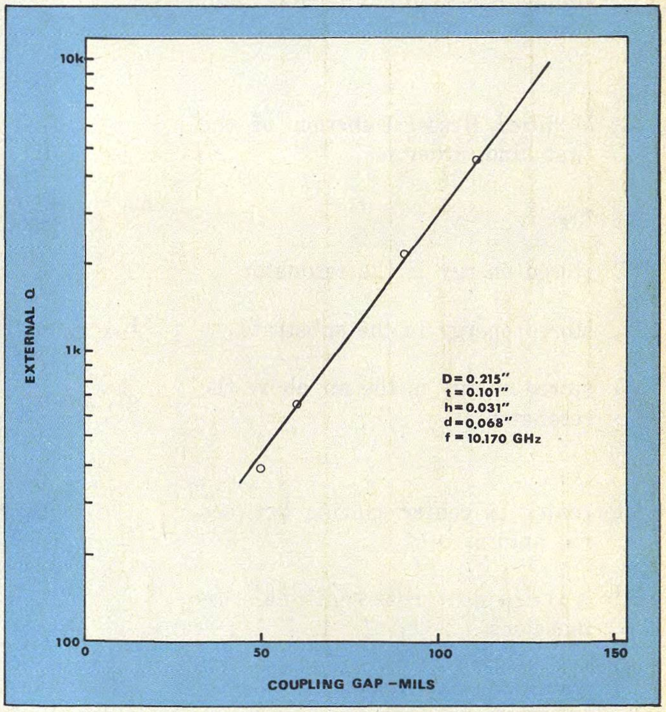

7. Lacking a good formula *for the evaluation of the squared term in the general external Q equation, experimental data relating Q_{EXT} to the coupling gap must be used.*

becomes available, experimental external Q data must be used. Typical results of such measurements are shown in Fig. 7.

Couple between the resonators

To utilize MIC dielectric resonators in bandpass filters, it is necessary to couple the end resonators to terminated transmission lines. The bandwidth passband response and stopband response depend upon the coupling values and number of resonators. Formulas [10] exist for computing the coupling values for the required bandwidth with maximally flat or equal-ripple response shape. But, none of these relate the coupling coefficient between a pair of resonators to the physical and electrical parameters of the MIC dielectric resonators, their center-to-center spacing, or the dimensions of the surrounding structure. Continuing this analysis, however, leads to these solutions.

Figure 1 shows that the resonators are cylindrical disks placed on the center line of a partially loaded cutoff waveguide. This partially loaded waveguide prevents radiation loss and undesired coupling to external fields. The external field of the fundamental resonant mode resembles that of a magnetic dipole directed along the axis of the disk. Because of this, an energized resonator excites many hybrid modes. The amplitude of these waves attenuates with longitudinal distance, since the waveguide is used below cutoff. The magnetic field of the waves excites the adjacent resonator and results in magnetic coupling between the pair of resonators. Because of the exponential decay of these waves, the coupling between nonadjacent resonators can be neglected.

The resonators are best represented as conducting loops in an enclosure, as shown in Fig. 8. The loops have an inductance, L, and are resonated at f_o by series capacitors, C. The magnetic dipole moment and the stored energy of the loop have already been defined. The EMF induced in the second loop is:

$$V_2 = -\oint E_2 \bullet d\ell = j\omega L_m I_1 \qquad (24)$$

By Stokes' theorem:

$$j\omega L_m I_1 = -\iint_{A_2} n_2 \bullet (\nabla \times E_2)ds = A_2(j\omega\mu_0 H_2) \qquad (25)$$

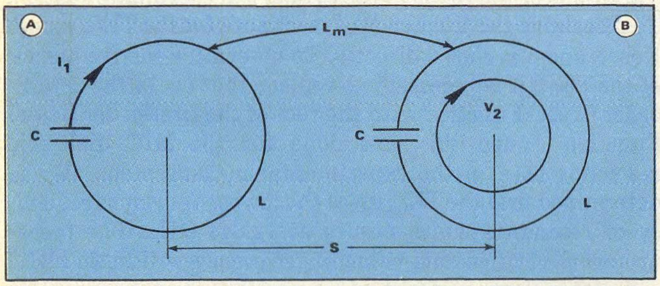

***8. Resonators represented as conducting loops** in an enclosure is one way to look at a resonator's coupling.*

The coupling coefficient

$$k = \frac{L_m}{L} \qquad (26)$$

becomes:

$$k = \frac{\mu_0 H_2 M_1}{2W_1} \qquad (27)$$

The magnetic field, H_z, is the field at position two, arising from a dipole M, at position one. This is expressed in terms of the normal modes of the partially loaded waveguide.

Using Collin's[7] notation, the electrical field of any waveguide mode is:

$$E_p = (e_p + e_{zp})\exp(k_p z) \qquad (28)$$

where the subscript p indicates the type and order of the mode. In a similar manner:

$$H_p = (h_p + h_{zp})\exp(k_p z) \qquad (29)$$

The following power normalization relationship applies to e_p and h_p of each mode.

$$\iint e_p \times h_p ds = 1 \qquad (30)$$

where the integration is over the transverse cross section of the waveguide.

The total fields are given by the following infinite summations over all possible modes.

$$E = \sum_p a_p E_p \qquad (31)$$

$$H = \sum_p a_p H_p \qquad (32)$$

The amplitudes for the waves of type and order p excited by the magnetic dipole are[7]:

$$a_p = j\left[\frac{\omega\mu_0 H_p M}{2}\right] \qquad (33)$$

Before determining the coupling coefficient, it is necessary to evaluate the normal modes of partially loaded waveguide shown in Fig. 1. In order to be excited, these modes must have an H field in the direction of the magnetic moment. For the case of interest, this narrows the analysis to LSE modes, since LSM modes do not have an H field in the proper direction.

To satisfy the boundary conditions at the conducting walls (Fig. 1):

$$\psi_1 = C_1\sin(k_{y1}x)\cos(n\pi y/a)\exp(-jkz) \qquad (34)$$

$$\psi_2 = C_2\sin\big(k_{y2}(b-x)\big)\cos(n\pi y/a)\exp(-jkz) \qquad (35)$$

Examination of Eqs. 34 and 35 reveals further that n has to be even to satisfy the H field requirement. The required fields and the propagation constants can now be determined with Maxwell's equations and boundary conditions.

It can be assumed that the most significant coupling occurs in the actual dielectric resonator, and that the field

H_2 is taken in the center of the resonator. The final result for the coupling coefficient is:

$$K = \frac{2F}{aVh}\left[\frac{(n\pi/a)^2 - \alpha_{mn}^2}{\alpha_{mn}}\right]\sin^2\left(k_{y2}(b-h-t/2)\right)\exp(-\alpha_{mn}s) \quad (36)$$

$$F = 32\pi\epsilon_r\left[\frac{\omega}{\gamma_r C}\right]^2\left[\frac{R}{\rho_{01}}\right]^2\left[\frac{\sin^2(\gamma_r t/2)}{t + (\sin(\gamma_r t)/\gamma_r)}\right] \quad (37)$$

$$V = \left[\frac{\sin(k_{y2}(b-h)}{\sin(k_{y1}h)}\right]^2\left[1 - \frac{\sin(2k_{y1}h)}{2k_{y1}h}\right]$$

$$+\left[\frac{b}{h} - 1\right]\left[1 - \frac{\sin(2k_{y2}\ (b-h)}{2k_{y2}\ (b-h)}\right] \quad (38)$$

These equations were analyzed by computer, and the theoretical results, with experimental comparisons, are shown in Fig. 9. As can be seen, the agreement is not very good. The reason for this is that in calculating the actual coupling between dielectric resonators in a practical filter structure, the assumption of infinitesimally small dipoles is violated. To overcome this and improve the agreement between theory and experiment, a distributed dipole moment is introduced:

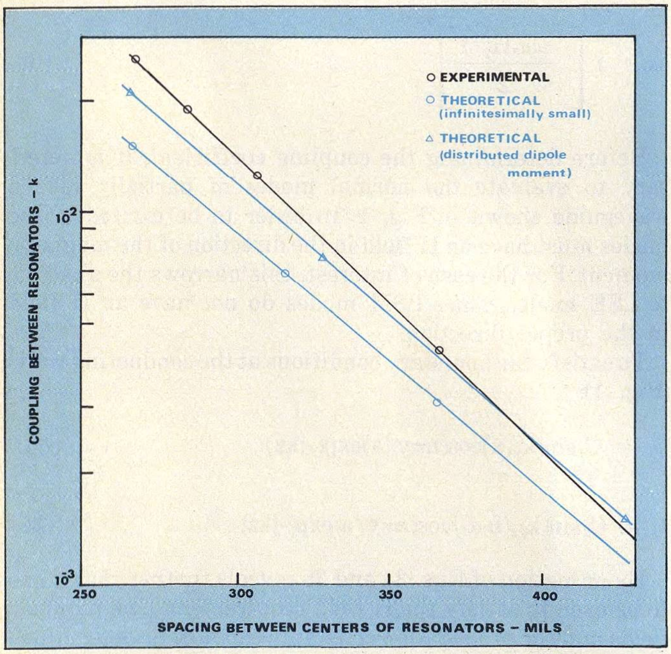

***9. Computer calculation points** out that resonator size —although very small—must be included in the coupling coefficient analysis.*

$$m(r,\Theta,z) = \frac{\epsilon(z)H(r,\Theta,z)M}{\iiint_v \epsilon(z)H(r,\Theta,z)dV} \quad (39)$$

The total coupling in this case is found from:

$$K = j\,\frac{\mu_0{}^2\omega}{4W_1}$$

$$\sum_q\left[\iiint_v h_q(x,y,z)m(r,\Theta,z)dV\right]^2 \exp(-\alpha_{mn}S) \quad (40)$$

The result after integration is:

$$K = \frac{2F}{bVh}\left[\frac{S_a}{1 - (K_{y2}/\gamma_1)^2}\right]^2\left[\frac{1}{(1 - (n\pi R/b\,\rho_{01})^2)^2}\right]$$

$$\left[\frac{(n\pi/b)^2 - \alpha_{mn}^2}{\alpha_{mn}}\right]\left[\frac{J_0{}^2 n\pi R}{b}\right]\exp(-\alpha_{mn}S) \quad (41)$$

where F and V are the same as defined in Eq. 39, and:

$$S_a = \sin\left(K_{y2}(d + t/2)\right)$$

$$\left[\cos\left(\frac{K_{y2}t}{2}\right) - \left(\frac{K_{y2}}{\gamma_1}\right)\left(\cot\left(\frac{\gamma_1 t}{2}\right)\right)\left(\sin\left(\frac{K_{y2}t}{2}\right)\right)\right] \quad (42)$$

These equations were analyzed by computer and the results plotted in Fig. 9. Notice how close the experimental and theoretical results are.

Locating spurious responses

A filter designer is often concerned with the location of spurious responses in the resonator. In the case of the MIC dielectric resonator, some of these responses can be determined with Eqs. 2 and 5. The resonance deduced from these equations would belong only to the TE family. But, the lowest order spurious responses in a dielectric resonator are caused by the TE mode excitation[11], therefore, the TM results need not be considered.

The $TE_{11\delta}$ or $TE_{10\delta}$ could be the closest to the dominant mode of operation. The subscripts denote the number of variations of the fields in the cylindrical coordinate system. To determine the frequency of resonance for the $TE_{10\delta}$ mode, Eqs. 2 and 5 are used directly. To determine the frequency of the $TE_{11\delta}$, it is necessary to replace the root of the zeroth-order Bessel Function with the root of the first-order Bessel Function. When this was done for the MIC dielectric resonator used in the experimental measurement, it was determined that the $TE_{11\delta}$ gives the lowest spurious frequency of resonance which occurs at 12.644 GHz. The measurements verified this value of frequency within 20 MHz.

Another source of potential spurious responses comes from the housing which is basically a partially loaded

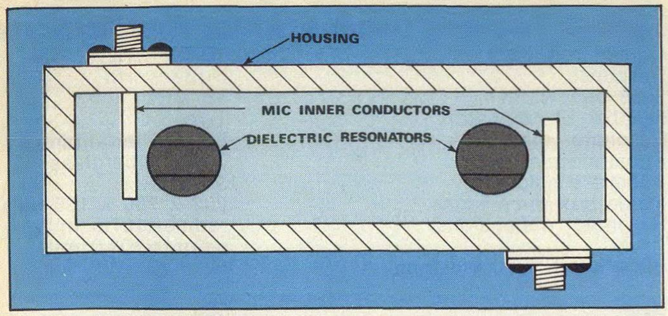

***10. Experimental filter** required sapphire dielectric tuning screws (not shown) to tune both resonators to the same frequency.*

waveguide cavity. The resulting equations for the TM case are:

$$K_{y1}^2 = -\epsilon_s\alpha_{y2}^2 + \left[\left(\frac{n\pi}{b}\right)^2 + \left(\frac{P\pi}{L}\right)^2\right](\epsilon_r - 1) \tag{43}$$

$$K_{y1}\tan(K_{y1}h) = \epsilon_s\alpha_{y2}\tanh\left[\alpha_{y2}(b-h)\right] \tag{44}$$

$$f_{mn}P = \frac{C}{2\pi}\sqrt{-\epsilon_s\alpha_{y2}^2 + \left(\frac{n\pi}{b}\right)^2 + \left(\frac{P\pi}{\ell_c}\right)^2} \tag{45}$$

These equations were analyzed by computer, and it was determined that the TM_{010} gave the lowest frequency of resonance. The computer results compared well with experimental measurements on the housing used for the three pole bandpass filter. The actual filter spurious frequencies, due to the partially loaded waveguide cavity, were somewhat lower because of the MIC inner conductor loading.

Two and three-pole bandpass filter design

The filter synthesis[10] is based on the well-known low pass prototype elements and a low pass to bandpass mapping. This permits synthesis of both Chebyshev and Butterworth responses. The design is completely determined by the following formulas:

$$Q_{EXT} = \frac{g_0 g_1}{w} \tag{46}$$

$$K_{j,j+1} = \frac{w}{\sqrt{g_j g_{j+1}}} \tag{47}$$

$$w = \frac{f_2 - f_1}{f_0} \tag{48}$$

$$f_0 = \sqrt{f_2 f_1} \tag{49}$$

The passband edges f_2 and f_1 are for the Chebyshev filters defined by the passband ripple level, while the bandwidth of the Butterworth filters is defined by the 3-dB points. Using these equations and the results of previous dis-

READER SERVICE NUMBER 39

Table 2: Two-pole bandpass filter specifications

Center frequency	10.170 GHz
Response	Butterworth
3-dB bandwidth	45 MHz
Number of resonators	Two
Resonator material	Barium tetratitanate
Substrate material	Teflon fiberglass
Substrate height	31 mils
Inside box dimensions	202 x 750 x 166 mils
Resonator dimensions	radius=107.5 mils height=101.0 mils
Butterworth filter elements	$g_0 = g_3 = 1$ $g_1 = g_2 = \sqrt{2}$
Q_{EXT}	300
k_{12}	3.32×10^{-3}
Spacing between resonators	166 mils

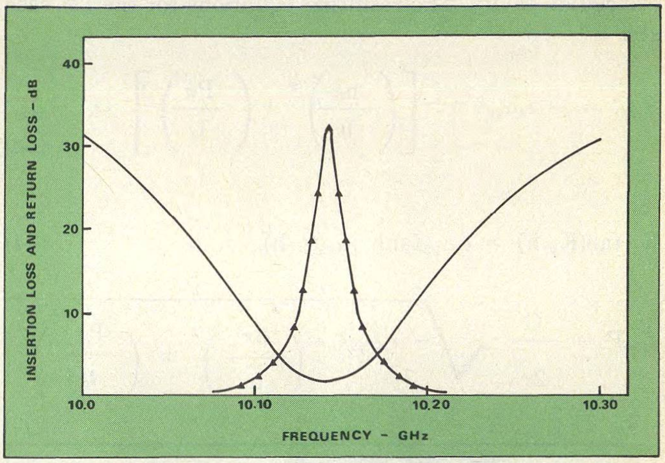

***11. Insertion and return loss** is plotted for a two-pole bandpass filter, designed using the analysis described.*

cussion, an experimental filter was designed with the parameters as listed in Table 2 (see Fig. 10).

The filter required sapphire dielectric tuning screws[5] above the MIC dielectric resonators to tune each resonator to the same frequency. Dielectric, rather than metallic tuning screws, were used to maintain the high unloaded Q. Based on the measured results and Cohn's formula,

$$Q_u = \frac{4.343}{w(\text{loss})} \sum_{1}^{n} g_i \qquad (50)$$

an overall unloaded Q of 1900 was calculated. The filter's performance is detailed in Fig. 11.••

References

1. R. D. Richtmyer, "Dielectric Resonators," *J. Appl. Phys.*, Vol. 10, pp. 391-398, (June, 1939).
2. A. Okaya and L.F. Barash, "The Dielectric Microwave Resonator," *Proc. IRE*, Vol. 50, pp. 2081-2092, (October, 1962).
3. H. Y. Yee, "Natural Resonant Frequencies of Microwave Dielectric Resonators," *IEEE Trans. Microwave Theory and Techniques* (Correspondence), Vol MTT-13, p. 256, (March, 1965).
4. J. C. Sethares and S. J. Naumann, "Design of Microwave Dielectric Resonators," *IEEE Trans. MTT*, Vol. MTT-14, pp. 2-7, (January, 1966).
5. S. B. Cohn, "Microwave Bandpass Filters Containing High-Q Dielectric Resonators," *IEEE Trans. MTT*, Vol. MTT-16, pp. 218-227, (April, 1968).
6. A. Karp, J.J. Shaw, and D. K. Winslow, "Circuit Properties of Microwave Dielectric Resonators," *IEEE Trans. MTT*, Vol. MTT-16, pp. 818-828, (October, 1968).
7. R. E. Collin, Field Theory of Guided Waves, New York, McGraw-Hill, (1960).
8. A. A. Oliner, and L. Goldstone, "Leaky - Wave Antennas," *IRE Trans.* Vol. AP-7, p. 307, (October, 1959).
9. S. B. Cohn and E. N. Torgow, "Investigation of Microwave Dielectric - Resonator Filters," Fifth Quarterly Report on Contract DA-36-039-AMC-02267 (E), 1 September 1964 to 30 November 1974, Rentec Corp., Project No. 31625.
10. G. L. Matthaei, L. Young, and E.M.T. Jones, Microwave Filters, Impedance - Matching Networks and Coupling Structures, New York, McGraw-Hill, (1964).
11. H. Y. Yee, "Natural Resonant Frequencies of Microwave Dielectric Resonators," *IEEE Trans. Microwave Theory and Techniques* (Correspondence), Vol. MTT-13, p. 256, (March, 1965).

Consider A Single Diode To Study Mixer Intermod

An accurate profile of the diode's conduction cycle is the key to analyzing third-order distortion. Sixth-order equations result, but a computer program plows through to find the best suppression method.

THERE are several schemes that can be applied to reduce the third-order, two-tone intermodulation (IM) level in a double-balanced mixer. These include using higher offset diodes, adding multiple diodes in series, and adding resistance in series with the diodes. More specifically, however, some fundamental questions arise concerning the quantitative effect of these schemes on third-order IM suppression. For instance:

- How does adding resistance in series with the diodes compare to using two diodes in series?
- Is one scheme more efficient in terms of local oscillator (LO) drive required to produce a given level of IM response?
- To what extent will just increasing the LO drive voltage in a low-level mixer decrease IM distortion?
- What effect does diode offset have?
- What is the effect of a wide temperature range (−54 to +100°C)?

Many of these questions can be answered in a general way by constructing mixers using the various schemes and making extensive measurements. However, if the questions are to be answered on a quantitative basis, results from mixer IM measurements alone leave uncertainties. The double-balanced mixer does not always behave well when measured for third-order IM because of phase cancellations. Thus, data taken as a function of frequency and as a function of temperature can be misleading. This is especially true when one is trying to ascertain the true temperature dependence of the third-order IM, or to discover to what extent certain circuit design approaches have on the overall suppression of the IM products.

The term suppression, as used here, should be clarified. Actually, the design approaches typically taken do not really suppress the IM, but rather they cause the level to be generated at a lower inherent value. This is in contrast to using feedback in an amplifier, a technique which does actually suppress the distortion since, at some point in the circuit, the IM level is higher than that seen by the outside world. Real suppression does occur in a mixer, but it is not deliberate and is the cause of the uncertainty in determining the true intercept point.

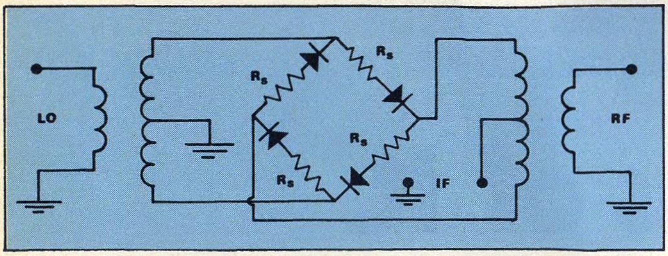

*1. **Classical double-balanced mixer circuit** employs series resistors (R_s) to limit intermodulation distortion.*

Daniel L. Cheadle, Head, Relcom Engineering, Solid-State Division, Watkins-Johnson Company, 3333 Hillview Avenue, Palo Alto, CA 94304.

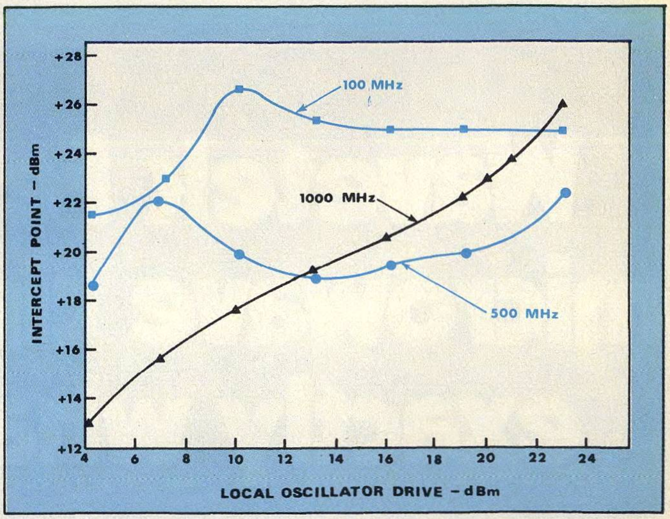

*2. **Note the difference between performance** at 1000 MHz and that at 100 and 500 MHz in this intercept plot.*

Evaluate a single diode

A classical mixer was constructed to demonstrate the nature of the problem in analyzing the full double-balanced mixer circuit (Fig. 1). The circuit was built in thin-film form on an alumina substrate to minimize stray reactances. Unencapsulated Schottky diode chips are bonded in series with 30-ohm tantalum-nitride resistors that are etched into the substrate.

The projected third-order, two-tone IM point is plotted in Fig. 2 as a function of LO drive level at approximately 100, 500 and 1000 MHz, with −10-dBm input tones used for each frequency. At 1000 MHz, the intercept point (IP) maintains a monotonic relationship to the LO drive level, but at both 100 and 500 MHz, there is a broad range of LO drive levels for which the IP remains essentially flat. In addition, the intercept point clearly peaks at lower LO drive levels at both 100 and 500 MHz. This peaking, which represents improved IM suppression, is due to phase cancellations in the double-balanced circuit. But this performance is highly dependent on the test setup and cannot be consistently repeated.

To eliminate this uncertainty, the analytical approach used here considers a single diode as a control element for both analysis and measurement since phase cancellations are not possible. It should further be clarified that in the ideal double-balanced mixer, the third-order product to be analyzed ($2f_{R1} - f_{R2} \pm f_L$) is not suppressed because of mixer balance, but is produced at a level that is dependent on the third-order nonlinearity of the diodes. Therefore, a single diode, used as a control element, can provide significant insight into the mechanisms of generating and reducing third-order IM distortion in a double-balanced mixer.

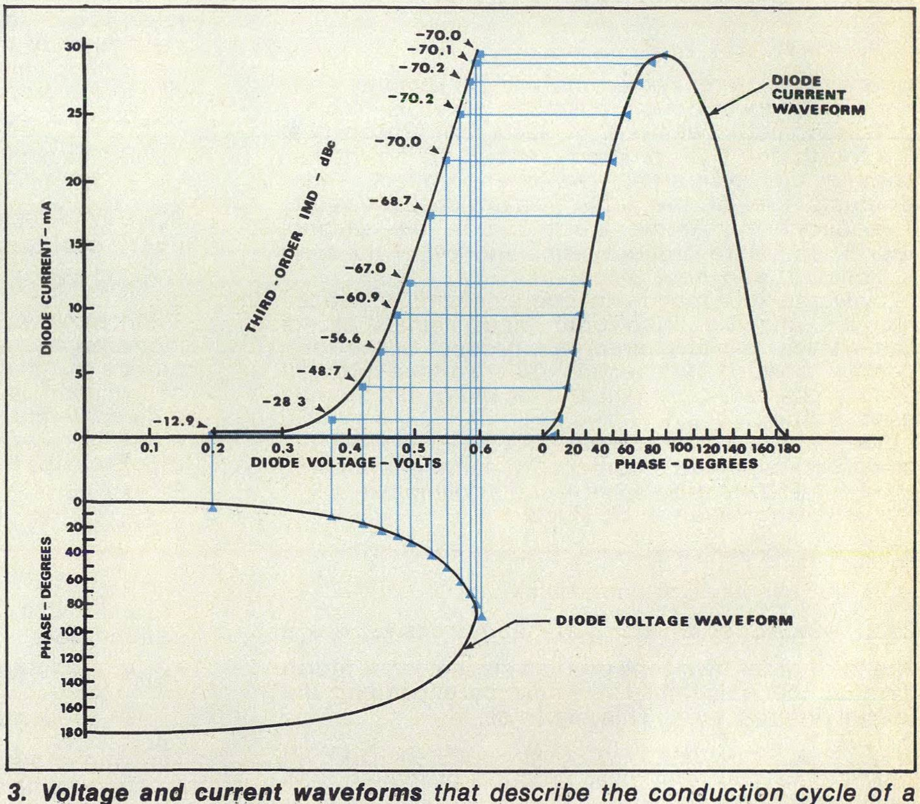

*3. **Voltage and current waveforms** that describe the conduction cycle of a Schottky-barrier diode are neither sinusoidal nor square wave. Data is taken with a 25-ohm series resistor at tone levels of −10 dBm.*

Drop restrictive assumptions

There have been many approaches to intermodulation analysis of mixer diodes, and some extensions of the analyses to single and double-balanced mixers in the past several years. The classical analysis technique uses a rather complicated mathematical approach which involves modified Bessel functions. Not only is the approach not readily assimilated or implemented, but certain restrictive assumptions are made to keep the analysis from becoming too unwieldy. For example, it is generally assumed that:

- The diode V-I curve is an exponential function.
- Either the LO source is a square wave, or DC bias is applied to the diodes.
- In the case of DC bias, the voltages across the diodes from both the LO and signal source are sinusoidal.
- The transition region can be ignored.

Let's consider the assumption of an exponential transfer characteristic. If a DC bias exists, then the approximation is not bad. In the real mixer world, however, the unbiased double-balanced mixer has established itself as the best choice for the vast majority of applications. These mixers most often are presented with sinusoidal LO voltages which means that the mixer diodes are switched gradually from an "off" state to a full "on" state. The assumption of a square-wave drive voltage is unrealistic in these cases.

The method of analysis incorporated here uses a sine wave input at the LO port and sweeps the full conduction cycle in steps beginning at very small conduction angles. The voltage and current waveforms of a typical Schottky diode transfer curve are shown in Fig. 3. Note that these waveforms are neither sinusoidal nor square-wave. The step intervals are shown by the lines connecting the current and voltage waveforms which pass through the diode curve.

Examine the transition region

The first 25 degrees of the LO conduction cycle represent the approximate transition region for a low-level mixer with nominal LO drive levels where the diode is not biased fully "off" nor is it biased fully "on". A significant amount of transition region intermodulation (TRIM) distortion exists in these cases. For a high-level mixer with 25 ohms resistance in each leg, the turn-on region is reduced to only about 15 degrees as shown by curves in Fig. 3. Even in this case, the distortion level for the first 5 degrees into the conduction cycle is only 12.9 dB below the desired signal. After 20 degrees, however, it has decreased to −56.6 dB.

Behind the program: Extracting direct mix and third-order products

The diode characteristic curve can be represented by a power series of the form

$$I_d = a_0 + a_1V_d + a_2V_d^2 + \ldots + a_nV_d^n$$

where I_d is the diode current and V_d is the diode voltage.

$$\text{Let} \quad x = A \cos \omega_1 t$$
$$x = B \cos \omega_2 t$$
$$z = C \cos \omega_o t$$

where ω_1 and ω_2 are the two signals present at the R port of the mixer and ω_o is the local oscillator frequency. A, B, and C are the respective amplitudes of each signal. Substituting into the power series gives

$$I_d = a_0 + a_1 [(x+y) + z] + a_2 [(x+y) + z]^2 + \ldots$$
$$+ a_n [(x+y) + z]^n$$

where the a_0 term represents any DC quantity present, which for a double balanced mixer, is zero.

Trigonometric analysis of each term shows that the fourth and sixth ordered terms of the polynomial contain the third-order, two-tone products. These products are of the form $\cos(2\omega_1 t)\cos(\omega_2 t)\cos(\omega_o t)$. The direct mix terms are found in the second, fourth, and sixth ordered terms and are of the form $(\omega_1 t)\cos(\omega_o t)$ and $\cos(\omega_2 t)\cos(\omega_o t)$.

Only the information in one sideband is needed for this analysis. With both input signals at the same level, only the direct mix product of the form $\cos(\omega_1 t) \cos(\omega_o t)$ is needed. The two-tone product used is $\cos(2\omega_1 - \omega_2 + \omega_o)t$ and the direct mix product used is $\cos(\omega_1 + \omega_o)t$.

The same results are obtained for the lower sideband since both sidebands contain the same information. From the second ordered term of the polynomial, $a_2V_d^2$, the following result is obtained:

$$a_2V_d^2 = a_2 (x+y)^2 = a_2 (x^2 + 2\,xz + z^2)$$

Only the center term contributes.

$$2a_2xz = 2a_2AC\cos \omega_1 t \cos \omega_o t = 2a_2AC \cos (\omega_1 + \omega_o)t$$

The third-order, two-tone product present in the fourth term of the polynomial is found by expanding the fourth ordered term. This becomes,

$$a_4V_z^4 = a_4 [(x+y)^4 + 4(x+y)^3 z + 6(x+y)z^2 + 4(x+y)z^3 + z^4]$$

Only the second term gives products of the required form, $\cos(2\omega_1 t)\cos(\omega_2 t)\cos(\omega_o T)$. The second term is expanded to form:

$$a_4[4(x+y)^3z] = 4a_4 (x^3 + 3x^2y + 3xy^2 + y^3)z$$

The significant term here is the second product, $3x^2yz$. Letting B=A and substituting for x, y, and z,

$$12a_4x^2yz = 12a_4A^3C\ (1/2 + 1/2 \cos 2\omega_1 t)\ (\cos \omega_2 t)\ (\cos \omega_o t)$$

$$= 3a_4A^3C\,[\cos (2\omega_1 - \omega_2)t \cos \omega_o t]$$
$$= 3/2a_4A^3C \cos (2\omega_1 - \omega_2 + \omega_o)t$$

Expanding the sixth ordered term of the polynomial gives

$$a_6V_2^6 = a_6 [(x+y)^6 + 6(x+y)^5z + 15(x+y)^4z$$
$$+ 20(x+y)^3z^3 + 15(x+y)^2z^4 + 6(x+y)z^5 + z^6]$$

It can be seen that only the second and fourth products yield terms of the proper forms. The second product has A^5 in it which, since A is small, will be negligible. The fourth product gives

$$20a_6(x+y)^3z^3 = 20a_6 [x^3 + 3x^2y + 3xy^2 + y^3]\, z^3$$

Taking the significant term,

$$60a_6x^2yz^3 = 60a_6A^3C^3 [(1/2+1/2\cos 2\omega_1 t)(\cos \omega_2 t)$$
$$(1/2+1/2 \cos 2\omega_o t) \cos \omega_o t$$
$$= 15/4a_6A^3C^3\cos(2\omega_1 - \omega_2 + \omega_o)t$$

Since the value of C can be greater than one for a high level mixer, terms with high powers of C and low powers of A that include the direct mix products must be included in the analysis. The fourth and sixth ordered terms of the polynomial have direct mix products involving single powers of A and high powers of C. From the fourth ordered term, the fourth product, $4(x+y)z^3$, gives

$$4a_4(x+y)z^3 = 4a_4AC^3 \cos \omega_1 \cos^3\omega_o t$$
$$= a_4AC^3 \cos (\omega_1 + \omega_o)t$$

From the sixth ordered term of the polynomial, the sixth product

$$6a_6(x+y)z^5 = 6a_6AC^5 \cos \omega_1 t \cos^5\omega_o t$$
$$= 3/4a_6AC^5 \cos (\omega_1 + \omega_o)t$$

The ratio of the amplitude of the third order two-tone products to the direct mix products then becomes:

$$\text{Ratio} = \frac{3/2a_4A^3C + 15/4a_6A^3C^3}{a_2AC + a_4AC^3 + 3/4a_6AC^5}$$

This analysis was made possible by the development of a special computer program (Table 1) that analyzes the IM performance of the diode across its full conduction cycle and, therefore, does not ignore the transition region. The basic approach is to trigonometrically reduce the products of the input signals and extract the direct mix and third-order products. The derivation of this reduction is shown in the accompanying sidebar. Amplitudes are compared by taking a ratio of the third-order, two-tone product ($f_L + 2f_{R1} - f_{R2}$) to the direct mix product ($f_L \pm f_R$), which is defined as diode intermodulation distortion (DIMD) and is given by:

$$\text{DIMD} = \frac{3/2a_4A^3C + 15/4a_6\ A^3C^3}{a_2AC + a_4AC^3 + 3/4a_6\ AC^5} \qquad (1)$$

where a_2, a_4 and a_6 are the polynomial coefficients, A is the signal voltage amplitude, and C is the LO drive voltage amplitude at the diode junction.

First, the diode DC transfer curve is accurately measured up to the level of highest peak current likely to be encountered in the circuit to be used. The coefficients of the polynomial are determined using a standard polynomial curve fit program available on several different computer systems. This program fits bivarite data to a polynomial using the "least squares approximation" method. Because of the squaring operation, the program requires the beginning and end points of the input data to be as near to the same order of magnitude as possible. This avoids large errors over the lower part of the curve. The analysis includes the entire conduction region including the transition region, so to accurately fit the transfer curve, four sets of polynomials are used. And, to obtain a high index of determination between the computer calculated polynomial

Table 1: BASIC program for analyzing IMD in mixer diodes

```
1      DATA 0,−1.13789E−04,3.98638E−03,−.055307,.381644,−1.31512,1.84086
2      DATA 0,−5.43593E−03,.147275,−1.54136,7.85016,−19.6006,19.3705
3      DATA 0,−8.77929,100.302,−454.962,1023.27,−1140.7,504.972
4      DATA 0,7.65458,−62.4819,200.616,−316.843,247.124,−76.2066
10     DIM A$[3]
20     DIM B$[3]
30     PRINT "THIRD - ORDER INTERMODULATION"
40     PRINT
50     PRINT
60     READ A0,A1,A2,A3,A4,A5,A6
70     PRINT "INITIAL, FINAL LO DRIVE (DBM), STEP INTERVAL (DB)";
80     INPUT D2,D3,D4
90     PRINT
100    PRINT "RF LEVELS DBM";
110    INPUT F1
120    PRINT
130    PRINT "DIODE EXT-SEP RES";
140    INPUT R2
150    PRINT
160    PRINT "TYPE /0/ IF DOUB-BAL OR /1/ IF SIN-DIODE MIXER";
170    INPUT K
180    PRINT
185    FOR D1=D2 TO D3 STEP D4
190    PRINT "ENTIRE SUMMARY (Y OR N)";
200    INPUT A$
210    PRINT
214    PRINT
220    IF A$="N" THEN 230
222    PRINT"I-DIODE    V-DIODE    IMD    R-DYNAMIC    PHASE"
224    PRINT
230    N=1
240    X1=0
250    W1=0
260    J1=0
270    P2=0
280    P4=0
290    P7=0
300    I1=0
310    I6=0
320    N1=0
330    N2=1
332    M8=0
340    V1=.01
350    E1=SOR(.05)*10^ (D1/20)*2*SOR(2)
360    F2=SOR(.05)*10^ (F1/20)*2
370    IF K=1 THEN 390
380    GOTO 410
390    R1=50
400    GOTO 420
410    R1=100
420    FOR X2=30 TO 90 STEP 10
430    IF X1 >= 31 THEN 460
440    FOR X1=5 TO 30 STEP 5
450    GOTO 470
460    X1=X2
470    Y1=X1*3.1416/180
480    E2=E1*SIN(Y1)
490    GOSUB 530
500    IF V3 >= V2 THEN 570
510    V1=V1+.01
520    GOTO 490
530    V2=E2-V1
540    DEF  FNA  (I1)=A0+A1*V1+A2*V1^ 2+A3*V1^ 3+A4*V1^ 4+A5*V1^
       5+A6*V1^ 6
542    I1=FNA(I1)
550    V3=(R1+R2)*I1
560    RETURN
570    V1=V1-.01
580    GOSUB 530
590    IF V3 >= V2 THEN 640
600    V1=V1+.001
610    GOTO 580
640    IF N1 >= 3 THEN 730
650    IF I1 >= .01 THEN 710
660    IF N1 >= 2 THEN 730
670    IF I1 >= .001 THEN 710
680    IF N1 >= 1 THEN 730
690    IF I1 >= .00001 THEN 710
700    GOTO 730
710    READ A0,A1,A2,A3,A4,A5,A6
720    N1=N1+1
730    IF I1 >= .008 THEN 760
740    S1=(V1-W1)/(I1-J1)
750    GOTO 790
760    V4=V1-.01
770    DEF  FNB(I4)=A0+A1*V4+A2*V4^ 2+A3*V4^ 3+A4*V4^ 4+A5*V4^
       5+A6*V4^ 6
774    I4=FNB(I4)
780    S1=.01/(I1-I4)
790    IF K=1 THEN 810
800    GOTO 840
810    I3=F2/(R1+R2+S1)
820    H1=I3*S1
830    GOTO 860
840    I3=F2/(100+(R2+S1)/2)
850    H1=(I3/2)*S1
860    M5=A2*H1*V1+A4*(4*H1^ 3*V1+H1*V1^ 3)
870    M6=A6*(H1^ 5*V1*81/8+10*H1^ 3*V1^ 3+H1*V1^ 5*3/2)
880    M3=M5+M6
890    M4=A4*H1^ 3*V13*V1·3/23*/2+A6*(H1^ 5*V1*15/2+H1^ 3*V1^ 3*15/4)
900    M1=20*LOG(M4/M3)*.4343
910    GOTO N OF 920,1460
920    IF A$="N" THEN 940
930    PRINT I1*10^ 3,V1,M1,S1,X1
940    IF X1<35 THEN 1000
950    P1=(M4^ 2/S1)/9
960    P6=(M3^ 2/S1)/9
970    P3=I1*V1/9
980    I5=(I1+J1)/18
982    M7=M1/9
990    GOTO 1040
1000   P1=(M4^ 2/S1)/18
1010   P6=(M3^ 2/S1)/18
1020   P3=I1*V1/18
1030   I5=(I1+J1)/36
1032   M7=M1/18
1040   P2=P2+P1
1050   P7=P7+P6
1060   P4=P4+P3
1062   M8=M8+M7
1070   W1=V1
1080   J1=I1
1090   I6=I6+I5
1100   NEXT X1
1110   X1=X1+1
1120   NEXT X2
1140   PRINT
1150   PRINT
1151   PRINT "     LO DRIVE = ",D1
1152   PRINT "     AVE IMD = ",M8
1170   PRINT "     AVE DIODE POWER = ";P4*10^ 3
1180   PRINT "     PEAK POWER = ";V1*I1*10^ 3
1190   PRINT "     PEAK CURRENT = ";I1*10^ 3
1200   N1=0
1210   N=2
1220   V1=.05
1240   IF I6 >= .01 THEN 1310
1250   IF I6 >= .001 THEN 1330
1260   IF I6 >= .00001 THEN 1350
1270   RESTORE
1274   READ A0,A1,A2,A3,A4,A5,A6
1310   RESTORE 4
1314   READ A0,A1,A2,A3,A4,A5,A6
1320   GOTO 1370
1330   RESTORE 3
1334   READ A0,A1,A2,A3,A4,A5,A6
1340   GOTO 1370
1350   RESTORE 2
1360   READ A0,A1,A2,A3,A4,A5,A6
1370   I7=FNA(I1)
1380   IF I7 >= I6 THEN 1410
1390   V1=V1+.005
1400   GOTO 1370
1410   V4=V1−.005
1420   I8=FNB(I4)
1430   S2=.01/(I7−I8)
1440   S1=S2
1450   GOTO 790
1460   PRINT "     AVE CURRENT = ";I6*10^ 3
1470   PRINT "     RD AVERAGE = ";S2
1490   PRINT
1500   PRINT
1510   PRINT "ABORT (Y OR N)";
1520   INPUT C$
1530   IF C$="Y" THEN 2000
1540   RESTORE
1550   READ A0,A1,A2,A3,A4,A5,A6
1560   PRINT
1570   NEXT D1
2000   END
```

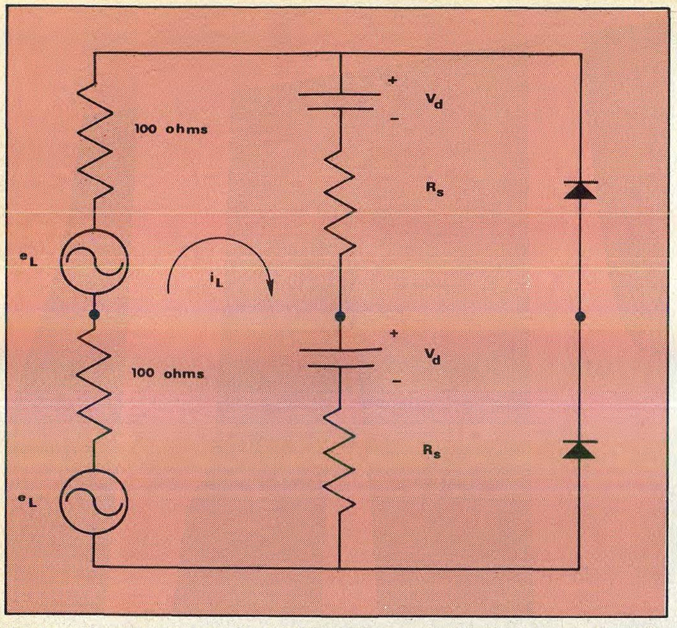

4. *Equivalent circuit for the LO port* *of a typical double-balanced mixer assumes a 4:1 impedance transformation ratio yielding two source impedances of 100 ohms.*

and the experimental data, it was found that at least a sixth-order equation is needed. By restricting the range over the transfer curve that each polynomial applied, and by using sixth-order polynomials, indicies of determination of 0.9998 or better can be obtained (an index of 1.0 represents a perfect fit). This close correlation insures that low level IM products can be extracted from the nonlinear diode curvature with reasonable accuracy.

Analyze equivalent circuits

The equivalent circuit for determining the diode conduction voltages and currents in the classical double-balanced mixer is shown in Fig. 4. This circuit represents the most common case where the LO transformer is constructed with a 2:1 turns ratio so that a 4:1 impedance transformation is obtained. This yields a source impedance for each half of the LO transformer of 100 ohms. Solving for the diode current i_d and the diode voltage V_d:

$$e_L - V_d = i_d\,(R_{LO} + R_s) \qquad (2)$$

Replacing i_d by its equivalent polynomial Eq. 2 yields:

$$\frac{e_L - V_d}{R_{LO} + R_s} = a_o + a_1V_d + a_2V_d^2 + a_3V_d^3 + a_4V_d^4 + a_5V_d^5 + a_6V_d^6 \qquad (3)$$

The computer program in Table 1 solves Eq. 3 using an iterative technique which first calculates e_L for the initial conduction increment for a given LO drive level. The first increment is 5 degrees into the turn-on cycle. A diode voltage level of 0.01 V is first assumed, and then incremented upwards in 0.01 V steps until Kirchhoff's voltage law is satisfied for the loop current in Fig. 4. After Eq. 3 is solved, the slope $(\frac{dV}{dI})$ of the transfer characteristic is determined by using the difference in the last voltage increment divided by the corresponding difference in the last current increment. This slope represents the diode dynamic resistance which is used to calculate the RF signal amplitude present at the diode junction. The level of IM produced at this point in the conduction cycle is calculated using Eq. 1. The LO source voltage is then calculated for the next 5-degree conduction increment and the above process is repeated. The diode transfer characteristic is represented by four different sets of sixth-order polynomials as previously stated. The program transfers to the next set of coefficients when the diode current exceeds the range of one set. The entire process is repeated until 90 degrees of conduction cycle is reached. The next 90 degrees is equal to the first 90 degrees since the drive voltage now swings back toward turn-off exactly in reverse.

The value of distortion for each increment in the LO conduction cycle is logarithmically averaged to determine the effective IM level as seen on a spectrum analyzer. This is done because the diode current is proportional to the log of its voltage, and the incremental IM levels are calculated based on the magnitudes of these voltages. A linear average would yield an effective value of IM which would predominate in the region before heavy conduction. Calculated results obtained using a linear average do not agree with measured results.

Experiments confirm the analysis

The equivalent circuit for determining the RF voltage

(continued on p. 170)

Table 2: Computed conduction-cycle characteristics

I-DIODE	V-DIODE	IMD	R-DYNAMIC	PHASE
−3.14673E−05	.088	−8.48973	−2.79656E+06	5
7.22212E−04	.175	−10.066	115434.	10
1.73294E−02	.259	−13.215	5058.06	15
.257891	.33	−16.5997	295.143	20
1.04397	.372	−29.2754	53.4298	25
2.13838	.396	−38.5265	21.9296	30
4.33207	.427999	−44.3741	14.5873	40
6.46305	.448999	−50.2916	9.85458	50
8.14629	.462999	−53.2327	8.23705	60
9.45473	.472999	−54.4328	7.71579	70
10.2777	.478999	−55.1472	8.92026	80
10.4311	.480999	−54.7631	9.17891	90

LO DRIVE = 4
AVE IMD = −41.1475
AVE DIODE POWER = 2.62251
PEAK POWER = 5.01733
PEAK CURRENT = 10.4311
AVE CURRENT = 5.12813
RD AVERAGE = 19.9539

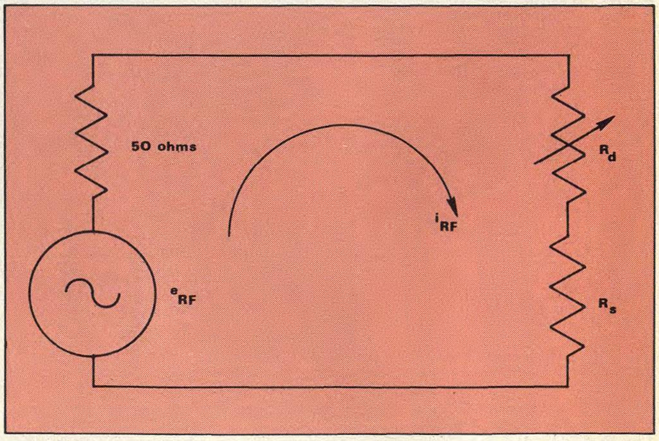

5. *RF voltage developed across a* *single diode circuit can be evaluated with this equivalent circuit.*

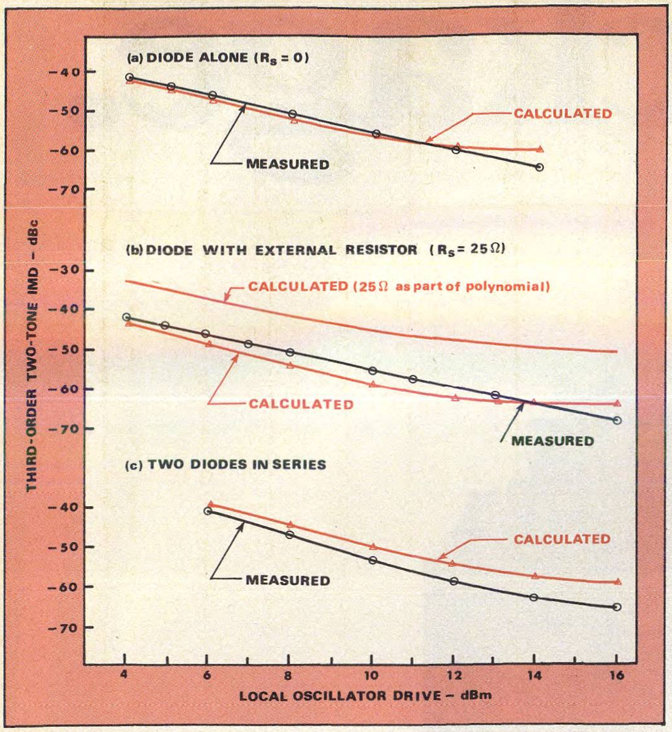

6. Series resistance offers the best IM suppression, *but series diodes can also be used effectively, especially when the individual device reverse breakdown voltage rating is low.*

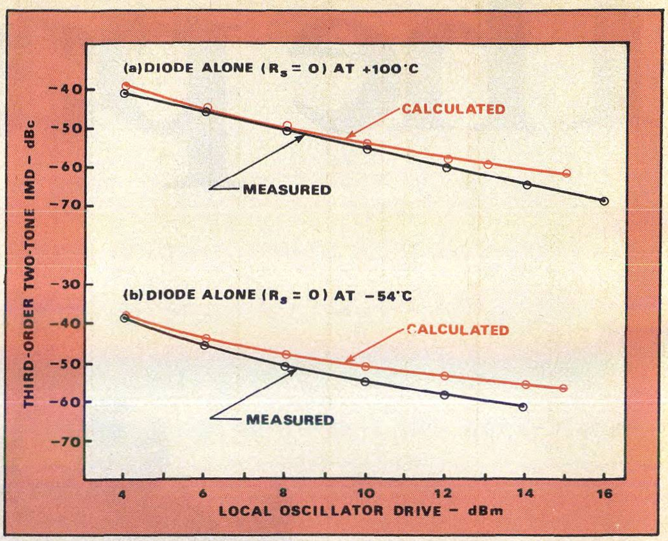

8. When internal series resistance *is extracted from the computation, measured and calculated values agree closely.*

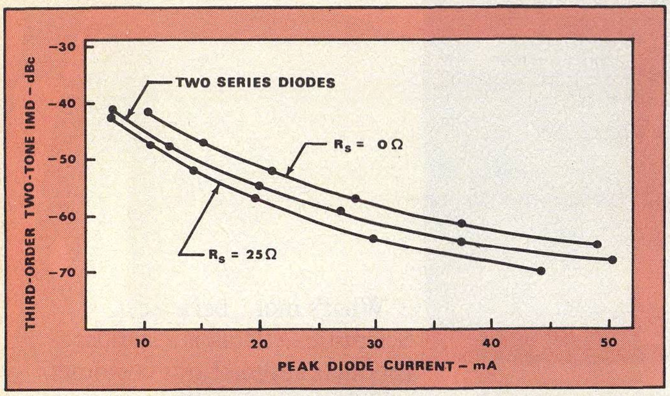

7. A comparison of IMD and peak diode current *confirms that series resistance most effectively blocks distortion.*

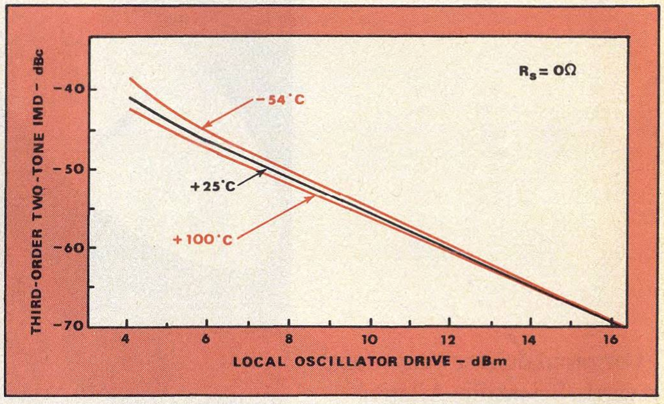

9. The change in the diode's offset voltage *with temperature causes the peak LO current to change which affects the distortion level. At higher LO levels, this effect is minimized.*

developed across the single diode circuit is shown in Fig. 5. Here, R_s is any series resistance added to the circuit, and R_d is the dynamic resistance of the diode which changes for each increment in the LO drive level.

The calculated and measured IM levels as a function of LO drive level are plotted in Fig. 6(a) for the diode alone—with no external resistors. The computer printout for this case is shown in Table 2 for a LO drive of +4 dBm. There is very close agreement between experiment and theory until the diode approaches higher LO drive levels. This descrepancy is caused primarily by the internal series resistance of the diode. This series resistance should be extracted from the diode's DC characteristic, and not included as part of the polynomial as Fig. 6(b) demonstrates. Here, a 25-ohm resistor was added in series with the diode. In one case, the 25-ohm resistor was included as part of the polynomial and over 10 dB in error occurred. When the resistor is separated from the polynomial, however, close agreement is obtained.

The performance of two diodes in series is shown in Fig. 6(c); the cumulative effect of each diode's internal series resistance slightly increases the error between measured and calculated values. The three conditions—the diode alone, the diode in series with a 25-ohm resistor, and two diodes in series—are replotted in Fig. 7 as a function of diode peak current for a given LO drive level. The 25-ohm resistor gives the highest suppression of third-order IM for a given value of peak current.

Figure 6 illustrates that each topology offers approximately equal suppression for a given applied LO drive level. The curves provide some answers to the first four questions posed at the beginning of this article. Series resistance provides the highest IM reduction, while two diodes in series offer the next best reduction. The curves also show that

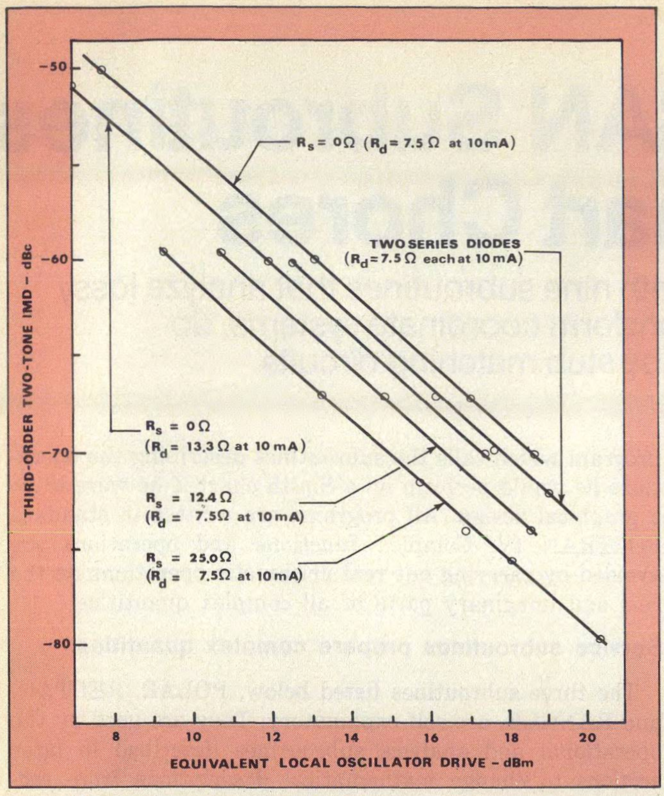

***10. When internal series resistance is extracted** from the computation, nonlinear behavior varies little with temperature.*

for two-tone signals (at −10 dBm levels) the added offset provided by an additional series diode has negligible effect on IM suppression. A word of caution is needed at this point, however, because this statement is correct only for the case low-level RF signals (<−10 dBm). When the RF signal becomes large, it can act as the LO. A higher offset is needed to prevent this. The diode internal series resistance increases by several ohms at both +100 and −54°C causing the calculated result to deviate from the measured value by 8 to 10 dB.

The analysis was reworked, and the major portion of this internal series resistance was extracted from the diode DC transfer characteristic and treated as an external series resistance. New polynomial coefficients were then determined, and the results are plotted in Fig. 8. Close agreement is obtained when the major portion of the internal series resistance is extracted.

The IM levels for the three temperatures are plotted as a function of LO drive in Fig. 9. At the lower LO levels, there is a greater difference due to the change in diode offset voltage which affects the amount of diode current that flows. For higher drive levels, this effect is reduced, which causes the IM levels to be nearly constant with temperature. If the IM levels are replotted as a function of current, they remain essentially constant from −54 to +100°C showing that the nonlinear behavior of the diode does not change appreciably with temperature.

To obtain additional insight into the double-balanced mixer, the drive levels used in the single-control circuits can be converted to an equivalent drive level in the double-balanced circuit for the classic case where the LO port uses a 4:1 impedance ratio transformer. Diodes with two values of internal series resistance—7.5 and 13.3 ohms—are compared in Fig. 10. In addition, the response of a device in series with a 25-ohm resistor is drawn. These results illustrate that the resistance decreases IM level approximately 0.3 dB/ohm. The decreased IM for the two series diodes is then attributed only to the increased series resistance provided by the second diode.

The diodes used in the analysis presented here are Hewlett-Packard devices (HP 5800-2810) that have a 15-V reverse breakdown capability. Many microwave quads can only support up to 2 V in the reverse direction. In this case, a greater benefit can be realized by using diodes in series, since the region of reverse nonlinear capacitance becomes more significant at higher frequencies and series diodes reduce this effect.••

Acknowledgement

The author thanks Jay Gaertner for his help in taking data and making measurements.

References

1. Dominic A. Fleri and Leonard D. Cohen, "Nonlinear Analysis of the Schottky-Barrier Mixer Diodes," *IEEE Transactions on Microwave Theory and Techniques*, Vol. MTT-21, No. 1, pp. 39-43, (January, 1973).
2. L. M. Orloff, "Intermodulation Analysis of Crystal Mixer," *Proceedings of the IEEE*, pp. 173-179, (February, 1964).
3. Robert L. Ernst, Peter Torrione and Wen Y. Pan, "Designing Microwave Mixers For Increased Dynamic Range," *IEEE Transactions on Electromagnetic Compatibility*, Vol. EMC-11, No. 4, pp. 130-138, (November, 1969).
4. William R. Gretsch, "The Spectrum of Intermodulation Generated in a Semiconductor Diode Junction," *Proceedings of the IEEE*, Vol. 54, No. 11, pp. 1528-1535, (November, 1966).
5. W. J. Warren and W. R. Hewlett, "An Analysis of the Intermodulation Method of Distortion Measurement," *Proceedings of the I. R. E.*, pp. 457-466, (April, 1948).
6. Daniel L. Cheadle, "Selecting Mixers for Best Intermod Performance," *Micro Waves*, Vol. 12, Nos. 11 and 12, pp. 48-54, pp. 58-62, (November, December, 1973).

Nine FORTRAN Subroutines Do Smith-Chart Chores

Expand your FORTRAN library with nine subroutines that analyze lossy or lossless transmission lines, transform coordinate systems, do Smith-chart rotations, and describe stub matching circuits.

THE Smith chart has been the main computational tool used in the analysis and design of transmission lines for over a quarter of a century.[1] One drawback of the Smith chart is its lack of accuracy, especially in the central region where the load impedance is roughly equal to the characteristic impedance of the line.[2] Another obstacle is the amount of work and time required when the transmission line analysis covers a span of frequencies.

Both of these shortcomings can be surmounted with the use of digital computers. *MicroWaves* first published a package of FORTRAN subroutines for solving transmission line problems some time ago.[3] This has been used to teach a course in distributed systems theory at Northeastern for several years. The present article develops a new subroutine package which extends and modifies the original programs in the following ways:

- A first course in transmission line theory usually begins with the study of specific types of lines and their first level parameters, namely resistance, inductance, capacitance, and conductance per unit length. Then it proceeds to derive the next level parameters from these, namely characteristic impedance, attenuation constant, phase constant, and propagation velocity. A subroutine, PARAM, was written, which computes second level parameters from the first, for any given frequency.
- The original program package, besides being very practical, is useful as a learning tool because each subroutine parallels a given graphical operation on a Smith chart, such as "enter the Smith chart," or "move the operating point on a constant VSWR circle." Because the method was so successful, it was decided to proceed in the same manner, but to include losses in the line which were neglected. Thus, the present package handles both lossy and lossless transmission lines.
- It is occasionally helpful to be able to determine the voltage as a function of position along the transmission line. A subroutine, CRANK, is included in the new package which allows the designer to determine this voltage.
- Since a great deal of a designer's time is often spent in matching transmission lines to antennas or other loads, it was decided to include a subroutine, MATCH, which allows one to determine the length and position of the required open-circuit or short-circuit matching stub.

An engineer does not have to be an expert programmer in order to use this package. He merely has to write a main program which calls the subroutines describing the operations he would perform on a Smith chart if he were to do a graphical design. All programs are written in standard FORTRAN IV. Complex functions and operations are avoided by carrying out real arithmetic operations on the real and imaginary parts of all complex quantities.

Wilfred J. Remillard, Professor, Northeastern University, 360 Huntington Avenue, Boston, MA 02115.

Service subroutines prepare complex quantities

The three subroutines listed below, POLAR, RECTAN, and RANGLE, are self-explanatory. They are used by the operational and analysis subroutines described in later sections to change mathematical descriptions from rectangular to polar coordinates and vice-versa, and to restrict operating angles to the range of −180 to +180 degrees.

Subroutine POLAR takes rectangular coordinates (X and Y) as inputs and produces the corresponding polar coordinates (RA and THETAD) as outputs. The letter D in THETAD is to remind the programmer that the polar angle is in degrees, not radians.

Subroutine RECTAN takes the polar coordinates (RA and THETAD) as inputs, and produces the corresponding rectangular coordinates (X and Y) as outputs.

Subroutine RANGLE converts any angle (THETAD) to its image in the range −180 to +180 degrees by adding or subtracting a suitable multiple of 360 degrees.

Subroutine computes second-level parameters

The subroutine PARAM takes as input parameters (R, AL, C, G, F) the resistance, inductance, capacitance and conductance per unit length of a transmission line, and the operating frequency. It produces as outputs (RO, XO, ALPHA, BETA) the real and imaginary parts of the characteristic impedance of the line, and the real and imaginary parts of the propagation constant, i. e., the attenuation and phase constants. The propagation velocity can also be obtained from PARAM since the velocity is equal to the radian frequency divided by BETA.

The formulas used by PARAM are:

$$\mathrm{RO}+j\mathrm{XO} = \sqrt{\frac{\mathrm{R}+j\mathrm{W}^*\mathrm{AL}}{\mathrm{G}+j\mathrm{W}^*\mathrm{C}}}$$

$$= \sqrt{\frac{\mathrm{R}+j\mathrm{B}}{\mathrm{G}+j\mathrm{X}}}$$

$$= \sqrt{\frac{\mathrm{ZM}\ \underline{/\mathrm{ZAD}}}{\mathrm{YM}\ \underline{/\mathrm{YAD}}}}$$

1. POLAR: Converts rectangular coordinates to polar form

```
      SUBROUTINE POLAR(X,Y,PA,THETAD)
C
C     CHANGE FROM RECTANGULAR TO POLAR COORDINATES
C
C     INPUT PARAMETERS:
C          X=ABSCISSA
C          Y=ORDINATE
C     OUTPUT PARAMETERS:
C          RA=MAGNITUDE
C          THETAD=ANGLE IN DEGREES BETWEEN -180 and +180
C
      RA=SQRT(X*X+Y*Y)
      THETAD=ATAN2(Y,X) *180./3.141592654
      RETURN
      END
```

2. RECTAN: Converts polar coordinates to rectangular form

```
      SUBROUTINE RECTAN(RA,THETAD,X,Y)
C
C     CHANGE FROM POLAR TO RECTANGULAR COORDINATES
C
C     INPUT PARAMETERS:
C          RA=MAGNITUDE
C          THETAD=ANGLE IN DEGREES
C     OUTPUT PARAMETERS:
C          X=ABSCISSA
C          Y=ORDINATE
C
      THETA=THETAD*3.14159265/180.
      X=RA*COS(THETA)
      Y=RA*SIN(THETA)
      RETURN
      END
```

3. RANGLE: Converts an angle to its image (−180 to +180°)

```
      SUBROUTINE RANGLE(THETAD)
C
C     CHANGES THETAD TO RANGE -180 to +180
C
C     INPUT:
C          THETAD=ANY ANGLE IN DEGREES
C     OUTPUT:
C          THETAD=SAME ANGLE CONVERTED TO RANGE
C                -180.LT.THETAD.LE.+180
C
    1 IF(THETAD.LT.360.)GO TO 2
      THETAD=THETAD-360.
      GO TO 1
    2 IF(THETAD.GE.0.)GO TO 3
      THETAD=THETAD+360.
      GO TO 2
    3 IF(THETAD.GT.180.)THETAD=THETAD-360.
      RETURN
      END
```

4. PARAM: Computes second-level transmission-line parameters

```
      SUBROUTINE PARAM(R,AL,C,G,F,RO,XO,ALPHA,BETA)
C
C     INPUT PARAMETERS:
C          R=RESISTANCE PER UNIT LENGTH
C          AL=INDUCTANCE PER UNIT LENGTH
C          C=CAPACITANCE PER UNIT LENGTH
C          G=CONDUCTANCE PER UNIT LENGTH
C          F=FREQUENCY IN HERTZ
C     OUTPUT PARAMETERS:
C          RO=REAL PART OF CHARACTERISTIC IMPEDANCE
C          XO=IMAGINARY PART OF CHARACTERISTIC IMPEDANCE
C          ALPHA=ATTENUATION CONSTANT
C          BETA=PHASE CONSTANT
C
      PI=3.141592654
      W=2.*PI*F
      B=W*C
      CALL POLAR(R,X,ZM,ZAD)
      CALL POLAR(G,B,YM,YAD)
      ZOM=SQRT(ZM/YM)
      ZOAD=(ZAD-YAD)/2.
      CALL RECTAN(ZOM,ZOAD,RO,XO)
C     TEST FOR NEGATIVE RO
      IF(RO.GE.O)GO TO 1
      RO=-RO
      XO=-XO
    1 GSM=SQRT(ZM*YM)
      GSAD=(ZAD+YAD)/2.
      CALL RECTAN(GSM,GSAD,ALPHA,BETA)
C     TEST FOR NEGATIVE ALPHA
      IF(ALPHA.GE.O.)GO TO 2
      ALPHA=-ALPHA
      BETA=-BETA
    2 RETURN
      END
```

5. REFLECT: Converts impedance to voltage reflection coefficient

```
      SUBROUTINE REFLECT(RO,XO,RR,XR,GM,GAD)
C
C     ENTER SMITH CHART BY OBTAINING REFLECTION COEFFICIENT
C
C     INPUT PARAMETERS:
C          RO=REAL PART OF CHARACTERISTIC IMPEDANCE
C          XO=IMAGINARY PART OF CHARACTERISTIC IMPEDANCE
C          RR=REAL PART OF RECEIVING-END IMPEDANCE
C          XR=IMAGINARY PART OF RECEIVING-END IMPEDANCE
C     OUTPUT PARAMETERS:
C          GM=MAGNITUDE OF REFLECTION COEFFICIENT
C          GAD=ANGLE OF REFLECTION COEFFICIENT IN DEGREES
C              BETWEEN -180 AND 180
C
      CALL POLAR(RR-RO, XR-XO,AN,ANAD)
      CALL POLAR(RR+RO, XR+XO,AD,ADAD)
      GM=AN/AD
      GAD=ANAD-ADAD
      CALL RANGLE(GAD)
      RETURN
      END
```

6. SPIRAL: Rotates a point around the Smith chart

```
      SUBROUTINE SPIRAL(GM1,GAD1,AN,ALPHA, BETA, GM2,GAD2)
C
C     MOVES OPERATING POINT ALONG SPIRAL IN SMIITH CHART FROM
C     STARTING REFLECTION COEFFICIENT TO FINISHING COEFFICIENT
C
C     INPUT PARAMETERS:
C          GM1=MAGNITUDE OF STARTING REFLECTION COEFFICIENT
C          GAD1=ANGLE IN DEGREES OF STARTING REFLECTION COEFFI
C          AN=LENGTH OF LINE IN WAVELENGTHS
C            =POSITIVE FOR MOVEMENT TOWARD GENERATOR
C            =NEGATIVE FOR MOVEMENT TOWARD LOAD
C          ALPHA=ATTENUATION CONSTANT
C          BETA=PHASE CONSTANT
C     OUTPUT PARAMETERS:
C          GM2=MAGNITUDE OF FINISHING REFLECTION COEFFICIENT
C          GAD2=ANGLE (DEGREES) OF FINISHING REFLECTION COEFFICIENT
C               BETWEEN -180 AND 180
C
      DGAD=720.*AN
      GAD2=GAD1-DGAD
      CALL RANGLE(GAD2)
      PI=3.141592654
      ATTN=-4.*PI*ALPHA*AN/BETA
      GM2=GM1*EXP(ATTN)
      RETURN
      END
```

7. IMPED: Restores reflection coefficient to impedance

```
      SUBROUTINE IMPED(RO,XO,GM,GAD,RS,XS)
C
C     LEAVE SMITH CHART BY CHANGING
C     FROM REFLECTION COEFFICIENT TO IMPEDANCE
C
C     INPUT PARAMETERS:
C          RO=REAL PART OF CHARACTERISTIC IMPEDANCE
C          XO=IMAGINARY PART OF CHARACTERISTIC IMPEDANCE
C          GM=MAGNITUDE OF REFLECTION COEFFICIENT
C          GAD=ANGLE OF REFLECTION COEFFICIENT IN DEGREES
C     OUTPUT PARAMETERS:
```

```
C          RS=REAL PART OF SENDING-END IMPEDANCE
C          XS=IMAGINARY PART OF SENDING-END IMPEDANCE
C
      CALL RECTAN(GM,GAD,GR,GI)
      CALL POLAR(1.+GR,GI,AN,ANAD)
      CALL POLAR(RO,XO,ZOM,ZOAD)
      CALL POLAR(1.-GR,-GI,AD,ADAD)
      CALL RECTAN(ZOM*AN/AD,ZOAD+ANAD-ADAD,RS,XS)
      RETURN
      END
```

8. CRANK: Determines voltage at a point on a line

```
      SUBROUTINE CRANK(RO,XO,R,X,AN,ALPHA,BETA,V1,V2)
C
C     USES CRANK METHOD FOR FINDING VOLTAGE V2 AT ANY
C     DISTANCE IN WAVELENGTHS (AN) FROM A POINT ON THE
C     LINE WHERE THE VOLTAGE IS GIVEN AS V1
C
C     INPUT PARAMETERS:
C          RO=REAL PART OF CHARACTERISTIC IMPEDANCE
C          XO=IMAGINARY PART OF THE CHARACTERISTIC IMPEDANCE
C          R=REAL PART OF IMPEDANCE AT POINT WHERE VOLTAGE IS V1
C          X=IMAGINARY PART OF IMPEDANCE WHERE VOLTAGE IS V1
C          AN=DISTANCE IN WAVELENGTHS BETWEEN POINTS WHERE
C               VOLTAGE IS V1 AND VOLTAGE IS V2
C             =POSITIVE WHEN MOVING TOWARD GENERATOR
C             =NEGATIVE WHEN MOVING TOWARD LOAD
C          ALPHA=ATTENUATION CONSTANT
C          BETA=PHASE CONSTANT
C          V1=VOLTAGE AT POINT ON LINE WHERE IMPEDANCE IS R+JX
C     OUTPUT PARAMETER:
C          V2=VOLTAGE AT DISTANCE AN-WAVELENGTHS FROM POINT
C               WHERE VOLTAGE IS V1
C
      PI=3.141592654
      CALL REFLECT(RO,XO,R,X,GM1,GAD1)
      CALL SPIRAL(GM1,GAD1,AN,ALPHA, BETA,GM2,GAD2)
      CALL RECTAN(GM2,GAD2,GR2,GI2)
      CALL RECTAN(GM1,GAD1,GR1,GI1)
      CALL POLAR(1.+GR2,GI2,AT,ANGT)
      CALL POLAR(1.+GR1,GI1,AB,ANGB)
      ATTN=ALPHA*AN*2.*PI/BETA
      V2=V1*AT*EXP(ATTN)/AB
      RETURN
      END
```

9. MATCH: Provides stub dimensions for matching a load and line

```
      SUBROUTINE MATCH(RO,ROS,RR,XR,N,WAVL,WAVLS)
C
C     STUB-MATCHING FOR LOSSLESS LINES AND STUBS
C
C     INPUT PARAMETERS:
C          RO=CHARACTERISTIC IMPEDANCE OF LINE
C          ROS=CHARACTERISTIC IMPEDANCE OF STUB
C          RR=REAL PART OF RECEIVING END IMPEDANCE
C          XR=IMAGINARY PART OF RECEIVING END IMPEDANCE
C          N=0, OPEN-CIRCUIT STUB
C           =1, SHORT-CIRCUIT STUB
C     OUTPUT PARAMETERS:
C          WAVL=WAVELENGTHS BETWEEN LOAD AND STUB
C          WAVLS=LENGTH OF STUB IN WAVELENGTHS
C
      CALL REFLECT(RO,0.,RR,XR,GM,ANG1)
      ANG2=ANG1+180.
      CALL RANGLE(ANG2)
      ANG3=ACOS(GM*180./3.141592654
      CALL IMPED(1.,0.,GM,ANG2,GRN,BRN)
      IF(GRN.GE.1.)WAVL=(ANG3+ANG2)/720.
      IF(ANG2.LT.0.)ANG2=ANG2+360.
      IF(GRN.LT.1.)WAVL=(ANG2-ANG3)/720.
      CALL IMPED(1.,0.,GM,ANG3,G1N,B1N)
      IF(GRN.GE.1.)B1N=-B1N
      B1=B1N/RO
      B2N=-B1*ROS
      CALL REFLECT(1.,0.,0.,B2N,GAM,ANG4)
      IF(ANG4.LT.0.)ANG4=360.+ANG4
      IF(N.NE.0)GO TO 30
      IF(B2N.GE.0.)GO TO 25
      WAVLS=(540.-ANG4)/720.
      RETURN
   25 WAVLS=(180.-ANG4)/720.
      RETURN
   30 WAVLS=(360.-ANG4)/720.
      RETURN
      END
```

$$= \sqrt{\frac{ZM}{YM}} \angle (ZAD\text{-}YAD)/2$$

$$= ZOM \angle ZOAD$$

and

$$ALPHA + jBETA = \sqrt{(R+jW^*AL)\ (G+jW^*C)}$$

$$= \sqrt{ZM \angle ZAD\ YM \angle YAD}$$

$$= \sqrt{ZM^*YM} \angle (ZAD+YAD)/2$$

$$= GSM \angle GSAD$$

An example program, TEST1, that uses PARAM to determine the propagation velocity as a function of frequency in the range of 300 to 4000 Hz, is shown in Fig. 1. The subroutines MINMAX and SIMPLOT used in TEST1 and in later examples are not described in this article since most installations have comparable service routines as part of their library. MINMAX finds the minimum and the maximum values in an array. SIMPLOT[4] produces a plot of one array of values (in this case, velocity) against a second array of values (in this case, frequency). The resulting plot is shown in Fig. 1.

The next three subroutines in the package, REFLECT, SPIRAL, and IMPED, correspond to the operations "enter the Smith chart," "rotate the operating point along a spiral,"

```
      PROGRAM TEST1(INPUT,OUTPUT)
C
C     PROGRAM TO TEST SUBROUTINE PARAM
C
      DIMENSION VP(38),F(38)
      REAL L
      PI=3.14159265
      R=2.56E-3
      L=1.94E-6
      C=6.22E-12
      G=6.8E-11
      DO 1 I=3,40
      J=I-2
      F(J)=100.*FLCAT(I)
C     F IS FREQUENCY IN HZ
      CALL PARAM(R,L,C,G,F(J),RO,XO,ALPHA,BETA)
    1 VP(J)=2.*PI*F(J)/BETA
C     VP IS PROPAGATION VELOCITY
      CALL MINMAX(F,38,FMIN,FMAX)
      CALL MINMAX(VP,38,VPMIN, VPMAX)
      CALL SIMPLOT(FMIN,FMAX,9HFREQUENCY,9,0,F,
     *VPMIN,VPMAX,8HVELOCITY,8,0,VP,38)
      STOP
      END
```

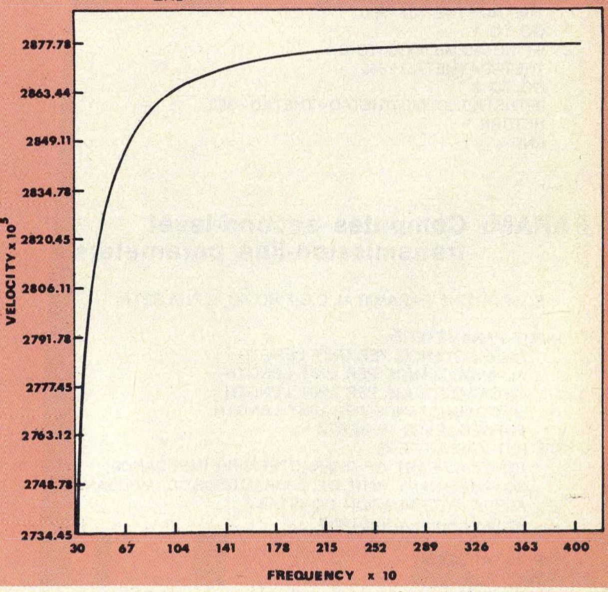

1. Test program uses PARAM *to determine propagation velocity as a function of frequency.*

and "leave the Smith chart," respectively.

Subroutine REFLECT accepts as inputs the real and imaginary parts of the characteristic impedance (RO and XO), and the real and imaginary parts of the receiving end impedance (RR and XR). It produces as outputs the corresponding magnitude and phase of the voltage reflection coefficient (GM and GAD). The formulas used in REFLECT are:

$$\begin{aligned} GM \underline{/GAD} &= \frac{(RR\text{-}RO) + j(XR\text{-}XO)}{(RR+RO) + j(XR+XO)} \\ &= \frac{AN \underline{/ANAD}}{AD \underline{/ADAD}} \\ &= (AN/AD) \underline{/(ANAD\text{-}ADAD)} \end{aligned}$$

Subroutine SPIRAL accepts as inputs the magnitude and phase of the voltage reflection coefficient at the starting point (GM1 and GAD1), the length of the line in wavelengths (AN), and the real and imaginary parts of the propagation constant (ALPHA and BETA). It produces as outputs the magnitude and phase of the voltage reflection coefficient at the finishing point (GM2 and GAD2). AN is positive for movement toward the generator, and negative for movement toward the load. The subroutine first assumes no losses, and rotates the operating point along a circle of constant VSWR. Then, it takes the entire attenuation into account in the last arithmetic statement, GM2=GM1*EXP (ATTN).

Subroutine IMPED accepts as inputs the real and imaginary parts of the characteristic impedance (RO and XO) and the magnitude and phase of the voltage reflection coefficient (GM and GAD). It produces as outputs the real and imaginary parts of the corresponding impedance (RS and XS). The formulas used by IMPED are:

$$\begin{aligned} RS+jXS &= (RO+jXO) \left[\frac{1+GM\underline{/GAD}}{1\text{-}GM\underline{/GAD}} \right] \\ &= ZOM\underline{/ZOAD} \left[\frac{(1+GR)+jGI}{(1\text{-}GR)\text{-}jGI} \right] \\ &= ZOM\underline{/ZOAD} \left[\frac{AN\underline{/ANAD}}{AD\underline{/ADAD}} \right] \\ &= (ZOM{*}AN/AD) \underline{/ZOAD+ANAD\text{-}ADAD} \end{aligned}$$

An example program, TEST2, that uses REFLECT, SPIRAL, and IMPED, is shown in Fig. 2. The transmission line in the problem is composed of four lossless sections, each of different characteristic impedance, and each of length AN. The receiving-end impedance is given as 100+j100 ohms, and the input VSWR is found as a function of AN for AN varying between 0 and 1. The Smith chart is entered (REFLECT) in transmission line section 0 (RO=60 ohms) at the load. The operating point is moved to the input end of this section (SPIRAL), and the Smith chart is exited (IMPED) and reentered (REFLECT) at the load end of the next section (R1=90 ohms). This process is repeated through all four sections. Finally, the VSWR, designated B (I), is found from the formula

B (I) = (1+GM7)/(1-GM7)

where GM7 is the magnitude of the voltage reflection coefficient in the fourth section. All of the above are calculated for 101 different values of AN by placing the calling statements in a DO-loop. Figure 2 shows the resulting graph of VSWR versus line length.

```
      PROGRAM TEST2(INPUT,OUTPUT)
C
C     PROGRAM TESTS REFLECT, SPIRAL, AND IMPED FOR LOSSLESS CASE
C
      DIMENSION B(101),C(101)
      RO=60.
      XO=0.
      R1=90.
      X1=0.
      R2=120.
      X2=0.
      R3=150.
      X3=0.
      RR=100.
      XX=100.
      ALPHA=0.
      BETA=1.
      DO 1 I=1,101
      AN=.01*FLOAT(I-1)
      CALL REFLECT(RO,XO,RR,XX,GM1,GAD1)
      CALL SPIRAL(GM1,GAD1,AN,ALPHA,BETA,GM2,GAD2)
      CALL IMPED(RO,XO,GM2,GAD2,RS,XS)
      CALL REFLECT(R1,X1,RS,XS, GM3,GAD3)
      CALL SPIRAL(GM3,GAD3,AN,ALPHA,BETA,GM4,GAD4)
      CALL IMPED(R1,X1,GM4,GAD4,RT,XT)
      CALL REFLECT(R2,X2,RT,XT,GM5,GAD5)
      CALL SPIRAL(GM5,GAD5,AN,ALPHA,BETA,GM6,GAD6)
      CALL IMPED(R2,X2,GM6,GAD6,RU,XU)
      CALL REFLECT(R3,X3,RU,XU,GM7,GAD7)
      B(I)=(1.+GM7)/1.-GM7)
      C(I)=AN
1     CONTINUE
      CALL MINMAX(B,101,BMIN,BMAX)
      CALL SIMPLOT(0.,1.,8HDISTANCE,8,0,C,BMIN,
     *BMAX,4HVSWR,4,0,B,101)
      STOP
      END
```

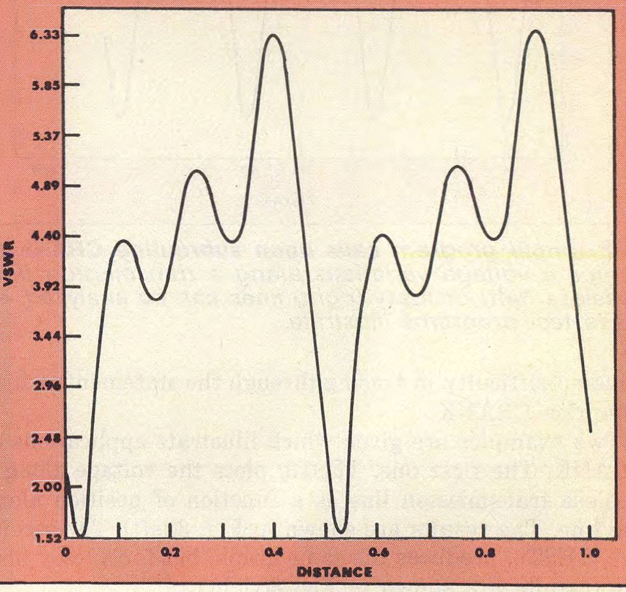

***2. Three subroutines, REFLECT, SPIRAL, and IMPED,** are used to analyze VSWR along a transmission line.*

Subroutines determine voltage, define matching stubs

Subroutine CRANK uses the crank method[5] to determine the voltage at any point on a transmission line if the voltage is known at any other point. It takes as inputs the real and imaginary parts of the characteristic impedance (RO and XO), the real and imaginary parts of the impedance at the point where the voltage is known (R, X), the distance in wavelengths (AN) between the known and unknown voltages, the attenuation constant (ALPHA), the phase constant (BETA), and the known voltage (V1). It produces as an output the unknown voltage (V2). Readers who are familiar with the crank method, and who understand the operational and service subroutines described in previous sections, will

```
      PROGRAM TEST3(INPUT,OUTPUT)
C
C     THIS PROGRAM TESTS CRANK FOR THE LOSSLESS CASE
C
      DIMENSION V1(151),A(151)
      R=1.52627
      X=3.2521
      DO 1 I=1,151
      A(I)=FLOAT(I-1)
      J=152-I
      AN=2.*A(I)/150.
      CALL CRANK(1.,0.,R,X,AN,0.,1,1.,V1(J))
    1 CONTINUE
      CALL SIMPLOT(0.,150.,8HDISTANCE,8,0,A,0.,1.5,
     *7HVOLTAGE,7,0,V1,151)
      STOP
      END
```

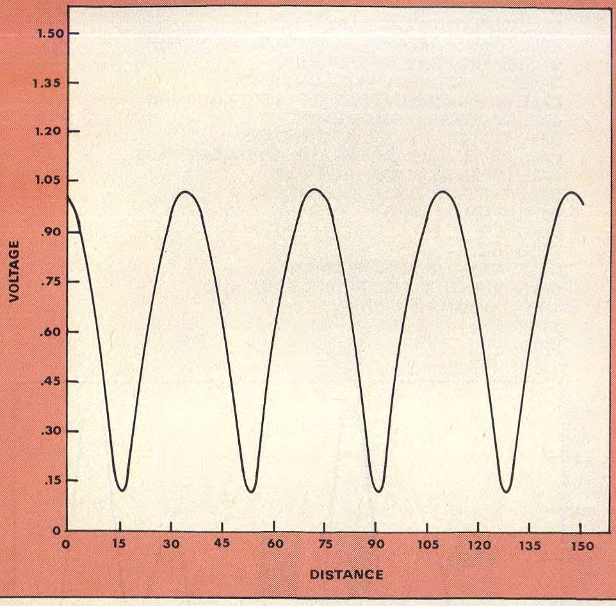


```
      PROGRAM TEST4(INPUT,OUTPUT)
C
C     THIS PROGRAM TESTS CRANK FOR THE LOSSY CASE
C
      DIMENSION V1(151),A(151)
      R=1.52627
      X=3.2521
      DO 1 I=1,151
      A(I)=FLOAT(I-1)
      J=152-I
      AN=2.*A(I)/150.
      CALL CRANK(1.,0.,R,X,AN,.0025,.1,1.,V1(J))
    1 CONTINUE
      CALL MINMAX(V1,151,VMIN,VMAX)
      CALL SIMPLOT(0.,150.,8HDISTANCE,8,0,A,VMIN,
     *VMAX,7HVOLTAGE,7,0,V1,151)
      STOP
      END
```

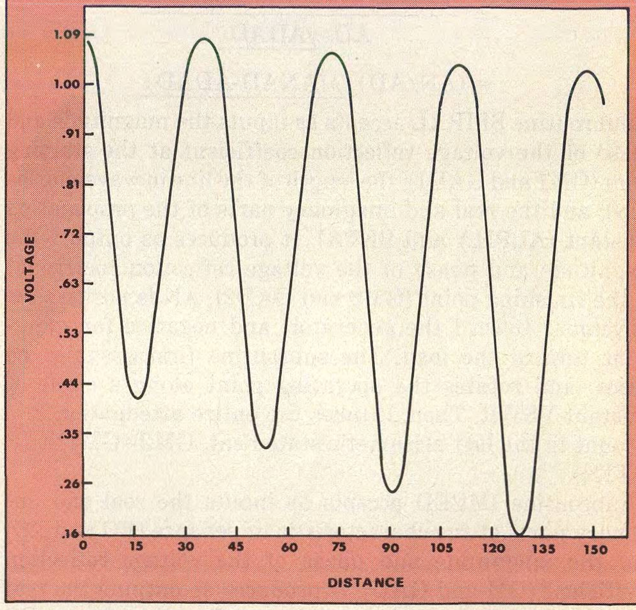

***3. Example program calls upon subroutine CRANK** to compute voltage variations along a transmission line. Lossless (left) or lossy (right) lines can be analyzed, as these test programs illustrate.*

have no difficulty in tracing through the statements which comprise CRANK.

Two examples are given which illustrate applications of CRANK. The first one, TEST3, plots the voltage along a lossless transmission line as a function of position along the line. The results are shown in Fig. 3(left). The second one, TEST4, produces the same graph, but for a lossy line. The results are shown in Fig. 3(right).

The last subroutine in the package, MATCH, is used for stub matching of a load to a lossless transmission line. It takes as inputs the characteristic impedance of the line (RO), the characteristic impedance of the stub (ROS), the real and imaginary parts of the load impedance (RR and XR), and an integer (N). When designing for an open-circuit stub, N is chosen as 0, and when designing for a short-circuit stub, N is chosen as 1. The outputs of MATCH are the distance from the load to the stub (WAVL) and the length of the stub (WAVLS).

MATCH uses the following procedure. First, the Smith chart is entered (REFLECT) at the load. The line impedance is then changed to an admittance by a 180-degree rotation on a constant VSWR circle. The phase angle (ANG3) of the voltage reflection coefficient is determined at the stub location. If the operating point for the load admittance lies outside the circle, r=1, the distance from the load to the stub is given by (ANG2-ANG3)/720, see Fig. 4. Otherwise, this distance is given by (ANG2+ANG3)/720. The determination of the length of the stub (WAVLS) follows in a similar straightforward manner.

An example, TEST5, is given, which determines the position and the length of a short-circuit stub as a function of frequency in the range 1 to 10 MHz. The characteristic impedance of the line (RO) is 100 ohms, while the characteristic impedance of the stub (ROS) is 50 ohms. The load consists of a resistance (RR) of 25 ohms in series with an inductance (AL) of 10^{-5} henries. The graph of WAVL and WAVLS versus frequency is shown in Fig. 5.

The package of subroutines presented in this article has proven to be useful as a design tool, and also as a learning mechanism for students just beginning in the field of microwaves. It is easy to use because the calling routines are simple to program, and the subroutines correspond to graphical operations used in analysis and design. Because distributed systems are not limited to transmission lines, these routines are also useful in the design of many other systems. For example, the author has found them invaluable in studies of underwater sound (ray tracing, etc.), and in architectural acoustics.••

References

1. P. H. Smith, "Transmission Line Calculator," *Electronics*, Vol. 12, No. 1, pp. 130-133, 318-325, (January, 1944).
2. W. C. Blanchard, "New and More Accurate Inside-Out Smith Chart," *MicroWaves*, Vol. 6, No. 11, pp. 38-42, (November, 1967).
3. Joseph W. Verizno, "Computer Programs For Smith-Chart Solutions (Part 1)," *MicroWaves*, Vol. 7, No. 7, pp. 57-61, (July, 1968).
4. Franklyn K. Brown, "Digital Computer Plotting," Northeastern University, (1969).
5. S. R. Seshadri, *Fundamentals of Transmission Lines and Electromagnetic Fields*, Addison-Wesley Publishing Company, (1971).

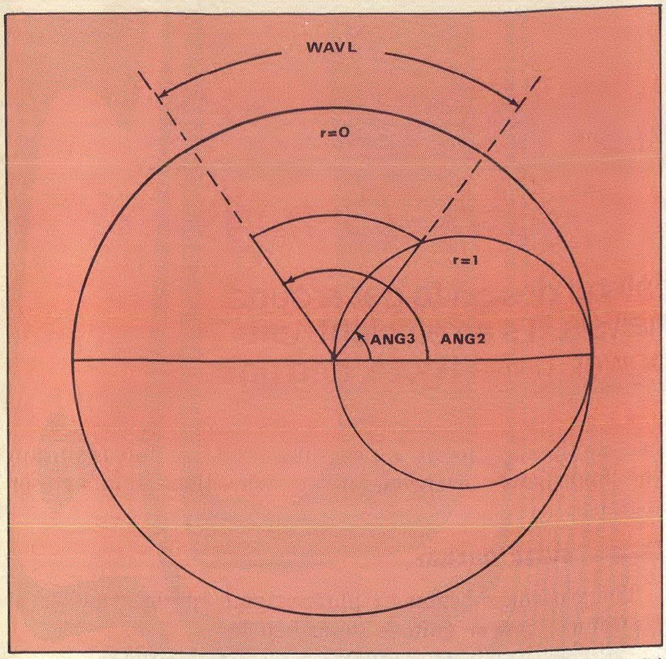

4. *A simple polar chart* *indicates whether angles should be summed or subtracted in MATCH.*

```
      PROGRAM TEST5(INPUT,OUTPUT)
C
C     THIS PROGRAM TESTS MATCH
C
      DIMENSION Z(202),F(202)
      RR=25.
      AL=1.E-5
      PI=3.141592654
      RO=100.
      ROS=50.
      DO 1 I=1,101
      F(I)=(91.+9.*FLOAT(I))*1.E4
      F(I+101)=F(I)
      XR=2.*PI*F(I)*AL
      CALL MATCH(RO,ROS,RR,XR,1,WAVL,WAVLS)
      Z(I)=WAVL
    1 Z(I+101)=WAVLS
      CALL MINMAX(Z,202,ZMIN,ZMAX)
      Z(101)=100.
      CALL SIMPLOT(1.E6,1.E7,9HFREQUENCY,9,0,F,
     *ZMIN,ZMAX,9HW-LENGTHS,9,0,Z,202)
      STOP
      END
```

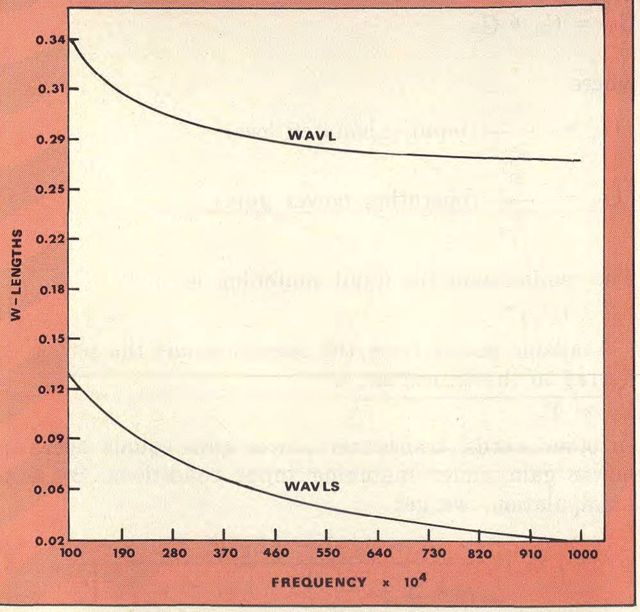

5. *Position (WAVL) and length (WAVLS)* *of matching stub are plotted for a range of frequencies specified by this test program.*

Easy-to-Plot Graphs Show Power-Gain Tradeoffs

Tired of plotting in circles? Try bilateral design to get around confusing low-power amplifier analysis. It's an efficient, universal tool that bullseyes output power, noise figure, and gain.

EFFICIENCY, being uppermost in the mind of the RF engineer charged with squeezing the last milliwatt out of a low-power amplifier design, is the ultimate Damoclesean sword. In attempting to extract maximum linear RF output power from a given input DC power, the designer realizes that one edge chops him down at a specific input level, while the other slices efficiency at other than a specific loading condition.

Plotting low-power efficiency need not leave the engineer hanging by a hair. Bilateral design, an analytic tool that enlists active-device scattering parameters, enables the designer to graphically visualize output power versus gain and input noise figure versus gain, at the preliminary design stages. It is a universal method that can be applied to amplifiers in which silicon bipolars, field effects, and GaAs FETs—anything that can be characterized by a set of s-parameters—are the active devices.

Bilateral design offers two advantages:

- constant-gain circles can be plotted as a function of load on a Smith chart when the input is matched, and
- constant output power circles can be calculated as a function of load. When these two families of circles are plotted on the same Smith chart, tradeoffs between gain and output power immediately become apparent. Furthermore, the points of tangency between the two families of circles and their loci are calculated as well; for a given output power, it is possible to pinpoint optimum load versus maximum gain.

Similarly, the technique works as well to describe input impedance. Constant gain circles can be plotted as a function of input impedance for a matched output. When this family of circles is plotted on a Smith chart together with constant noise figure circles, noise figure versus gain tradeoffs may further be used to blunt the blade.

Basically, bilateral design takes a three-step approach:

- the scattering parameters of the device are taken, either from a manufacturer's data sheet or via a network analyzer,
- calculations of seven criteria affecting maximum gain are performed, and
- a series of gain circles are constructed from matched input and output conditions. The designer does not solve for one answer; a locus of load reflection coefficients of the circles yields the same output power. The designer, now able to see the circles depicting maximum gain and output power, can manipulate the DC quiescent point (and thus maintain the input power level constant) to draw these points closer together.

David Rosemarin and **Moty Chorev**, One Sapir Street, Ramat Gan, Israel.

Output stage design

The procedure begins by plotting gain circles.[1,2] Bilateral transducer power gain is described by:

$$G_T = |S_{21}|^2 \bullet \frac{1-|\Gamma_s|^2}{|1-S'_{11}\Gamma_s|^2} \bullet \frac{1-|\Gamma_L|^2}{|1-S_{22}\Gamma_L|^2} \qquad (1)$$

where

$$S'_{11} = S_{11} + \frac{S_{12}S_{21}\Gamma_L}{1-S_{22}\Gamma_L}$$

The reflection coefficients of source and load are written Γ_s and Γ_L, respectively. Bilateral transducer power gain may be generally considered as:

$$G_T = \frac{\text{Power delivered to load}}{\text{Power available from source}}$$

$$= \frac{P_\alpha}{P_{av}} = \frac{P_{in}}{P_{av}} \times \frac{P_\alpha}{P_{in}}$$

or

$$G_T = G_S \bullet G_P$$

where

$$G_S = \frac{P_{in}}{P_{av}} \text{ (input mismatch loss)}$$

$$G_P = \frac{P_\alpha}{P_{in}} \text{ (operating power gain)}$$

The requirement for input matching is:

$$\Gamma_s = (S'_{11})^* \qquad (2)$$

Available power from the source equals the power delivered to the transistor, or

$$P_{in} = P_{av} \qquad (3)$$

In other words, transducer power gain equals operating power gain under matching input conditions. By some manipulation, we get

$$G_P = |S_{21}|^2 \frac{1-|\Gamma_L|^2}{|1-S_{22}\Gamma_L|^2 - |S_{11}-\Delta\Gamma_L|^2} \qquad (4)$$

where

$$\Delta = S_{11}S_{22} - S_{12}S_{21}$$

Table I. Constant Gain Circles

g(dB)	DISTANCE(−R)	RADIUS(−ρ)
6.63	0.957	0
5.63	0.881	0.117
4.63	0.786	0.213
3.63	0.692	0.308
2.63	0.601	0.399
1.63	0.516	0.484

Table II. Constant Output Power Circles

P_{out}(dB)	G_L(mmho)	Distance R	Radius ρ	Γ_{opt}†	
−10	20.0	0.500	0.500	0.219	102.66°
−5	6.32	0.240	0.760	0.588	52.14°
−2	3.17	0.137	0.863	0.768	49.28°
0 = 25 mW	2.0	0.091	0.909	0.847	48.73°
−10	0.2	0.010	0.990	0.983	48.38°
−20	0.02	0.001	0.999	0.998	48.38°

Notes: (1) G_L calculated via Eqs. 12 or 13
(2) Distance R calculated via Eqs. 14 and 15
(3) Radius ρ calculated via Eqs. 14 and 16
(4) Γ_{opt} calculated via Eq. 19

Γ_{opt}† Inserting the value of Γ_{opt} instead of Γ_L in Eq. 4 solves for maximum power gain available for a given output power.

Operating power gain can be expressed as:

$$G_P \triangleq |s_{21}|^2 \bullet g \qquad (5)$$

For constant operating gain, taking g as a parameter, we get a family of circles on a Smith chart. The centers of the circles are located at:

$$r = \frac{g \bullet c_2^*}{1 + g(|s_{22}|^2 - |\Delta|^2)} \qquad (6)$$

where

r is a radius vector from center of the Smith chart. The vector radii are:

$$\rho = \frac{(1 - 2K\,g\,|s_{12}s_{21}| + g^2|s_{12}s_{12}|^2)^{1/2}}{1 + g(|s_{22}|^2 - |\Delta|^2)} \qquad (7)$$

where

$$c_2 \triangleq s_{22} - \Delta\, s_{11}^*$$

$$\Delta \triangleq s_{11}s_{22} - s_{12}s_{21}$$

and

$$K \triangleq \frac{1 + |\Delta|^2 - |s_{11}|^2 - |s_{22}|^2}{2|s_{12}s_{21}|}$$

If the value K is greater than unity, maximum gain is:

$$G_{PMAX} = G_{TMAX} = \left|\frac{s_{21}}{s_{12}}\right| K_m \qquad (8)$$

where:

$$K_m \triangleq K \mp \sqrt{K^2 - 1}$$

In the preceeding expression, use a plus sign when B_1 is negative, a minus sign when B_1 is positive.

$$B_1 \triangleq 1 + |s_{11}|^2 - |s_{22}|^2 - |\Delta|^2$$

$$B_2 \triangleq 1 + |s_{22}|^2 - |s_{11}|^2 - |\Delta|^2$$

Thus, the load reflection coefficient for maximum gain is:

$$\Gamma_{ML} = \frac{B_2 \mp \sqrt{B_2^2 - 4|c_2|^2}}{2c_2} \qquad (9)$$

Constant power circles

The power calculations rely on knowing the collector load admittance, in a bipolar design. The linear output power delivered to a load is largely determined by the shunt load resistance. In other words, the output power is determined from the output conductance. It is important to realize that the transistor delivers maximum power to the load not only when the load conductance is chosen, but also when the collector current and voltage are in phase and operate along a truly resistive load line. Or, the susceptive part of the load must conjugately match the transistor output susceptance.

From the quiescent point determined by V_{CC}, and I_C, the quiescent load conductance, G_o (the slope of the load line), can be calculated.

$$G_o\ (\text{mmho}) = \frac{I_c\ (\text{mA})}{V_{cc}\ (\text{V})} \qquad (10)$$

The maximum linear output power is:

$$P_{MAX}\ (\text{mW}) = \frac{I_c^2}{2G_o} \qquad (11)$$

Actual conductance, G_L, which is greater or smaller than G_O, is considered as:

$$|G_L| > |G_o|$$

thus

$$P_L\ (\text{mW}) = \frac{I_c^2}{2G_L}$$

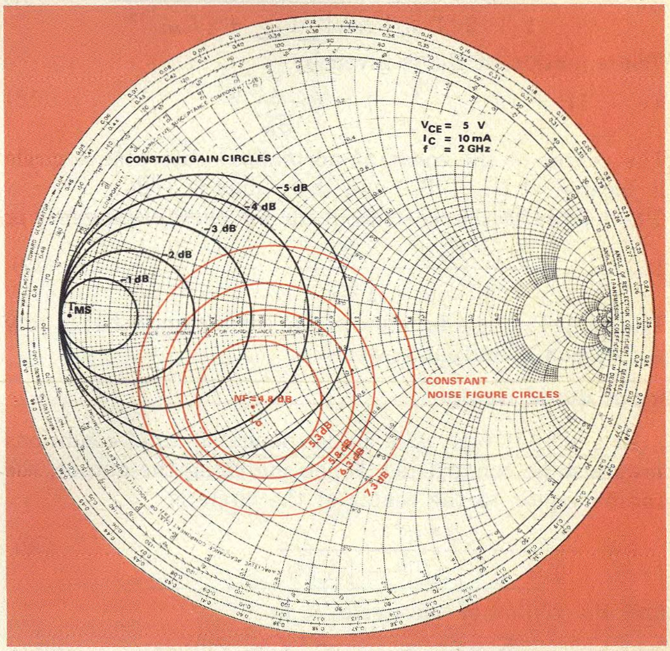

*1. **For the points of tangency,** the load susceptance is a conjugate match to the transistor susceptance.*

from which we get the expression

$$G_L = G_o \frac{P_{MAX}}{P_L} \qquad (12)$$

For $|G_L| < |G_o|$

$$P_L(mW) = \frac{V_{cc}^2}{2} G_L$$

from which we get

$$G_L = G_o \frac{P_L}{P_{MAX}} \qquad (13)$$

The ratio P_L/P_{max}, which is less than unity, can be expressed in dB. It is called P (dB). For each ratio, two values of load conductance are achieved. The normalized conductance, G_{LN}, is:

$$G_{LN}\ (mmho) = \frac{G_L\ (mmho)}{20} \qquad (14)$$

The contour of constant conductance is a circle in which the center lies on $\Gamma = 1\ \angle 180°$. The center of the constant conductance circle, r, is:

$$r = \frac{G_{LN}}{1 + G_{LN}} \qquad (15)$$

and its radius is:

$$\rho = \frac{1}{1 + G_{LN}} \qquad (16)$$

The family of constant conductance circles is equivalent to the constant output power circles.[3]

Balance gain and power

When plotting the two families of circles, Fig. 1, a tradeoff between gain and linear output power is apparent. To find the points of tangency of the two families, take the following approach. Bodway's transformation expresses the impedances referred to the matched generator and load impedances. The calculations show that the locus of the points of tangency is a constant normalized susceptance, independent of constant power circles. The locus is given by:

$$B_N = -\frac{2\,|\Gamma_{ML}|\sin\angle\Gamma_{ML}}{1 + 2\,|\Gamma_{ML}|\cos|\angle\Gamma_{ML}| + |\Gamma_{ML}|^2} \qquad (17)$$

The equation of B_N is given by:

$$(u + 1)^2 + (v + \frac{1}{B_N^2}) = (\frac{1}{B_N})^2 \qquad (18)$$

The center of the constant normalized susceptance circle is located at $(-1, 1/B_N)$ and the radius is $1/B_N$.

The load reflection coefficient for the point of tangency is:

$$\Gamma_{opt} = \frac{1 - G_{LN} - j\,B_N}{1 + G_{LN} + j\,B_N} \qquad (19)$$

The value Γ_{opt} is a function of the conductance that is only a function of output power.

Input stage design

In a similar way, gain circles depicting input conditions may also be constructed. When matching the output, the radius vector to the center of the circle is:

$$r = \frac{g \bullet c_1^*}{1 + g\,(|S_{11}|^2 - |\Delta|^2)} \qquad (20)$$

and the radius of the circle, ρ, is:

$$\rho = \frac{(1 - 2K\,g\,|S_{12}S_{21}| + g^2\,|S_{12}S_{21}|^2)^{1/2}}{1 + g\,(|S_{11}|^2 - |\Delta|^2)} \qquad (21)$$

where

$$c_1 \triangleq S_{11} - \Delta\,S_{22}^*.$$

The final step is to plot noise figure circles. The centers are located at:

$$r = \frac{\Gamma_o}{1 + N_i} \qquad (22)$$

and the radii are at:

$$\rho = \frac{1}{1 + N_i}\sqrt{N_i^2 + N_i\,(1 - |\Gamma_o|^2)} \qquad (23)$$

where

$$N_i = \frac{F - F_{MIN}}{4R_N}\,|1 + \Gamma_o|^2$$

F_{MIN} = minimum noise figure
R_N = equivalent input noise resistance
Γ_o = source reflection coefficient required for F_{MIN}

After the two families of circles are plotted, a tradeoff between gain circles and noise figure circles, as a function of source reflection coefficient, can be attempted.

As an example of bilateral design, a bipolar device is considered, in which the load impedance for maximum output power is determined when the input is matched. The gain is also calculated. The s-parameters of the transistor, an HP 35866E, are given by:

$S_{11} = 0.530\ \angle -166°$
$S_{12} = 0.056\ \angle 39°$
$S_{21} = 3.64\ \angle 71°$
$S_{22} = 0.60\ \angle -40°$

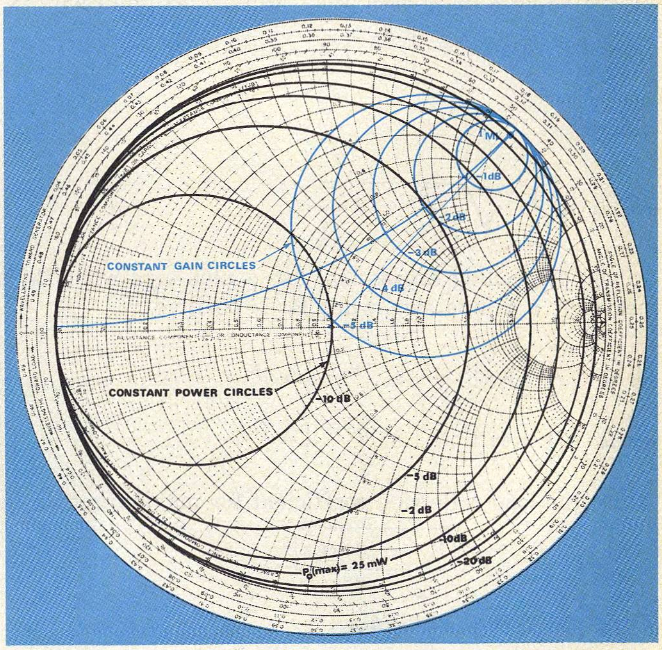

***2. The constant gain circles** are taken from Table I. The circles are constructed in 1-dB steps, according to Equations 5, 6, and 7. The constant power output circles are taken from Table II.*

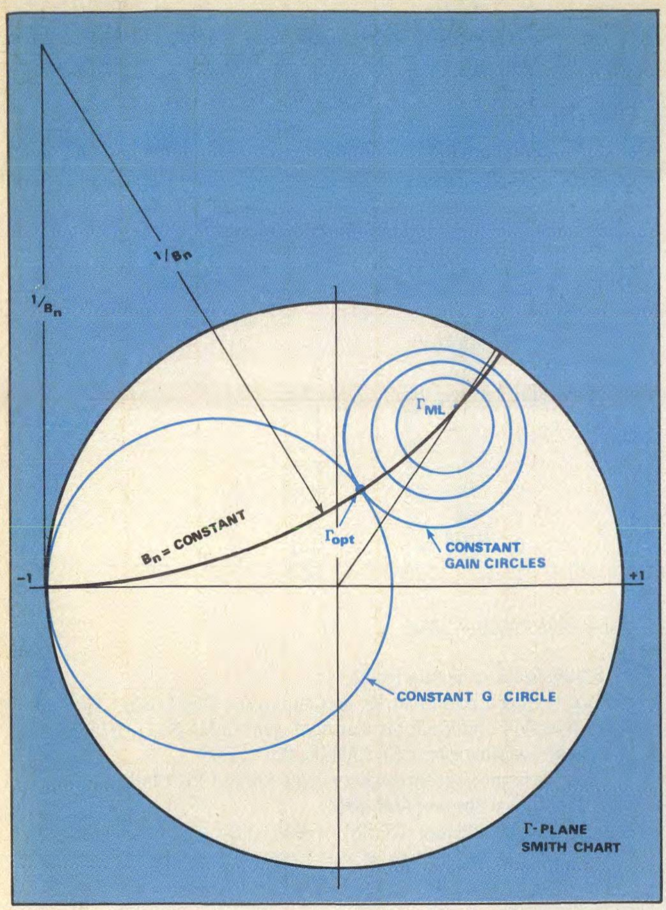

3. The tradeoff between amplifier noise figure versus constant gain *becomes apparent when the respective circles are plotted on the same Smith chart.*

and the bias is:

$V_{CE} = 5v$

$I_C = 10$ mA

The solution follows:

Stability factor (Eq. 7)

$$K = 1.002$$

Maximum gain (Eq. 8)

$$G_{PMAX} = 17.85 \text{ dB}$$

Reflection coefficient for maximum gain (Eq. 9)

$$\Gamma_{ML} = 0.975 \angle 48.4°$$

Gain circles (input matched) (Eqs. 5, 6, 7)

$$\bar{G}(dB) = 10 \log |s_{21}|^2 = 11.22 \text{ dB}$$

$$g_{MAX} = G_{PMAX} - \bar{G}(dB) = 6.63 \text{ dB}$$

The gain circles are constructed in 1-dB steps, as shown in Table 1.

Optimum conductance (Eq. 10)

$$G_O = 2 \text{ (mmho)}$$

Conductance (or power) circles of maximum power (Eq. 11)

$$P_{MAX} = 25 \text{ (mW)}$$

The locus of points of tangency of the two families of circles is a constant susceptance circle (Eq. 17) where

$$B_N = -0.449.$$

The circle has a center at (−1, 2.23) (Eq. 18) and a radius of 2.23. The radius and center of conductance circles, as well as the point of tangency, are shown in Table II.

The plot in Fig. 2 shows that maximum gain, which is identical to Γ_{ML}, falls on the −20 dB linear output power circle, which corresponds to 0.25 mW. Using the circle of maximum output power (25 mW) at the point of tangency, the gain lies within the −1 dB constant gain circle. To calculate the gain degradation, take Γ_{opt} from Table II. From the table, Γ_{opt} equals 0.847 $\angle 48.73°$. Inserting this in Eq. 4, power gain is:

$$G_p = 17.28 \text{ dB}$$

The final answer is:

$$G_p - G_{pmax} = 17.28 - 17.85 = -0.57 \text{ dB}$$ ••

S—PARAMETERS AMPLIFIER DESIGN

Transistor: HP35866E
Bias: 5.0 V, 10 mA
Frequency: 1500.0 MHz

S11=	.530	-166.0
S12=	.056	39.0
S21=	3.640	71.0
S22=	.600	-40.0

Stability Factor = 1.002

UNILATERAL CALCULATIONS

Unilateral figure of merit, U = .141

GT = Transducer power gain = P delivered to load / P available from source
GTU = Unilateral transducer power gain under the assumption of S12=0
GTU (dB) = GS (dB) + GO (dB) + GL (dB)
Where GS (dB) = Gain of input matching network
GO (dB) = 20*Log (S21)
GL (dB) = Gain of output matching network

Maximum unilateral transducer gain, GTUMAX (dB) = 14.592
Maximum gain of input network, GSMAX (dB) = 1.432
Maximum gain of output network, GLMAX (dB) = 1.938

Input Constant Gain Circles
D1 = Distance of center of circle from center of Smith chart
R1 = Radius of the circle

GS (dB)	D1	R1
-5	.154	.807
-4	.190	.760
-3	.233	.701
-2	.284	.628
-1	.344	.535
0	.414	.414
1	.493	.227

Output Constant Gain Circles
D2 = Distance of center of circle from center of Smith chart
R2 = Radius of the circle

GL (dB)	D2	R2
-5	.170	.802
-4	.209	.755
-3	.255	.698
-2	.309	.629
-1	.371	.545
0	.441	.441
1	.520	.303

BILATERAL CALCULATIONS

Simultaneous conjugate match
Source reflection coefficient for maximum gain, GAMA (MS) = .970, 177.2
Load reflection coefficient for maximum gain GAMA (ML) = .975, 48.4
Maximum available gain (dB), GAMAX (dB) = 17.85
Input constant transducer gain circles (Output matched)
Center of the circles on GAMA (MS)
GS = GT/GAMAX GS (dB) = GT (dB) - GAMAX (dB)
D1 = Distance of center of circle from center of Smith chart
R1 = Radius of the circle

GS (dB)	D1	R1
0	.970	.000
-1	.862	.135
-2	.756	.242
-3	.655	.344
-4	.560	.439
-5	.474	.526

Output constant transducer gain circles (Input matched)
Center of the circles on GAMA (ML)
GL = GT/GAMAX GL (dB) = GT (dB) - GAMAX (dB)
D2 = Distance of center of circle from center of Smith chart
R2 = Radius of the circle

GL (dB)	D2	R2
0	.975	.000
-1	.881	.117
-2	.786	.213
-3	.692	.308
-4	.601	.399
-5	.516	.484

Data was taken from the computer program shown *to plot circles on the Smith chart for the design of input and output stages. For example, when the circuit is adjusted for simultaneous conjugate match, linear output power decreases by 20 dB referred to the maximum output power available. But it is possible to achieve maximum power with a decrease of only 0.5 dB in gain.*

References

1. Hewlett-Packard, High Frequency Circuit Design Seminar.
2. Ralph S. Carson, *High Frequency Amplifiers*, John Wiley & Sons, New York, (1975)
3. K. Richter, "Predicting Linear Power Amplifier Performance," *Micro Waves*, Vol. 13, No. 2, pp. 56-59 (February, 1974).
4. G. E. Bodway, "Two Port Power Flow Analysis Using Generalized Scattering Parameters," *Microwave Journal*, Vol. 10, No. 6 (May, 1967).

Output Constant Conductance Circles
Center of the circles on B = 0 line
GO = IC/VCE   PMAX = (VCE*IC)/2 = 25.00 mW
IF G>GO Then P = PMAX *GO/G
IF G<GO Then P = PMAX * G/GO
D = Distance of center of circle from center of Smith chart
R = Radius of the circle
GAMA (L) = Point of tangency
GL (dB) = Gain at GAMA (L)
The locus of all points of tangency of constant power circles
and constant gain circles is a constant susceptance circle
Norm B = -.449
The radius of this circle is 2.226
The center of this circle is 2.441   114.188

G(MMHO)	P(dB)	D	R	GAMA(L)		GL (dB)
200.000	-20	.909	.091	.819	179.48	-13.149
20.000	-10	.500	.500	.219	102.66	-4.641
6.325	-5	.240	.760	.588	52.14	-1.944
3.991	-3	.166	.834	.717	49.83	-1.256
3.170	-2	.137	.863	.768	49.28	-.987
2.518	-1	.112	.888	.811	48.95	-.761
2.000	0	.091	.909	.847	48.73	-.575
1.589	-1	.074	.926	.876	48.60	-.422
1.262	-2	.059	.941	.900	48.52	-.300
1.002	-3	.048	.952	.920	48.47	-.203
.632	-5	.031	.969	.949	48.41	-.072
.200	-10	.010	.990	.983	48.38	-.024
.020	-20	.001	.999	.998	48.38	-1.465

NOISE FIGURE

Minimum noise figure (Ratio), FMIN = 3020E+01
Minimum noise figure (dB) = 4.8
Equivalent input noise resistance, RN = .800
Source reflection coefficient for FMIN, GAMA = .430, -133

Noise Figure Circles
F = Noise figure desired
C = Center of circle
R = Radius of circle

F (dB)	C	R
4.8	.430	.000
5.3	.402	.231
5.8	.375	.327
6.3	.349	.401
6.8	.323	.462
7.3	.299	.516
7.8	..275	.563

Take the Guesswork Out of Thick Microstrip K

Don't guess thickness correction when calculating the effective dielectric constant of thick microstrip. Instead, use a simple graph to put K_{eff} on the line.

TO simplify the analysis of thin microstrip lines, make a zero-thickness conductor approximation. But when considering lines with thicker conductors such as those found on copper-clad circuit boards, make believe you never heard of the zero-thickness approximation.

The characterization of microstrip structures used as TEM transmission lines has been the subject of many recent papers.[1,2] Two major parameters appear in most: characteristic impedance (Z) and effective dielectric constant (K_{eff}). The characteristic impedance is defined as the ratio of instantaneous voltage to current at a particular point on the line. The effective dielectric constant is the dielectric constant of a homogeneous material having the same phase velocity as the inhomogeneous microstrip transmission line.

The K_{eff} and Z parameters of thick microstrip lines have been calculated [3,4], but not in a way that can be easily duplicated. In the process of calculating the K_{eff} of thick microstrip lines, a high-capacity digital computer was used. This is a drawback for the designer having access to only a handheld or desktop calculator.

Wheeler's dilemma

In his benchmark paper on thick microstrip line, H. A. Wheeler[5] briefly discusses a width correction factor applied to the zero thickness case to compensate for the effects of a thicker-than-zero conductor. Others[6,7] have repeated Wheeler's compensating expression, and have expanded on his work to determine the attenuation constant of microstrip lines.[8,9]

The problem is, Wheeler formulated for free space, where the material has a relative dielectric constant of 1. As Wheeler points out, the expression becomes less accurate as the dielectric constant increases; he suggests dividing the width correction factor by the relative dielectric constant. This works for Z but not for K_{eff}.

TUCLIV solves the dilemma

A computer program, TUCLIV, may be used to characterize thick microstrip more accurately. The program encompasses strip width, substrate height, and conductor thickness at a specific dielectric constant, Fig. 1 (a). An example of the data obtained from TUCLIV is shown in Fig. 2; microstrip parameters are plotted for strip-width-to-substrate-height ratios (W/H) and conductor-thinkness-to-

Kurt P. Schwan*, Member of the Staff, MIT Lincoln Laboratory, 244 Wood Street, Lexington, MA 02173.
*Work done while employed at Rockwell International

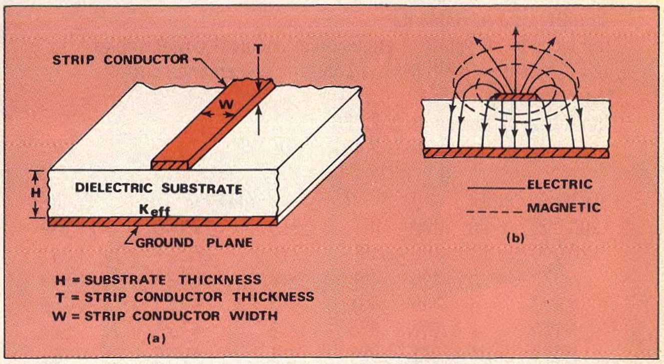

1. A thick microstrip transmission line, seen in cross section, has a finite dielectric substrate thickness, as well as strip conductor thickness and width. These factors are usually quantified as zero-thickness approximations (a). As the conductor becomes thicker, lines below the conductor (in the dielectric) are affected slightly while the number of lines above the dielectric increase (b).

Thick Microstrip Characteristics (K=10)

TUCLIV			vs. WHEELER			
			No 1/K		With 1/K	
W/H	Z	K_{eff}	Z	K_{eff}	Z	K_{eff}
T/H = 0.0						
0.2	89.00	6.154	89.43	6.129		
1.0	48.66	6.708	49.02	6.674		
2.0	32.98	7.177	32.78	7.400		
T/H = 0.002						
0.2	88.61	6.125	88.80	6.134	89.37	6.130
1.0	48.48	6.700	48.90	6.677	49.01	6.674
2.0	32.98	7.172	32.73	7.402	32.77	7.401
T/H = 0.012						
0.2	87.38	6.017	86.61	6.151	89.13	6.132
1.0	48.28	6.661	48.47	6.688	48.96	6.675
2.0	32.91	7.150	32.55	7.409	32.76	7.401
T/H = 0.078						
0.2	82.16	5.616	78.64	6.218	88.12	6.139
1.0	47.14	6.454	46.64	6.737	48.77	6.680
2.0	32.46	7.005	31.78	7.438	32.68	7.404

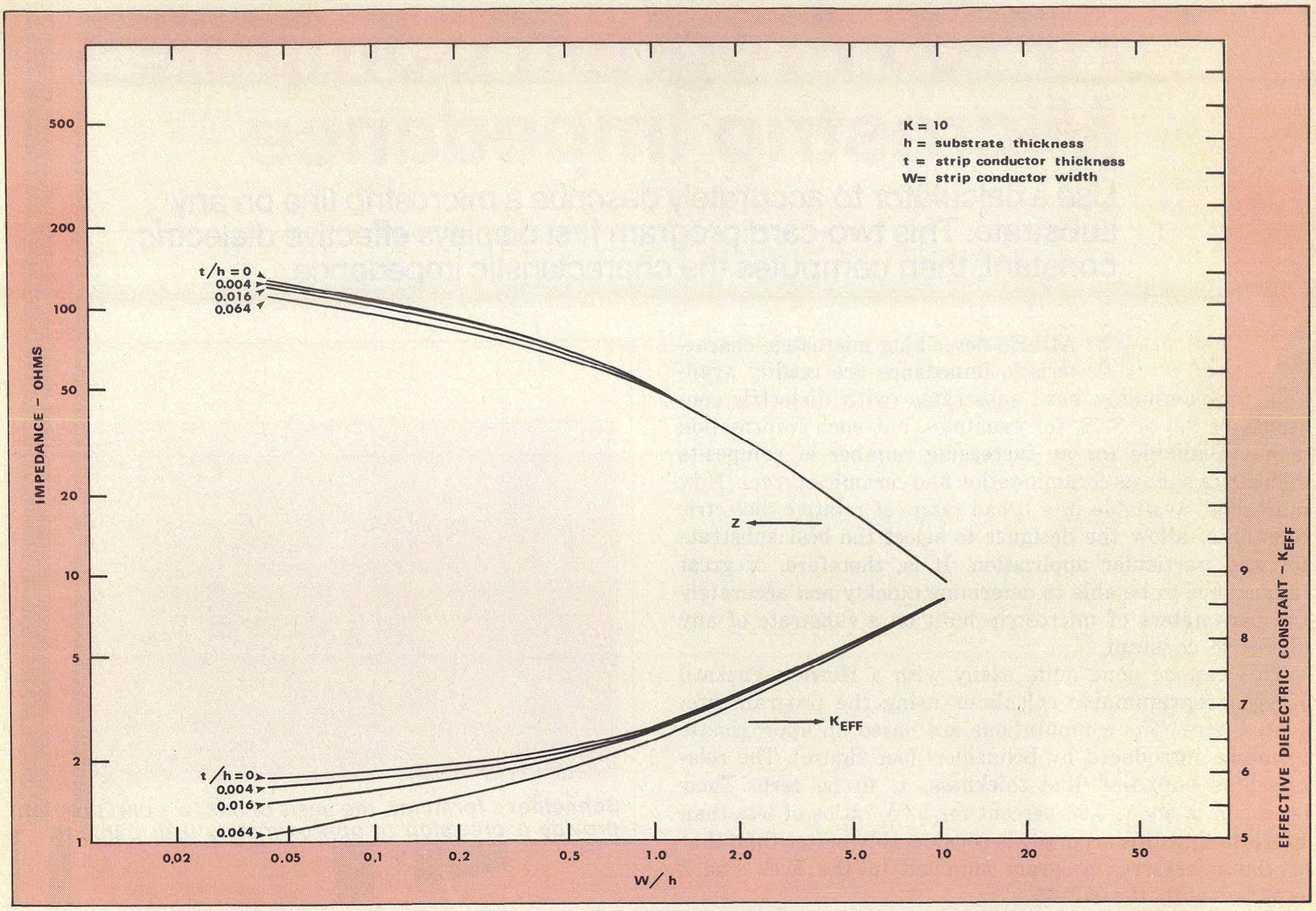

2. The computer program TUCLIV is used to generate the plots of microstrip parameters. Various strip-width-to-substrate-height ratios (W/H) and conductor-thickness-to-substrate-height ratios (T/H) are given for a dielectric constant (K) = 10.

substrate-height ratios (T/H) for a substrate dielectric constant (K) = 10. The table shows values of Z and K_{eff} generated via TUCLIV, and compares the values against those calculated using Wheeler's formulas, both with and without additional correction of dividing by the dielectric constant (1/K).

For zero thickness (T/H = 0) there is good agreement between Wheeler and TUCLIV. However, as conductor thickness increases, both impedance values calculated by Wheeler's formulas diverge from the TUCLIV values. This is to be expected, when you remember Wheeler's comments regarding the intuitive nature of the correction factor.

The table serves yet another purpose. It emphasizes the discrepancies when the designer relies on a fudge factor for K_{eff}. Using Wheeler's formulas, the effective dielectric constant increases as the conductor size increases. In other words, K_{eff} is going the wrong way. In Figure 2, values for K_{eff} decrease as conductor thickness increases.

Imagine what happens to the electric field lines surrounding a conductor as it thickens. In Fig. 1 (b), as the conductor becomes thicker, lines below the conductor (in the dielectric) are affected slightly; the number of lines above the dielectric add. Since more lines pass through the vacuum above the dielectric material, K_{eff} decreases.

On the other hand, if an incremental width is added to the conductor to approximate a thicker conductor (as Wheeler suggests), the opposite results occur. The field lines above the dielectric are little affected, while those below the conductor in the dielectric increase, resulting in a high K_{eff}.••

References

1. Sven Hagelin and Lars-Davis Wernlund, "Properties of Microstrip Transmission Lines," (June, 1974), available as report N76-73858, National Technical Information Service, US Department of Commerce, Springfield, VA 22161.
2. M. A. R. Gunston, *Microwave Transmission-Line Impedance Data*, Ch. 3, Van Nostrand Reinhold Company, Landon (1972).
3. Harold E. Stinehelfer, "An Accurate Calculation of Uniform Microstrip Transmission Lines," *IEEE Trans. Microwave Theory and Techniques*, Vol. MTT-16, No. 7, pp. 439-444 (July, 1968).
4. Kurt P. Schwan, "Thick Coupled Unequal Microstrip Lines," Masters dissertation at the Catholic University of America, Washington, DC (1977).
5. Harold A. Wheeler, "Transmission-Line Properties of Parallel Strips Separated by a Dielectric Sheet," *IEEE Trans. Microwave Theory and Techniques*, Vol. MTT-13, pp. 172-185 (March, 1965).
6. M. Caulton, J. J. Hughes, and H. Sobol, "Measurements on the Properties of Microstrip Transmission Lines for Microwave Integrated Circuits," *RCA Review*, pp. 377-391 (September, 1966).
7. Dr. I. J. Bahl and D. K. Trivedi, "A Designer's Guide to Microstrip Line," *MicroWaves*, Vol. 16, No. 5, pp. 174-182 (May, 1977).
8. M. V. Schneider, "Microstrip Lines for Microwave Integrated Circuits," *The Bell System Technical Journal*, pp. 1421-1444 (May-June, 1969).
9. Robert A. Pucel, Daniel J. Massi, and Curtis P. Hartwing, "Losses in Microstrip," *IEEE Trans. Microwave Theory and Techniques*, Vol. MTT-16, No. 6, pp. 342-350 (June, 1968).

HP-65 Program Computes Microstrip Impedance

Use a calculator to accurately describe a microstrip line on any substrate. This two-card program first displays effective dielectric constant, then computes the characteristic impedance.

TABLES describing microstrip characteristic impedance are readily available for commonly used substrates (with dielectric constants of 9.6 or 3.78, for example), but such information is not available for an increasing number of composite dielectrics such as ceramic-teflon and ceramic-styrene. New materials, available in a broad range of relative dielectric constants, allow the designer to select the best substrate for any particular application. It is, therefore, of great importance to be able to determine quickly and accurately the parameters of microstrip built on a substrate of any dielectric constant.

This can be done quite easily with a Hewlett-Packard HP-65 programmable calculator using the program presented here. The computations are based on approximate formulas introduced by Schneider[1] (see figure). The relationships supposed line thickness, t, to be zero. Their precision is about 0.25 percent for h/W ratios of less than 10. Note that this accuracy is considerably better than that of the microstrip program supplied in the E.E. Pac 2 supplied with the HP-65.

The program does not fit on a single magnetic program card, due to the limited memory size of the calculator. Thus, it is written on two cards which must be introduced successively. The values of h/W and K_e are calculated from the first program card, which also stores the input data K and W/h in registers 1 through 4. The program on the second card uses all these values to calculate the characteristic impedance, Z_o.

The following steps are used to execute the program. Remember, since values for W/h, h/W and K_e are stored in the calculator while program cards are being exchanged, don't make any "clear register" operation before introducing the second card.

- Clear program.
- Read the first card.
- Write K, ENTER, write W/h.
- Depress D to display K_e; the register contents are now: R1: K, R2: W/h, R3: h/W, and R4: K_e.
- Clear program, but do not clear register.
- Read the second card.
- Depress E to display Z_o.

To calculate new parameters, simply go back to the first step. The display is automatically set to .5 by the program. To change it, make a DSP.n after reading the first card. ••

Fred E. Gardiol, Professor, and **J. F. Zürcher,** Ecole Polytechnique Féderale de Lausanne, Chemin de Bellerive 16, CH-1007, Lausanne, Switzerland.

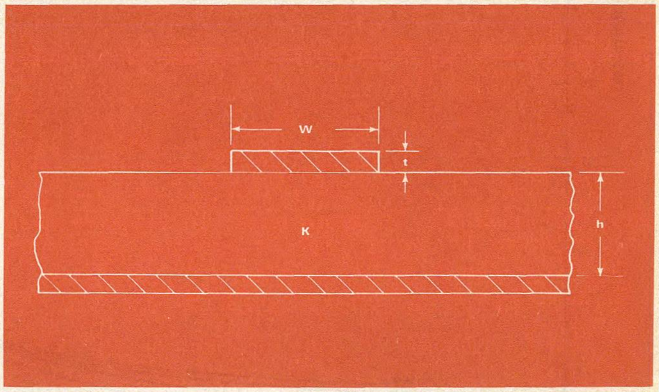

Schneider's formulas, *the basis of this two-part program, provide a precision of approximately 0.25 percent.*

K = dielectric constant
K_e = effective dielectric constant
W = microstrip line width
h = substrate thickness
t = microstrip line thickness
Z_o = characteristic impedance of the microstrip line

KEY EQUATIONS

$$K_e = \frac{K+1}{2} + \frac{K-1}{2}\left(1 + \frac{10h}{W}\right)^{-1/2}$$

For $0 \leq W/h \leq 1$:

$$Z_o = \frac{1}{\sqrt{K_e}}\, 59.952 \ln\left(\frac{8h}{W} + \frac{W}{4h}\right)$$

For $1 < W/h \leq 10$:

$$Z_o = \frac{1}{\sqrt{K_e}} \; \frac{119.904\,\pi}{(W/h) + 2.42 - 0.44(h/W) + (1 - h/W)^6}$$

Reference

1. M.A.R. Gunston, Microwave Transmission-Line Impedance Data, pp. 42-43, Van Nostrand Reinhold Co., New York, 1972.

Card 1: Calculation of effective dielectric constant (K_e)

LINE	KEY ENTRY	CODE SHOWN	COMMENTS	LINE	KEY ENTRY	CODE SHOWN	COMMENTS
01	LBL	23		24	CHS	42	
02	D	14		25	g	35	
03	DSP	21		26	y^x	05	calculation of K_e
04	.	83	sets display to .5	27	↑	41	
05	5	05		28	RCL 1	34 01	
06	STO 2	33 02	stores W/h in register 2	29	↑	41	
07	g X⇄Y	35 07		30	1	01	
08	STO 1	33 01	stores K in register 1	31	−	51	
09	RCL 2	34 02		32	2	02	
10	g	35		33	÷	81	
11	1/x	04		34	×	71	
12	STO 3	33 03	stores h/W in register	35	↑	41	
13	f	31		36	RCL 1	34 01	
14	CLR STK	42		37	↑	41	
15	RCL 3	34 03		38	1	01	
16	1	01		39	+	61	
17	0	00		40	2	02	
18	×	71		41	÷	81	
19	1	01		42	+	61	
20	+	61		43	STO 4	33 04	stores K_e in register 4
21	↑	41		44	RTN	24	
22	.	83		45	gNOP	35 01	
23	5	05					

Card 2: Calculation of characteristic impedance (Z_o)

LINE	KEY ENTRY	CODE SHOWN	COMMENTS	LINE	KEY ENTRY	CODE SHOWN	COMMENTS
01	LBL	23		49	2	02	
02	E	15		50	+	61	
03	f	31		51	RCL 3	34 03	
04	CLR STK	42		52	↑	41	
05	1	01		53	.	83	
06	↑	41		54	4	04	
07	RCL 2	34 02	test W/h > or ≤ 1	55	4	04	
08	g X≤Y	35 22		56	×	71	
09	g NOP	35 01		57	−	51	
10	GTO	22		58	1	01	
11	B	12		59	↑	41	
12	GTO	22		60	RCL 3	34 03	
13	C	13		61	−	51	
14	RTN	24		62	↑	41	
15	LBL	23		63	6	06	
16	B	12		64	g	35	
17	RCL 2	34 02		65	y^x	05	
18	4	04		66	+	61	
19	÷	81		67	g	35	
20	↑	41		68	1/x	04	
21	RCL 3	34 03		69	1	01	
22	8	08		70	1	01	calculation of Z_o for: $1 < W/h \leq 10$
23	×	71		71	9	09	
24	+	61		72	.	83	
25	f	31		73	9	09	
26	LN	07	calculation of Z_o for $0 \leq W/h \leq 1$	74	0	00	
27	5	05		75	4	04	
28	9	09		76	×	71	
29	.	83		77	g	35	
30	9	09		78	π	02	
31	5	05		79	×	71	
32	2	02		80	RCL 1	34 01	
33	×	71		81	f	31	
34	↑	41		82	$\sqrt{x}$	09	
35	RCL 4	34 04		83	g	35	
36	f	31		84	1/x	04	
37	$\sqrt{x}$	09		85	×	71	
38	g	35		86	↑	41	
39	1/x	04		87	RCL 1	34 01	
40	×	71		88	↑	41	
41	RTN	24		89	RCL 4	34 04	
42	LBL	23		90	÷	81	
43	C	13		91	f	31	
44	RCL 2	34 02		92	$\sqrt{x}$	09	
45	↑	41		93	×	71	
46	2	02		94	RTN	24	
47	.	83		95	g NOP	35 01	
48	4	04					

1977 ANNUAL INDEX

Abbreviations: (TA) - Technical Article, (N) - News, (CF) - Cover Feature, (PF) - Product Feature, (SR) - Staff Report

Acoustic Wave Devices

□ *Interdigital SAW Transducer Poses Its Bidirectionality*, (N), Sept, p. 42.

□ *Magnetic Field Tunes SAW Oscillator*, (N), Nov, p. 37.

□ *Nondispersive Delay Line Operates From 7 to 11 GHz*, (N), Mar, p. 24.

□ *Radar Systems Mature With SAW Technology*, (TA), May, p. 162.

□ *You Can't Shake Up SAW Sources*, (N), May, p. 37

Amplifiers

□ *Compact Radial Power Combiner Teams Up A Dozen Power GaAs FETs*, (N), Oct, p.9.

□ *Easy To Plot Graphs Show Power-Gain Tradeoffs*, (TA), Dec, p. 178.

□ *Impatt Amp Designed For Digital Transmitters*, (N), July, p. 14.

□ *Noise Temp Of A K-Band Satcom Amp Drops To A Quiet 90°K*, (PF), Sept, p.126.

□ *Spot Compression Points With Equal-Gain Circles*, (TA), Oct, p. 60.

□ *Stretch FET Amp Design Beyond Octave Bandwidths*, (TA), May, p. 54.

□ *Ultra-Wideband Lab Amplifier Delivers 4 Watts From 1 To 1000 MHz*, (PF), Sept, p. 126.

□ *Update Amplifier Design With Network Synthesis*, (TA), Oct, p. 50.

Antennas and Phased Arrays

□ *Microwave Reflector Antennas Reviewed*, (N), Dec, p. 142.

□ *Modified Backfire Lowers Cross-Polarization Levels*, (TA), June, p. 70.

□ *NRL Is Touting New Millimeter Antenna*, (N), Feb, p. 20.

□ *Offset Feed Antenna Tested At 100 GHz*, (N), May, p. 37.

□ *Propagation Study Focuses On Weather*, (N), Jan, p. 32.

□ *Reshaped Subreflectors Reduce Antenna Sidelobes*, (TA), May, p. 170.

CATV

□ *Cable TV Wins Big In Two DC Courts*, (N), May, p. 21.

□ *Part Of Pay Cable Ruling To Be Appealed By FCC*, (N), June, p. 22.

□ *Opposition Growing To CATV Via Satellites*, (N), Oct, p. 27.

Commercial Applications

□ *European Conference Showcases Innovative Commercial Applications*, (N), Sept, p. 12.

□ *300-Channel Microwave Net Links Power Grid Over 1280-km Route*, (N), Oct, p. 36.

□ *X-Band Instrument Measures Moisture*, (N), June, p. 26.

Communications

□ *AT&T Won't Eliminate Its Telpak Service*, (N), Sept, p.30.

□ *Appeals Court Says Yes To MCI's Execunet*, (N), Sept, p. 27.

□ *Appeals Court Upholds FCC Interstate Jurisdiction*, (N), Aug, p. 24.

□ *Bell Systems To Begin SSB Field Trials* (N), Aug, p. 46.

□ *Brazil Is First With 8 GHz PCM Radio System*, (N), Feb, p. 22.

□ *"Carrier's Carrier" Needed, Says FCC Chairman*, (N), May, p. 24.

□ *Common Carrier Explored Before Communications Panel*, (N), Nov, p. 26.

□ *Communications Act Rewrite Is Priority Number One*, (N), Feb, p. 20.

□ *Congress Flexes Muscle Against "Bell Bill,"* (N), Apr, p. 23.

□ *Congress Goes To School On Telecommunications*, (N), May, p. 24.

□ *Congress Will Study Broadband Communications*, (N), Jan, p. 18.

□ *Convolution Program Tests Two Interfering Signals*, (TA), Nov, p. 68.

□ *DC Court Will Rule On MCI's Execunet*, (N), July, p. 21.

□ *Execunet Decision Heads To Supreme Court*, (N), Oct, p. 30.

□ *FCC Offers Grim Word To MCL, SPC Services*, (N), Apr, p. 26.

□ *FCC Okays ITT Private Line Network*, (N), Aug, p. 24.

□ *FCC's SBS Approval Is Appealed In Court*, (N), May, p. 24.

□ *FCC Urged To Allocate "Communicasting" Service Frequencies*, (N), Mar, p. 12.

□ *FCC Will Study Revenues From Telephone Equipment*, (N), Jan, p. 20.

□ *House Panel Pursues Communications Rewrite*, (N), July, p. 24.

□ *Industry WARC Comments Being Surveyed By FCC*, (N), Oct, p. 30.

□ *Industry Will Study Intercity Competition*, (N), Sept, p. 27.

□ *Japanese Designers Stress High-Capacity Links*, (N), Aug, p. 43.

□ *Lower Crosspole Levels For Safe Frequency Reuse*, (TA), Nov, p. 48.

□ *MCI Asks Supreme Court Not To Rule On Execunet, (N), Dec., p. 30.*

□ *Microwaves May Star In Rural Communications*, (N), June, p. 21.

□ *Mobile Radio At 900 MHz. . . 'Logical' Design Relaxes Tough Crystal Standards*, (TA), Aug, p. 52.

□ *New Mobile Radio Service Proposed For 900-MHz Band*, (N), July, p. 10.

□ *RCA Is The Target Of A Complaint To FCC*, (N), Jan, p. 28.

□ *Saudi Microwave System Won By Western Electric*, (N), July, p. 28.

□ *Scandinavian Mobile Phone System Seen For 1980s*, (N), Sept, p. 36.

□ *Space Diversity Combats Deep Fading Problems*, (N), June, p. 36.

□ *Supreme Court Lets Stand FCC Telephone Ruling*, (N), Feb, p. 19.

□ *Users Turn From AT&T As Telpak Phases Out*, (N), July, p. 21.

□ *Washington Reacts To Reports Of Soviet Telephone Tapping*, (N), Sept, p. 24.

□ *Wiley To Hold FCC Helm, At Least For A While*, (N), Mar, p. 22.

Components

□ *Active Circuits Keep Systems On The Level*, (TA), Mar, p. 62.

□ *Apply Standard Curves To Strange Substrates*, (TA), Sept, p. 116.

□ *Are Mixers A Victim Of Coherent Shot Noise?*, (N), July, p. 32.

□ *Dielectric Resonators Add Q To MIC Filters*, (TA), Dec, p. 150.

□ *Drop-In Circulator Spans 4-8 GHz Band*, (PF), Aug, p. 72.

□ *Edge-Guide: One Path To Wideband Isolator Design, Part I*, (TA), Jan, p. 54.

□ *Edge-Guide: One Path To Wideband Isolator Design, Part II*, (TA), Feb, p. 50.

□ *GaAs Varactors Offer High Qs*, (PF), Aug, p. 72.

□ *H-P 65 Program Computes Microstrip Impedance*, (TA), Dec, p. 186.

□ *Is Video Leakage Your System Problem?*, (TA), Feb, p. 58.

□ *Magnetic Field Adjusts Directional Coupler*, (N), Jan, p. 32.

□ *Mixers Add MM-Wave Capabilities To Spectrum Analyzers*, (PF), Aug, p. 70.

□ *Mixers Combine High Isolation With Rugged Mechanical Design*, (PF), Aug, p. 70.

□ *NBS Study Focuses On SMA Connectors*, (N), Apr, p. 14.

□ *New Cable Rules To Impact Costs and Availability*, (N), Sept, p. 10.

□ *Nine FORTRAN Subroutines Do Smith Chart Chores*, (TA), Dec, p. 172.

□ *Nondispersive Delay Line Operates From 7 To 11 GHz*, (N), Mar, p. 24.

□ *Power Transistors Debut With Stepped-Electrode Construction*, (PF), Aug, p. 72.

□ *Radar Systems Mature With SAW Technology*, (TA), May, p. 162.

□ *Speed Circulator Design With Computer Modeling*, (TA), June, p. 54.

□ *Take The Guesswork Out Of Thick Microstrip K*, (TA), Dec, p. 184.

□ *Temperature Stable Dielectric Resonators Replace Expensive Invar, Boost Q in MICs*, (N), Dec, p. 14.

□ *Upgrade Coax Switches For High Power Transfer*, (TA), Jan, p. 48.

Design

□ *CAD: Programs Grow In Flexibility As Designers Learn About Optimization*, (SR), June, p. 49.

Diodes

□ *A Low-Frequency Look At Millimeter-Wave Diodes*, (N), Nov, p. 37.

□ *A More Ideal GaAs Mixer Diode*, (N), Dec, p. 10.

□ *All Epitaxial PINs Switch At Lower Voltage*, (N), Dec, p. 142.

□ *Consider A Single Diode To Study Mixer Intermod*, (TA), Dec, p. 162.

□ *Low-Cost Detector Design Is Ideal For RF Monitors*, (TA), Mar, p. 58.

□ How The New Schottkys Detect Without DC Bias, (TA), Feb, p. 44.

□ Impatts Surge To Higher Powers And Frequencies, (N), Apr, p. 9.

□ Mesa Structure Raises Beam-Lead PIN Diode Performance, (PF), May, p. 192.

□ New Impatt R&D Drives Up Efficiency; Processing Key To Improved Specs, (N), Dec, p. 9.

□ Schottky-Diode Area-Loss Relationship Examined, (N), Apr, p. 35.

□ Series-Connected Impatts Pack A 22-W Punch, (N), Sept, p. 42.

□ Super Schottky Turns in Record Performance, (N), June, p. 38.

□ Varactor Shows Strongly Nonlinear C/V Characteristics, (N), Aug, p. 32.

Economic Outlook

□ Appeals Court Upholds Comsat Rate Decision, (N), Dec, p. 30.

□ Carter Would Curb Overseas Arms Sales, (N), June, p. 21.

□ Commerce Dept. Sees Industrial Outlook Bright, (N), Mar, p. 19.

□ Defense Funding Dominates FY 78 Budget, (N), Mar, p. 10.

□ DOD Eyes New Incentive: Government Guaranteed Loans, (N), June, p. 24.

□ DOD Will Liberalize Its Export Policy, (N), Nov, p. 26.

□ EW Funding: Large Gains Seen For Device And Component Development, (N), May, p. 9.

□ F-15 Is Target For Congress-DOD Battle, (N), May, p. 21.

□ Import Growth In Electronic Components, (N), Aug, p. 24.

□ Microwave Studies Set In Intelsat's New Budget, (N), Jan, p. 20.

□ Military Navigation Market Flies High, (N), July, p. 12.

□ Pentagon Gives Nod For Cruise Missiles, (N), Mar, p. 22.

□ Pentagon's Harold Brown: Big News For R&D?, (N), Feb, p. 20.

Electronic Warfare

□ Air Force Will Build A Killer Satellite, (N), Nov, p. 23.

□ "Buck Rogers" Beam Weapon May Be Close To Reality, (N), July, p. 28.

□ Boeing, General Dynamics In Cruise Missile Contest, (N), Nov, p. 26.

□ Carter's B-1 Decision: Boon To Cruise Missiles?, (N), Aug, p. 24.

□ Congress Is Debating In-House Defense Work, (N), July, p. 24.

□ Lockheed Wins Air Force Approval to Build Precision Location/Strike System, (N), Nov. p. 14.

□ Microprocessors: Changes Ahead For ECM Architects, (TA), May, p. 46.

□ NATO Weighs Important Airborne EW Decisions, (N), Feb, p. 22.

□ Next Carter Target: Cruise Missile Control, (N), July, p. 24.

□ Pentagon Concerned About Soviet Killer Satellites, (N), Jan, p. 20.

□ US, European Firms Race For New EW Markets, As Japanese Manufacturers Sprint To Catch Up, (N), Nov, p. 10.

Filters

□ Bandpass Multiplexers Now Cover 9:1 Bandwidths, (PF), Jan, p. 64.

Front Ends

□ BASIC Computer Algorithm Spots Spurious Responses, (TA), Mar, p. 42.

□ Josephson Junction Mixers: Approaching The Final Frontier?, (N), May, p. 14.

□ Ku-Band Front-Ends Shrink To Meet Big Demands, (N), June, p. 14.

□ Thin-Film Mixers Team Up To Block Out Image Noise, (TA), Mar, p. 34.

Instrumentation and Measurement

□ Calculator-Controlled Six-Port Junction Seen As Everyman's Network Analyzer, (N), Aug, p. 14.

□ Computer Control Brings More Capabilities and Higher Performance To Spectrum Analysis, (PF), Sept, p. 122.

□ Count And Stabilize: One Instrument Does Both To 18 GHz, (CF), Apr, p. 66.

□ Define Dynamic Range For Better Spectrum Analysis, (TA), Aug, p. 62.

□ How Accurate Is Your Power Meter?, (TA), Sept, p. 106.

□ Licensees Sought To Produce NBS-Developed RF Power Meter, (N), Aug, p. 12.

□ Measurement Accuracy Hinges On Coupler Design, (TA), Apr, p. 41.

□ Meterless Monitoring Of Radiation Now In Sight, (N), Aug, p. 10.

□ Microprocessor-Controlled Frequency Counter Thinks Fast, Acts Smart And Costs Less, (CF), Nov, p. 74.

□ Resonant Method Measures Package Parasitics, (N), July, p. 32.

□ Self-Calibrating ANA Eyes S-Parameters From 0.1 To 18 GHz, (PF), Sept, p. 124.

□ Simple Setup Measures Complex Dielectric Data, (TA), Apr, p. 64.

□ Spectrum Analyzer Resolves To 30 Hz At 12 GHz, Works To 60 GHz With External Mixers, (PF), May, p. 193.

□ Swept Measurements Speed Gain Compression Tests, (TA), Apr, p. 48.

□ Superconductor May Be The New RF Attenuation Standard, (N), June, p. 12.

□ Sweeper And Signal Generator Features Combined In One Package, (PF), Jan, p. 64.

□ Test Set Measures Low-Level Intermod Noise, (N), June, p. 36.

□ Ultra-Fast RF Power Meter Eases Multi-Detector Power Struggle, (PF), Dec, p. 195.

□ Vector Voltmeters Perk Up With High-Speed Sampling, (TA), Apr, p. 56.

Lasers and Integrated Optics

□ Acousto-Optics Light The Path To Broadband ESM Receiver Design, (SR), Sept, p. 54.

□ British Hope To Be First With Telephone Fiber Optics, (N), June, p. 17.

□ Chicago Hosts First Optical Communication Installation, (N), May, p. 10.

□ Italian Telephone System Tests 140 Mbls Optical Link, (N), Nov, p. 28.

□ Laser-Based System Scans Road For Wear, (N), Oct, p. 36.

□ Laser Triggers High-Speed RF Switch, (N), Apr, p. 28.

□ LED Method Speeds Optical Fiber Tests, (N), Mar, p. 26.

□ Optical Fibers Will Link Japan's "Wired Cities", (N), Jan, p. 22.

□ Opto Branch Readily Made, Report Siemens Researchers, (N), Sept, p. 36.

□ Remote Laser Technique Measures Air Pollution, (N), Mar, p. 24.

Microwaves and Medicine

□ Cancer Therapy, Detection Aided By Microwave Technology, (N), Sept, p. 22.

□ Direct-Contact Diathermy Probes Found Safer, (N), May, p. 12.

□ Effects Of Non-Ionizing Radiation Given Priority Status By Congress, (N), Aug, p. 9.

□ Is That Microwaves You Hear?, (N), Aug, p. 32.

□ Microwaves and Biology Next Hot Issue In DC, (N), Apr, p. 23.

□ Soviets Are Studying Microwave Effects On Health, (N), Jan, p. 18.

Millimeter Waves

□ A Low-Frequency Look At Millimeter-Wave Diodes, (N), Nov, p. 31.

□ Millimeter-Wave "Pipe" Dream Nears Reality In Great Britian, (N), Jan, p. 22.

□ Mixers Add MM-Wave Capabilities To Spectrum Analyzers, (PF), Aug, p. 70.

□ NRL Is Touting New Millimeter Antenna, (N), Feb, p. 20.

□ Offset Feed Antenna Tested At 100 GHz, (N), May, p. 37.

□ Weather Affects MM-Wave Missile Guidance Systems, (TA), Sept, p. 62.

□ With Outputs Of Milliwatts To Megawatts, Millimeter Wave Radar Is Coming On Strong, (N), Nov, p. 9.

Miscellaneous

□ Appeals Court Remands FCC's Fee Schedule, (N), Feb, p. 19.

□ Business Employs Fewer Scientists, Engineers, (N), Aug, p. 21.

□ Carter Outlines NASA Space Goals, (N), Aug, p. 21.

□ Dilemma Is Seen On Electronics Smuggling, (N), May, p. 21.

□ DOD's Sealed Bids Chided In Congress, (N), Dec, p. 27.

□ European Climate Unhealthy For Fledgling Technical Firms, (N), Aug, p. 28.

□ Ferris, Brown Fill Vacancies At FCC, (N), Nov, p. 23.

1977 ANNUAL INDEX

Abbreviations: (TA) - Technical Article, (N) - News, (CF) - Cover Feature, (PF) - Product Feature, (SR) - Staff Report

(Miscellaneous (cont.)

□ *Fort Monmouth Reorganization Confirmed,* (N), May, p. 12.

□ *Future Of OTP In Limbo Again,* (N), Mar, p. 22.

□ *Geller Will Head Telecommunications Office,* (N), Dec, p. 30.

□ *Government Will Fight Microwave Eavesdropping,* (N), Oct, p. 27.

□ *NASA-Air Force To Duel Over "Waterhole" Spectrum,* (N), Oct, p. 30.

□ *National Science Board Plans Public Posture,* (N), Apr, p. 26.

□ *New Communications Office Will Join The DC Scene,* (N), Sept, p. 30.

□ *New Science Advisor Hopes For Key Role,* (N), July, p. 21.

□ *OTP To Be Scuttled By White House,* (N), Aug, p. 21.

□ *Paperwork Eased For Small DOD Purchases,* (N), Dec, p. 30.

□ *Personnel Shifts Expected In DC Science Community,* (N), Jan, p. 20.

□ *77 Experiments Chosen For Spacelab,* (N), June, p. 26.

R&D

□ *Airborne Ice Clouds Fading Issue,* (N), Apr, p. 35.

□ *Cornell Plans Submicron Lab,* (N), Sept, p. 24.

□ *Damages Charged To Lightning,* (N), Oct, p. 40.

□ *Josephson Junction Mixers: Approaching The Final Frontier?,* (N), May, p. 14.

□ *Quasars Guide ARIES In Seaslope Quest,* (N), July, p. 9.

Radar

□ *Airport Radar Will Be Linked By Microwaves,* (N), June, p. 24.

□ *Microprocessor Muffles Auto Radar False Alarms,* (N), Mar, p. 24.

□ *Multimode F-16 Radar Begins Flight Tests,* (N), May, p. 17.

□ *New Combining And Cooling Techniques Developed For 1-kW L-Band Transmitter,* (N), Sept, p. 9.

□ *NOAA Tracks Twisters In Doppler Tests,* (N), June, p. 24.

□ *Radar Systems Mature With SAW Technology,* (TA), May, p. 162.

□ *Robot Radars Eyed For New DEW Line,* (N), Apr, p. 14.

□ *Spaceborne Radar Needs Correction,* (N), Nov, p. 37.

□ *Synthetic Array Radar To Map The Surface Of Venus,* (N), Jan, p. 12.

□ *Weather Affects MM-Wave Missile Guidance Systems,* (TA), Sept, p. 62.

□ *With Outputs of Milliwatts To Megawatts, Millimeter-Wave Radar Is Coming On Strong,* (N), Nov, p. 9.

Satellite Communications

□ *Arabsat Group To Announce Consultant Bid On $84-Million Program,* (N), Oct, p. 36.

□ *Brown Says Russians Have Killer Satellities,* (N), Dec, p. 134.

□ *Chinese Earth Station Surprises EIA Delegation,* (N), Nov, p. 28.

□ *Comsat Will Build New Earth Station,* (N), Dec, p. 27.

□ *ESA Lays Plans For Direct Broadcast Satellite,* (N), Feb, p. 22.

□ *Earth Stations Slim Down To Meet Grass-Root Demands,* (SR), Jan, p. 36.

□ *Earth Stations To Triple By 1985, As Systems Move Up To 30 GHz,* (N), Aug, p. 48.

□ *Earth Station Weighs Just 25 Pounds,* (N), Aug, p. 48.

□ *Evolution Of Satellite Communications Traced,* (N), Mar, p. 26.

□ *Experimental Comsat To Fly For ESA,* (N), Sept, p. 36.

□ *FCC Okays SBS Satellite Venture,* (N), Mar, p. 19.

□ *FCC Okays Satellites For Public Broadcasters,* (N), Apr, p. 26.

□ *Five-Year Term Granted For Marisat Satellites,* (N), Feb, p. 20.

□ *4.5-Meter Earth Stations Win FCC Approval,* (N), Feb, p. 19.

□ *Indians Borrow Symphonie For Two-Year Experiment,* (N), Aug, p. 28.

□ *Indian National Satellite (INSAT) Set For '81 Launch,* (N), Oct, p. 36.

□ *Mail By Satellites? Postal System Urged To Consider,* (N), Mar, p. 22.

□ *NASA Will Alter Its Public Satellite Contracts,* (N), Dec, p. 27.

□ *Processors To Play Key Roles In Future Military Satellites,* (N), Aug, p. 47.

□ *Satellites Beam Solar Power To Earth* (N), Dec, p. 142.

□ *Satellite Links Studied For North Sea Wells,* (N), May, p. 28.

□ *Satellite Links Two Radio Observatories,* (N), Mar, p. 14.

□ *Satellite-To-Home TV: Only $40 Million A Year?,* (N), Sept, p. 27.

□ *WARC Comments Needed On Small Earth Stations,* (N), June, p. 21.

□ *Western Union Proposes Interchangeable Satellites,* (N), Aug, p. 21.

□ *Western Union Wins $796-M Satcom Program,* (N), Mar, p. 14.

Semiconductors and MICs

□ *A Designer's Guide To Microstrip Line,* (TA), May, p. 174.

□ *Amorphous Semiconductor Modulates Without Delay,* (N), Oct, p. 40.

□ *Ask Tough Questions About GaAs FET Specs,* (TA), Oct, p. 82.

□ *Balanced Transistors: A New Option For RF Design,* (TA), June, p. 42.

□ *Barritts Are Best For Self-Mixing Radars,* (N), Feb, p. 29.

□ *Careful MIC Design Prevents Waveguide Modes,* (TA), May, p. 188.

□ *80 GHz DDR Impatt Breaks Mid-Power Barrier,* (N), Dec, p. 134.

□ *GaAs FETs Gain Ground In Oscillators, Mixers and Limiters,* (N), June, p. 9.

□ *GaAs FETs Slash Noise Figures,* (N), Oct, p. 40.

□ *GaAs FET Speeds Data Transfer,* (N), Aug, p. 32.

□ *Gigabit Logic: Speed Rises As Power Falls,* (N), Apr, p. 12.

□ *Glowing GaAs FET Sheds Light On New Internal Field Structure,* (N), Dec, p. 18.

□ *Gunn-Device Voltages Profiled By SEM,* (N), Jan, p. 32.

□ *Illumination Improves Trapatt Performance,* (N), Jan, p. 14.

□ *InP Gunn-Effect Devices Begin To Surface In The US,* (N), Feb, p. 12.

□ *Is There A Josephson Junction In Your Future?,* (TA), Mar, p. 50.

□ *Master The T-Junction And Sharpen Your MIC Designs,* (TA), May, p. 184.

□ *MOSFET Developments Up Power And Frequency To Challenge Bipolars At VHF To Microwave,* (N), Oct, p. 10.

□ *PNP Bipolar Transistor Developed For High-Speed Complementary Amplifier,* (N), Mar, p. 9.

□ *POWER (9.5 W) & Low-Noise (0.7 dB NF) GaAs FETs In Lab Now, Say Researchers At Cornell Conference,* (N), Oct, p. 18.

□ *Prices on FETs Lowered; The Start Of An Industry Trend?,* (N), Sept, p. 18.

□ *POWER! GaAa FETs Star In A New Role,* (SR), Feb, p. 36.

□ *Power Transistor Elevates Emitters,* (N), June, p. 17.

□ *Semiconductor and Circuit Designs Team Up To Score New Performance Highs,* (N), Feb, p. 9.

□ *Semiconductor Material Analyzed Without Contact,* (N), Feb, p. 29.

□ *Sixteen-Cell Bipolar Reaches 40 W At 2 GHz,* (N), Sept, p. 20.

□ *Super-Cooled System Quiets GaAs FET,* (N), Apr, p. 35.

□ *TDA Distortion Traced To Velocity-Field Curve,* (N), May, p. 37.

□ *Theory Says GaAs Quieter Than InP For FETs,* (N), Feb, p. 29.

□ *Two-Layer FET Structure Boosts Performance,* (N), Sept, p. 42.

Sources

□ *Design VCOs Accurately with Computer Analysis,* (TA), July, p. 70.

□ *GaAs FET Oscillators Break Into K Band,* (PF), July, p. 92.

□ *GaAs FETs Rival Gunns In YIG-Tuned Oscillators,* (TA), July, p. 42.

□ *Oscipliers: K-Band VCOs You Build With Bipolars,* (TA), Nov, p. 62.

□ *Power GaAs FET Shows Promise In Oscillator,* (N), July, p. 12.

□ *Relativistic Source Development Speeds Up,* (N), July, p. 14.

□ *VCO Subsystems: What To Test, How To Test It, Part I,* (TA), May, p. 60.

□ *VCO Subsystems: What To Test, How To Test It, Part II,* (TA), July, p. 82.

□ *You Can't Shake Up SAW Sources,* (N), May, p. 37.

□ *Depolarization Related To Radio Performance,* (N), July, p. 32.

□ *Doppler-Scanner Dialogue Displays US-UK Flap,* (N), Sept, p. 30.

□ *MLS "Test-Off" Set For November,* (N), Oct, p. 20.

□ *Scanning Beam MLS Wins First Round,* (N), May, p. 28.

Systems

□ *British Decline Invitation To Display Doppler MLS,* (N), Dec, p. 134.

□ *FAA Reverses Field on Doppler/TRSB Fly Offs,* (N), Nov, p. 23.

Tubes

□ *Focus On High-Power Tube Developments,* (N), Mar, p. 26.

□ *1-kW 38-GHz TWT Runs Silent, Runs Deep,* (N), Apr, p. 28.

□ *Tube Manufacturers Stress Power And Efficiency Gains,* (N), Jan, p. 9.